E.O. Paton Electric Welding Institute of the National Academy of Sciences of Ukraine

International Scientific-Technical and Production Journal

CONTENTS

INTERVIEW WITH PROF. S.I. KUCHUK-YATSENKO, THE DEPUTY DIRECTOR OF THE E.O. PATON ELECTRIC WELDING INSTITUTE

The welding society in Ukraine and far abroad is familiar with the amazing achievements of the E.O. Paton Electric Welding Institute (PWI) in the field of flash-butt welding. This direction is headed by Prof. Sergey I. Kuchuk-Yatsenko, the academician of the NAS of Ukraine, the merited worker of science and technology of the former UkrSSR. His research activity is associated with the fundamental research works of physical-metallurgical processes in welding of different metals in the solid phase, purposeful study of rapid-running processes of heating and fracture of single contacts at the high energy concentrations. He obtained new data on the peculiarities of formation of joints with the formation of thin layer of melt on the contact surfaces of parts being welded, its behavior under the effect of electrodynamic forces and interaction with gas environment in the contact zone. The new regularities were established characterizing power characteristics of the process of contact melting of metals, the algorithms of automatic control of basic process parameters were determined with the purpose of obtaining the best conditions of heating and deformations of the parts being welded.

The practical result of fundamental research works, carried out by Prof. S.I. Kuchuk-Yatsenko and his staff, was highly appraised:

1966 — the Lenin prize for the development and implementation of machines for flash-butt welding of rails in the repair and construction of seamless railroads;

1976 — the State Prize of the UkrSSR for creation and industrial implementation of new technology and highly-efficient assembly-welding complexes for serial production of large-sized structures of unified elements;

1986 — the State Prize of the USSR for creation of technologies and equipment for flash-butt welding of structures of high-strength aluminium alloys;

2000 — the E.O. Paton Prize of the NAS of Ukraine.

Prof. S.I. Kuchuk-Yatsenko published over 350 scientific papers in the authoritative specialized journals, received 740 author's certificates and patents, prepared 11 Candidates and 2 Doctors of Technical Sciences. He was decorated with two orders of the Red Banner of Labour, Order of the «Badge of Honour», Order of Prince Yaroslav the Wise of the Fouth and the Fifth classes, and medals.

On the eve of the 85th birthday anniversary of Prof. S.I. Kuchuk-Yatsenko the Editorial Board of the Journal recorded the interview with the jubilee person connected to one of the directions of his activity: welding of rails.

Dear Professor, how the permanent interest to the topic «Welding of rails» may be explained?

Indeed, the publication of articles on the topics related to welding of rails is regularly continuing in «The Paton Welding Journal», and at the PWI scientists deal with this problem for several decades. In fact, the PWI deals with creation of flash-butt welding technology of rails and design of equipment from the early 1960s.

At the PWI for the first time in the world practice the technology of flash-butt welding of thick-walled parts was developed using the continuous flashing of large-section parts, providing a great improvement of power characteristics of the process, namely 3–4 times reduction of the specified capacity of the source and enabling its full automation. In the development of this technology Professors B.E.

Prof. S.I. Kuchuk-Yatsenko

Paton and V.K. Lebedev actively participated. On the basis of this technology the original generation of welding equipment was created patented in the leading countries of the world. For the first time in the world flash-butt welding was used to join the rails directly on the track in the construction of seamless high-speed railways.

How widespread did the created technology of welding rails become at that time? Was there a feeling that the problem had been solved completely?

The technology and equipment quickly gained a wide application on the railroads of the USSR. The production of new welding equipment according to the PWI documentation was mastered by Kakhovka Plant of Electric Welding Equipment, with which we have many years of fruitful cooperation. This development was highly appraised by the state: it was awarded the Lenin Prize. We had every reason «to rest on laurels». But the development of any direction does not allow even a temporary stop. At first, new production demands arise with the development of transport systems, and secondly, under competitive conditions there is a need for continuous improvement of the technology and equipment. For these

Machine K155, 1959
(S.I. Kuchuk-Yatsenko *at the left*)

purposes the PWI Center «Pressure Welding» was established in 1987 for industrial implementation and a wide mastering of the PWI developments. The base of its staff formed the PWI specialists.

How did the technical and commercial relations with foreign companies develop?

Even under the conditions of closed market, starting since the 1970s, the leading international railway companies of Austria, France, Japan, the United States and other countries showed an interest to the technology and equipment. Already from the beginning of the 1970s the export of rail welding equipment with accompanying technologies for welding began from Ukraine. On the one hand, it encouraged our producers for modernization of equipment and, on the other hand, for establishment of long-term fruitful cooperation with the Austrian company «Plasser & Theurer», US «Norfolk Southern Corporation», «Holland LP», «Progress Rail Service Corporation», Canadian «E.O. Paton International Holdings Inc.» etc. At the present time we stilll continue to cooperate with the foreign companies, improving the technology and equipment taking into account the most rigid requirements in this area. In several decades, the PWI has developed more than 10 generations of rail welding machines, which production was mastered by Kakhovka Plant of Electric Equipment with the participation of the PWI. Now almost in all the continents of the world more than 1,500 rail welding machines operate, being designed at the PWI and manufactured at Kakhovka. The PWI specialists provide engineering maintenance of this equipment and it is not only limited by setting up the equipment and staff training. With improvement of the structure of railway transport and construction elements of the railway track the new challenges appear to be solved by welders.

How would you characterize the newly emerging challenges?

Until the mid-1970s in welding of rails the our proposed technology with a continuous flashing was used, and after a while the technology of pulsed flashing was offered by the PWI. Already in 1976 the first machine was sold to the USA, and since 1976 until the beginning of the 1980s, over 35 machines such as K355A were sold. The construction of new high-speed mainline railroads required solving of two main problems: the use of high-strength rails, characterized by an increased wear resistance, and meeting the higher requirements to the geometrical dimensions of track.

In the last decade many countries experience an intense reconstruction of railways and rail track. Here, high-strength rails having hardness of up to *HB* 400 are used. According to the technological specifications a practical full strength of welded joints with the base metal of rail steel and high plastic properties are required. It was not managed to obtain these characteristics using the traditional technology. At the PWI the systematic studies of weldability of new high-strength rails of different world producers (Austria, China, Russia, USA, Ukraine, Japan) are carried out to develop welding technologies, providing the required mechanical properties. This meantime raises the need in a substantial change of control systems of welding machines and designs of their separate units.

What new approaches were realized in welding of rails?

In particular, it was found that for a high quality welding of high-strength rails the technology of contact heating and mechanical part of design of machines need a substantial change to provide 1.5−2 times increase in compression forces. It was also found that to produce the stable high quality of high-strength rails joining the strictly preset energy input in welding is required. For this purpose the electronic system was developed providing the stabilization of energy input at changes of different conditions of operation of the equipment, as well as at its operation under the field conditions. In the development of systems of automatic computerized control of weld-

**Yaroslav Mikitin,
the Management Director of Kakhovka Plant
of Electric Welding Equipment**

A close cooperation connects KPEWE with PWI and Prof. S.I. Kuchuk-Yatsenko has been a reliable support to this unity of production and science already more than 50 years. He was among the pioneers of the electric welding machines production at the South of Ukraine in Kakhovka. He has been always a driving force in implementation of new models of equipment which later were recognized throughout the world. Taking into account a many-year experience of business and personal relationships with Sergey Ivanovich, I would like to say the following: he is a world famous scientist in the field of flash-butt welding, and welding of rails, railway frogs and pipes is the priority of his research. I, personally, consider him to be my teacher. I am proud that the destiny disposed me to be almost all my conscious labor life together with Sergey Ivanovich. Sergey Ivanovich, I am eternally grateful to You for the plant and the business You adore. I wish You a strong health, new creative ideas and realizations!

Valery Krivenko, the Director of Engineering Centre «Pressure Welding»

Sergey I. Kuchuk-Yatsenko together with Boris E. Paton were initiators of foundation of the engineering centre «Pressure Welding» in 1987. At that time it was only a beginning of wide-scale industrial implementation of machines and technologies for flash-butt welding of pipes and rails both in the USSR as well as abroad. Already in those years they could foresee that a wide-scale implementation of new welding technologies is impossible without a special research engineering department being a part of the PWI. The fundamental base of the new engineering centre was composed of engineers of the PWI Experimental Design Technological Bureau having already the experience of implementation of welding equipment and technologies to the industry.

Since the end of the 1980s the area of industrial implementation of rail welding equipment of the PWI was sufficiently widened due to making the contracts for sale of rail welding machines to Canada, USA, China and later India, Turkey, South-Eastern Asia, South America, Australia. Sergey Ivanovich was a direct participant of all technical and commercial negotiations and conclusion of many export contracts, which allowed bringing the PWI research engineering developments to the world market.

Machine K900 (Singapore, 1994)

ing process another significant problem was solved allowing during welding the simultaneous stabilization of the position of long-rail sections after welding.

It is known that in the process of service of seamless track the stresses occur in fixed rails caused by change in temperature, i.e. under the influence of environment. Their effect leads to deformation of rail sections, violation of preset sizes of the track, and in critical situations leads to accidents. The most dangerous are compressive stresses, which may lead to «ejection» of a section.

A bold decision was suggested: in welding of rails of infinite length to create tensile stresses in the sections of such value that at the preset range of changing temperatures in the rails the compressive stresses could not occur. For this purpose during welding it is necessary to provide the tension for value, correlating with proper calculated value of drop of temperatures. The applied technology of flash-butt welding allows performing this operation, as it envisages the bringing the parts together in the process of flashing. An understanding was reached that it is necessary to provide control of welding process with simultaneous control of tension force of sections being welded. This problem was solved by creation of algorithms of control of the welding process basic parameters.

What types of the designed equipment allow meeting the updated requirements of the customers?

As a result of carried out developments a new generation of welding machines and technology, named «pulsating flashing», was developed and patented in the leading foreign countries. The first machines of this type K900, K920 and K921 were designed at the PWI and tested at the railways of the USA together with «Norfolk Southern Corporation» and other US customers.

From the mid-1990s at the PWI a new generation of rail welding machines for welding of rail sections with tension of K922 type was designed. Their production was mastered by Kakhovka Plant of Electric Welding Equipment. All the rail welding enterprises of Ukraine were equipped with these machines (more than 10 machines). They were also delivered

Machine K921 (USA, 1994)

Machine K922 (produced since 2003)

Machine K945 (Great Britain, Wales, 2013)

to the rail welding enterprises of Russia and China, where with their help the construction of seamless high-speed railways was realized.

How promising is the use of high-strength rails?

Since 2011, at the Ukrainian enterprises the production of high-strength rails was started and at the same time at the PWI the technology of their welding is being tested. In addition, on demands from different countries the developments of welding technologies of new generations of high-strength rails are performed at the PWI. At the present time, the task of laying out the rails is put forward, providing a cargo capacity of 1.2 billion gross tons, which is 2–3 times higher than wear resistance of the operated rails. The organizing of works on laying out the rails during construction of high-speed roads is improved. At the request of English company «Network Rail» a new generation of rail welding machines such as K945, designed for welding with tension of long sections of up to 1000 m was developed at the PWI, was patented and manufactured at Kakhovka Plant of Electric Welding Equipment in 2014.

How is the quality control of rail joints organized?

The algorithms for estimation of quality of welded rails in real time were determined. Computerized system of in-process quality control of the rails joints on the basis of integrated evaluation of the influence of real deviations of welding parameters from the set optimal values was developed.

In the system of rail welding enterprises of «Ukrzaliznytsya» a unified system with the use of Internet for system control of quality of welded joints of rails on the main areas of railway communications was created, allowing processing information for 60,000 butts per year, evaluating their quality, performing rejection and providing information on the state of equipment and need in its preventive measures.

The readers are probably interested to know whether there is an experience in the application of rail welding machines, designed and manufactured in Ukraine, for welding rails in the subway?

Yes, today there is a successful experience in welding of rail tracks using the developed equipment and technology for the subway in the USA, China, Singapore, Russia and Azerbaijan, and the joining of sections is carried out directly in the tunnels.

Thank you, Professor, for the interesting and detailed information on the touched topic. We wish you a good health, many long years of successful work, every happiness and prosperity.

Editorial Board of «The Paton Welding Journal»

Dennis Shears, the Ex-President of «E.O. Paton International Holding Inc.»

Our continuous cooperation with the PWI and Prof. S.I. Kuchuk-Yatsenko is continuing since early 1990s after we had purchased first rail welding machine K355 for «Norfolk Southern Corporation».

During our first contact with the Institute the welding process and machine were little known to us.

Prof. S.I. Kuchuk-Yatsenko worked very close with us and provided a great amount of information and materials, which allowed our company to develop itself and become a main buyer of machines for flash-butt welding. Such cooperation allowed establishing the strong mutual relations with the PWI and, in particular, became the ground for our great respect to Prof. S.I. Kuchuk-Yatsenko.

Soon after concluding the contract with the PWI we found some more market variants for machines of the new designs. The first one appeared to be the new machine with upsetting force of 100 t allowing obtaining the tightness of rail not applying any additional devices. That machine was very successful and a great deal of its sales proved it. Due to such success one more machine for welding was created, including welding of closing butt directly on the track, which also gained a great popularity and was successfully replicated with many modifications.

The machines of the mentioned designs appeared due to a fruitful work of Prof. S.I. Kuchuk-Yatsenko. Today we are at the final stage of creating the machine with new design of head for welding of rail switches and frogs. In combination with new process it will allow considerable extension of market capabilities for the machines for flash-butt welding of rails.

We very appreciate our cooperation with Prof. S.I. Kuchuk-Yatsenko and the help he renders us during such a long period.

We send our best wishes to Prof. S.I. Kuchuk-Yatsenko on the day of his jubilee and hope to continue our cooperation and friendship.

FLASH BUTT WELDING OF RAILWAY FROGS THROUGH CAST AUSTENITIC INSERT

S.I. KUCHUK-YATSENKO[1], **Yu.V. SHVETS**[1], **A.V. KAVUNICHENKO**[1], **V.I. SHVETS**[1],
S.D. TARANENKO[1] and **V.A. PROSHCHENKO**[2]

[1]E.O. Paton Electric Welding Institute, NASU
11 Bozhenko Str., 03680, Kiev, Ukraine. E-mail: office@paton.kiev.ua
[2]Company «Dnepropetrovsky Strelochny Zavod»
181 Belostotsky Str., 49098, Dnepropetrovsk, Ukraine

The technology of flash butt welding of rail frogs with rail ends using an austenitic insert of rolled metal of stainless steel of type 18-10 has found a wide application. In the present paper the experiments on evaluation of possibility of using a shaped casting of steel of type 18-10 as an insert are described. It is shown that fundamental differences in the structure and properties of metal of different zones of welded joints using rolled or cast inserts are not observed. Further increase in efficiency and physical and mechanical properties of welded joints can be realized by optimizing the chemical composition and structure of the insert metal. 8 Ref., 3 Tables, 2 Figures.

In 1990 the company «Vereinigte Oesterreichische Eisen und Stahlwerke-Alpine Montan AG» (Austria) proposed a method of joining parts of switches of austenitic high-manganese steel casting with the rail of carbon steel [1], at which the austenitic insert of chrome-nickel steel of type 18-10, stabilized by niobium or titanium, is used. Moreover the content of niobium in the insert must be at least 10-fold, and that of titanium not less than 5-fold of carbon content.

In 1990 at the E.O. Paton Electric Welding Institute the technology of joining of rail frogs of high-manganese steel 110G13L with rail ends of steel M76 was developed using the method of flash butt welding with a pulsating flashing [2]. The distinctive feature of this technology is the ability to produce quality joints at the minimum energy input, providing minimization or elimination of formation of the undesired structural transformations in welds capable to reduce the ductile properties of the joints. This opened up the new possibilities for optimizing the welding technology, in particular, allowed reducing the requirements to regulation of chemical composition of the insert and eliminating power-intensive heat treatment operation.

This technology was successfully implemented at the company «Dnepropetrovsky Strelochny Zavod». During 14 years about 1,500 rail frogs with welded-in ends were welded and suc-cessfully operated. A considerable experimental material [3–7] was accumulated, which allowed improving the welding technology, specifying the requirements to the composition of steel 110G13L, in particular, as to the content of phosphorus in it, evaluating the structural and phase states in different zones of welded joint and the metal of insert. It was also established that prepa-ration of austenitic semi-products of standard rolled sheet metal of steels of type 18-10 is asso-ciated with increase in labor intensity of works and, in a number of cases, their chemical com-position did not satisfy the quality requirements of the produced joints. Thus, in some specimens of welded frogs in the area of metal of type 18-10 steel insert (free from δ-ferrite) close to the fusion boundary with the rail steel, intergranular mi-crocracks were detected having the character of hot microcracks.

Furthermore, during the test of joints for static bending the most frequent locations of frac-ture appeared to be the areas of base metal near the fusion line on the side of rail steel M76 [3]. The cracks bear longitudinal nature oriented along the axis of joint zone, and are probably associated with delayed fracture, initiated by martensitic transformation.

The aim of this work was to establish at the first stage the possibility of using cast austenitic inserts of stainless steel of type 18-10 in the joint of frogs with rail ends. In case of a positive result it is possible further to optimize the chemical and structural composition of the insert to provide high levels of mechanical properties of the joints.

Figure 1. Microstructure of chrome-nickel insert: *a* — rolled steel; *b* — cast steel 1; *c* — cast steel 2 (*a* — ×250; *b*, *c* — ×100)

Table 1. Chemical composition of inserts

Type of insert	Mass fraction of elements, %					
	C	Cr	Ni	Ti	S	P
Rolled	0.08	17.8	9.7	0.57	0.006	0.03
Cast 1	0.05	21.3	11.5	0.07	0.005	0.02
Cast 2	0.17	19.0	9.9	0.09	0.006	0.03

tallographic examinations were carried out in optical microscope «Neophot-32» and in scanning electron microscope JAMP 9500 F. After welding of specimens and grinding of joint surface it was subjected to non-destructive (capillary) testing. The mechanical tests on static bending were carried out in hydraulic press MPS-300 according to the requirements of [8].

In Table 1 the chemical composition of rolled and pilot cast inserts is shown. Figure 1 shows microstructure of metal of the inserts.

The microstructure of rolled insert optimal by its chemical composition represents a typical structure of polygonal austenite with inclusions of δ-ferrite elongated along the direction of rolling (Figure 1, *a*). The microstructure of cast insert 1 (Figure 1, *b*) is typical of the cast state. Its base is composed of primary austenite grains. Between austenite grains the ferrite grains are located, edged with more etched areas, probably caused by intergranular liquation. In microstructure of cast alloy 2 the volume fraction of ferrite is higher. The inclusions of ferrite are edged with a structural component of dark color, enriched with titanium.

In the macrostructure of welded joint (Figure 2) such typical areas are observed:
• transition zone at the interface of rail steel M76 and insert; and
• transition zone at the interface of steel 110G13L and insert.

The structural components in the transition zones of welds with cast insert are similar to those formed using the rolled insert [3–5].

The transition zone at the interface of steel 110G13L and cast insert has a stable austenitic structure. Its distinctive feature is the presence of increased content of chromium and nickel in the near-contact layer of steel 110G13L.

The works were carried out jointly with the specialists of «Dnepropetrovsky Strelochny Zavod» using the equipment for production of shaped casting of austenitic steel available at the Plant.

The chemical composition of the insert was controlled by spectral analysis. The welding of specimens was performed at basic mode [3]. Me-
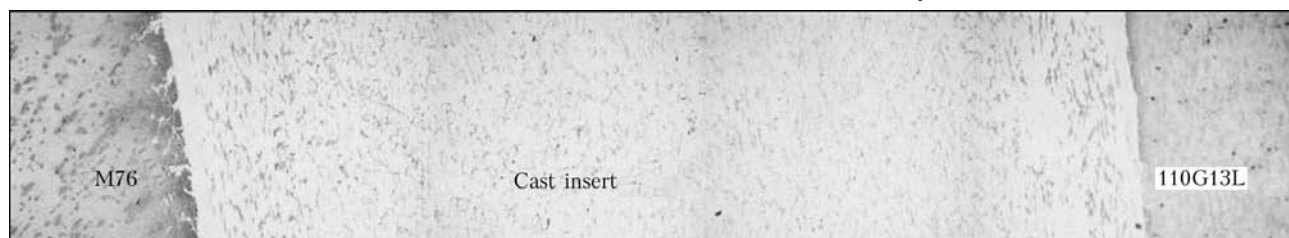

Figure 2. Macrostructure (×25) of welded joint of frog with rail ends

Table 2. Mechanical properties of parent metal of insert

Type of insert	Tensile strength, MPa	Yield strength, MPa	Elongation, %
Rolled	480−520	200−220	40−44
Cast 1	387−474	205−263	36−58

Table 3. Test results of welded specimens on static bending (profile R65)

Type of insert	Fracture force, N	Bending deflection, mm
Rolled	$\frac{940-1330}{1115}$	$\frac{16-36}{22.5}$
Cast 1	$\frac{1120-1190}{1140}$	$\frac{29-48}{38}$
Cast 2	$\frac{855-1100}{994}$	$\frac{18-29}{24}$

Near the boundary of joint of steel M76 with the cast insert (on the side of steel M76), as well as in the joint with the rolled inserts, local formation of hardening structures is possible that can reduce the ductile properties of joints in this area.

Table 2 shows the results of testing the mechanical properties of parent metal of inserts. The test results show that the insert metal meets the requirements to inserts as to yield strength (200−250 MPa) and elongation (40 %).

The test results of specimens on static bending are shown in Table 3.

One of the reasons of more stable mechanical properties of welded joints produced through the cast insert may consist in the fact that non-metallic inclusions in them have a globular shape and are relatively uniformly distributed across the section of insert, and in the rolled insert they are concentrated in strips of rolling and so during welding the probability of getting them to the butt zone is higher.

Thus, the prospects of application of cast inserts in the joints of railway frogs with rail ends in flash butt welding using pulsating flashing are experimentally confirmed. The further investigations on optimization of chemical and structural composition of the insert metal are rational in order to improve the efficiency of process and stability of mechanical properties.

1. (1991) *European application for patent 0467881A1*. Publ. Number 91890157.0.
2. Kuchuk-Yatsenko, S.I., Didkovsky, O.V., Bogorsky, M.V. et al. *Method of resistance butt welding*. Pat. 46820 Ukraine. Publ. 17.06.02.
3. Kuchuk-Yatsenko, S.I., Shvets, Yu.V., Dumchev, E.A. et al. (2005) Flash-butt welding of railway frogs with rail ends using an intermediate insert. *The Paton Welding J.*, **1**, 2−4.
4. Kuchuk-Yatsenko, S.I., Shvets, Yu.V., Gordan, G.N. et al. (2006) Features of formation of structure of joints of rail steel M76 to steel 110G13L made by flash-butt welding. *Ibid.*, **1**, 2−8.
5. Kuchuk-Yatsenko, S.I., Shvets, Yu.V., Kavunichenko, A.V. et al. (2007) Influence of the width of stainless steel insert on performance of joints of railway frogs with rail ends. *Ibid.*, **3**, 2−5.
6. Kuchuk-Yatsenko, S.I., Shvets, Yu.V., Kavunichenko, A.V. et al. (2008) Performance of flash butt welded joints on railway frogs. *Ibid.*, **9**, 30−33.
7. Kuchuk-Yatsenko, S.I., Shvets, V.L., Shvets, Yu.V. et al. (2010) Causes of crack formation in the HAZ of cast high-manganese steel in flash-butt welding. *Ibid.*, **7**, 4−7.
8. *TUU 27.3-26524137-1342:2006*: Frogs and points with welded-on rail ends of R65, R50 and UIC60 type. Valid from 10.08.2006.

INFLUENCE OF THERMODYNAMIC AND STRUCTURAL PARAMETERS OF MULTILAYER FOILS ON SHS PROCESS CHARACTERISTICS

M.V. KRAVCHUK and **A.I. USTINOV**

E.O. Paton Electric Welding Institute, NASU
11 Bozhenko Str., 03680, Kiev, Ukraine. E-mail: office@paton.kiev.ua

Characteristics of the process of self-propagating high-temperature synthesis (SHS) to foil with multilayer structure based on elements, capable of formation of intermetallic compounds, are determined by many thermodynamic and structural parameters. This significantly complicates the possibility of prediction of the features of SHS reaction running in them at the change of the foil structure and chemical composition. In the study, analysis of effectiveness of these parameters influence on SHS reaction front temperature and velocity in multilayer foil was performed within the framework of a phenomenological model. It is shown that the velocity of SHS front propagation and heat generation intensity nonmonotonically depend on structural parameters. In the case of Ni/Al multilayer foil, structural parameters were established, for which maximum values of heat generation intensity are reached in the foil in SHS process, and the method for their determination was proposed. 8 Ref., 1 Table, 11 Figures.

It is known [1–3] that under certain conditions the process of self-propagating high-temperature synthesis (SHS) with intensive heat evolution can be initiated in multilayer foils (MF) based on intermetallic-forming elements. Such MF are regarded [3] as heat sources, which can provide local heating of the joint zone, necessary for realization of the process of material joining by welding or brazing. It is shown that the velocity and temperature of SHS reaction front in MF depend on its chemical composition and structure. In practical terms, it is necessary to know MF parameters, which can ensure the maximum level of heat generation in SHS process.

As searching for optimum structure of foil with high reactivity is related to solving a multiparametral problem, it was necessary to assess the effectiveness of the influence of various MF parameters on its characteristics, including not only its microstructural characteristics, but also thermodynamic parameters such as the coefficient of element interdiffusion, diffusion activation energy and thermodynamic stimulus for intermetallic formation.

In this work, the influence of MF structural and thermodynamic characteristics on their reactivity in the mode of stationary SHS process was studied within the framework of a phenomenogical model [4–6].

Investigation procedure. It is known [4] that in the mode of stationary process of SHS front propagation in MF it is possible to correlate MF structural and thermodynamic parameters by simultaneously solving the equations of heat conductivity and diffusion between the reaction elements.

Schematically, MF structure (Figure 1) can be presented as alternation of layers of elements A and B, with multilayer period $4l(\lambda)$, which are separated by an interlayer of thickness Δy_0 of intermetallic phase forming in the foil during its production. In [4] it was shown that the velocity of SHS front propagation in the case of foil equiatomic composition can be presented as
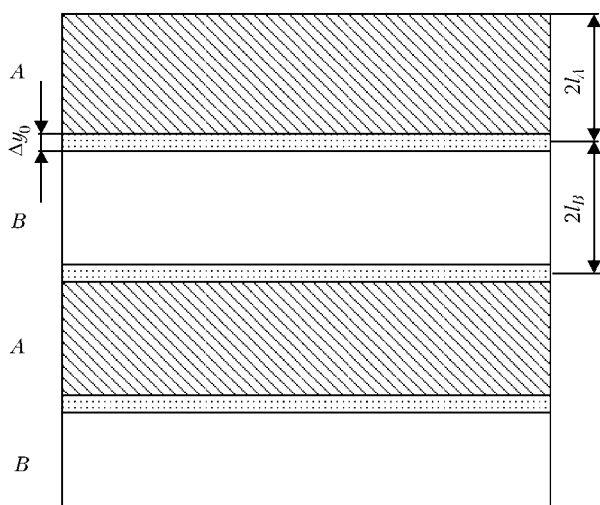

Figure 1. Schematic structure of multilayer foil

$$V = \sqrt{32.32 \, \frac{a^2 D_0 \Delta g}{(4l^2 - \Delta y_0^2)} \, \frac{T_0(kT_f + Q)}{Q^2(T_f - T_0)} \exp\left(-\frac{Q}{kT_f}\right)}, \quad (1)$$

where D_0 is the coefficient of interdiffusion; T_0 is the initial foil temperature; Q is the energy of interdiffusion activation; Δg is the thermodynamic stimulus of intermetallic phase formation; a^2 is the thermal diffusivity; k is the Boltzmann constant; T_f is the front temperature which is calculated by the following formula:

$$T_f = T_0 + \frac{\Delta g}{3k} f, \quad (2)$$

where $f = (2l - \Delta y_0)/2l$ is the foil effectiveness (volume fraction of unreacted elements). Thermodynamic stimulus Δg is the free energy of intermetallic phase formation from elements A and B.

The above equations (1) and (2) show that thermodynamic parameters are determined by elements, which are the basis for multilayer structure formation, and structural parameters are determined by foil preparation conditions. If all the parameters included into equations (1) and (2) have been determined, it is possible to calculate foil reactivity characteristics in the mode of SHS stationary propagation.

For real systems part of these parameters are not determined, and some of them depend on foil preparation conditions and they can change within certain limits. While, for instance, MF multilayer period is determined with sufficient accuracy by studying its cross-sectional microstructure, intermediate layer thickness determination by direct microstructural studies is difficult, as by theoretical estimates it can be equal to several nanometers. However, if two foils are manufactured on the basis of one A/B system under similar conditions with different multilayer periods λ_1 and λ_2 (provided $\lambda_1 > \lambda_2$), then, having determined for such foils SHS front temperatures T_{f_1} and T_{f_2}, it is possible to apply equation (2), solving it for parameter Δy_0:

$$\Delta y_0 = \frac{\lambda_1 \lambda_2 (T_{f_1} - T_{f_2})}{2[(T_{f_1} - T_0)\lambda_1 - (T_{f_2} - T_0)\lambda_2]}. \quad (3)$$

On the other hand, considering that structural and thermodynamic parameters can have an estimated value, it is important to determine the effectiveness of the influence of each of these parameters on foil reactivity. This enables not only forecasting its characteristics, depending on thermodynamic and structural parameters, but also assessing their «sensitivity» to the accuracy of these parameters determination.

Results and their discussion. To determine these values, the influence of thermodynamic and structural parameters was studied in the case of multilayer Ni/Al foil of equiatomic composition. The same values of thermodynamic parameters of Ni/Al system were taken as in [4]: $D_0 = 1.5\cdot10^{-5}$ m^2/s, $Q = 2.7\cdot10^{-19}$ J, $a^2 = 7.42\cdot10^{-5}$ m^2/s, $T_0 = 300$ K, $\Delta g = 7.36549\cdot10^{-20}$ J.

In [4] it is shown that there exists a linear dependence of SHS reaction front temperature on foil effectiveness coefficient at different values of initial interlayer thickness. Let us consider the influence of thermodynamic parameters on SHS front temperature and its propagation velocity. With this purpose, SHS front temperature was calculated from equation (2), depending on thermodynamic stimulus at different structural parameters of the foil. It is seen (Figure 2) that SHS front temperature grows linearly at increase of thermodynamic stimulus, irrespective of foil structure. However, the level of SHS front temperature is essential influenced by foil structural characteristics. So, for instance, at $\Delta g = 7.36549\cdot10^{-20}$ J, SHS front temperature varies in the range from 1400 up to 2000 K at increase of multilayer period from 50 up to 300 nm and reduction of interlayer thickness from 8 to 4 nm. In this connection, dependencies of front temperature on interlayer thickness Δy_0 and multilayer period λ at constant value of thermodynamic stimulus were calculated. It is seen (Figure 3) that for any multilayer period SHS front temperature drops at increase of interlayer thickness. Reduction of multilayer period also leads to lowering of SHS front temperature, and the stronger, the larger the intermediate layer thickness (Figure 4).
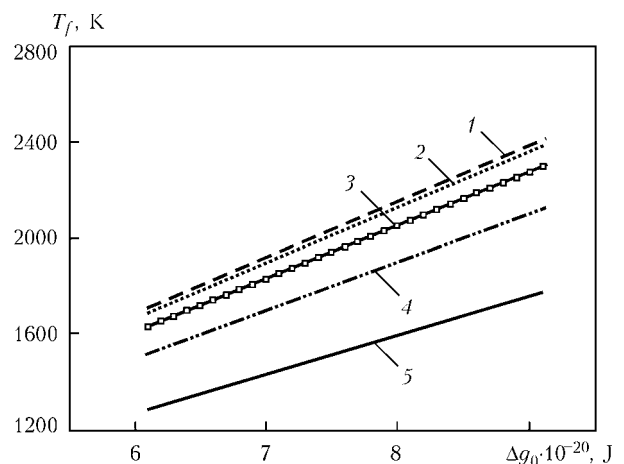
**Figure 2.** Dependence of SHS front temperature on thermodynamic stimulus: *1* — $\lambda = 300$ nm, $\Delta y_0 = 4$ nm; *2* — $\lambda = 50$ nm, $\Delta y_0 = 1$ nm, *3* — $\lambda = 100$ nm, $\Delta y_0 = 4$ nm; *4* — $\lambda = 50$ nm, $\Delta y_0 = 4$ nm; *5* — $\lambda = 50$ nm, $\Delta y_0 = 8$ nm
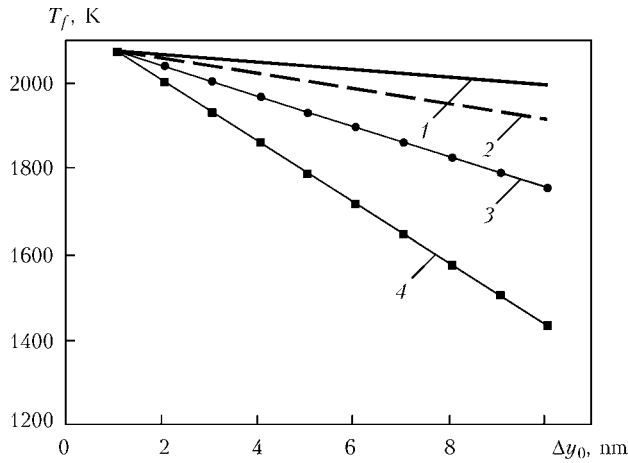
Figure 3. Dependence of SHS front temperature on inter-layer thickness Δy_0 for Ni/Al foil with different multilayer periods: *1* — λ = 400; *2* — 200; *3* — 100; *4* — 50 nm

Thus, the conducted analysis showed that SHS front temperature depends both on thermodynamic stimulus, and on foil structural characteristics. In order to generalize such an interdependence, SHS front temperature dependencies on Δgf value (furtheron referred to as thermodynamic coefficient of effectiveness of foil) were calculated. They are determined both by physical nature of elements forming the foil laminated structure, and by its structural characteristics. It is found that (Figure 5) dependence of SHS front temperature on thermodynamic coefficient of effectiveness is linear and invariant to structural characteristics.

As Δg value is determined by the nature of elements forming the multilayer structure, increasing the thermodynamic coefficient of foil effectiveness requires increasing the volume fraction of elements, which did not enter into the reaction during foil preparation. According to (2), this can be achieved through reducing the interlayer thickness and increasing the multilayer period.
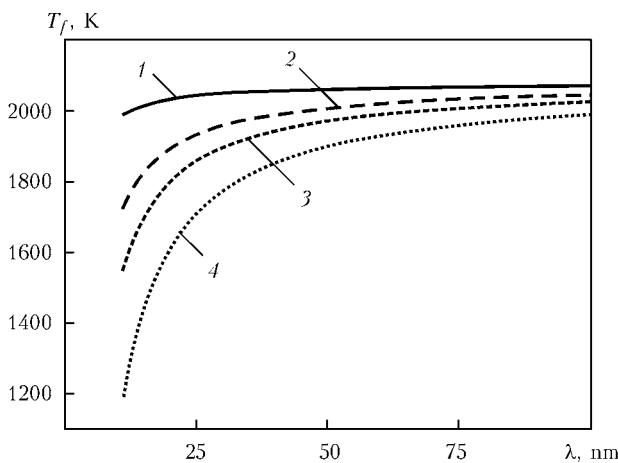
Figure 4. Dependence of SHS front temperature on multilayer period for Ni/Al foil with different interlayer thicknesses: *1* — Δy_0 = 1; *2* — 4; *3* — 6; *4* — 10 nm
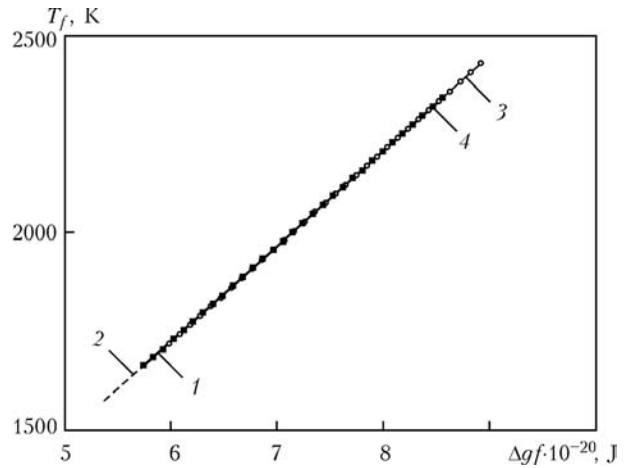
Figure 5. Dependence of combustion front temperature on thermodynamic coefficient of effectiveness of Ni/Al foil: *1* — λ = 50 nm, Δy_0 = 1 nm; *2* — λ = 50 nm, Δy_0 = 3 nm; *3* — λ = 100 nm, Δy_0 = 1 nm, *4* — λ = 100 nm, Δy_0 = 3 nm

On the other hand, at practical application of MF as a local heat source, not only SHS front temperature, but also its propagation velocity will determine foil effectiveness for local heating of the joint zone during reaction welding or brazing. At a low velocity of SHS front propagation, heat removal into the joint zone will decrease the foil capacity for local heating of this zone. Negative influence of this process can be reduced through increase of SHS front propagation velocity.

According to (1) thermodynamic stimulus is one of the parameters affecting the velocity of SHS front propagation. As is seen from Figure 6, the velocity of SHS front propagation is different from zero only in the case, when its magnitude is higher than a certain critical value, otherwise SHS reaction will not take place. It can be assumed that in systems, in which the thermodynamic stimulus is below a certain critical value,
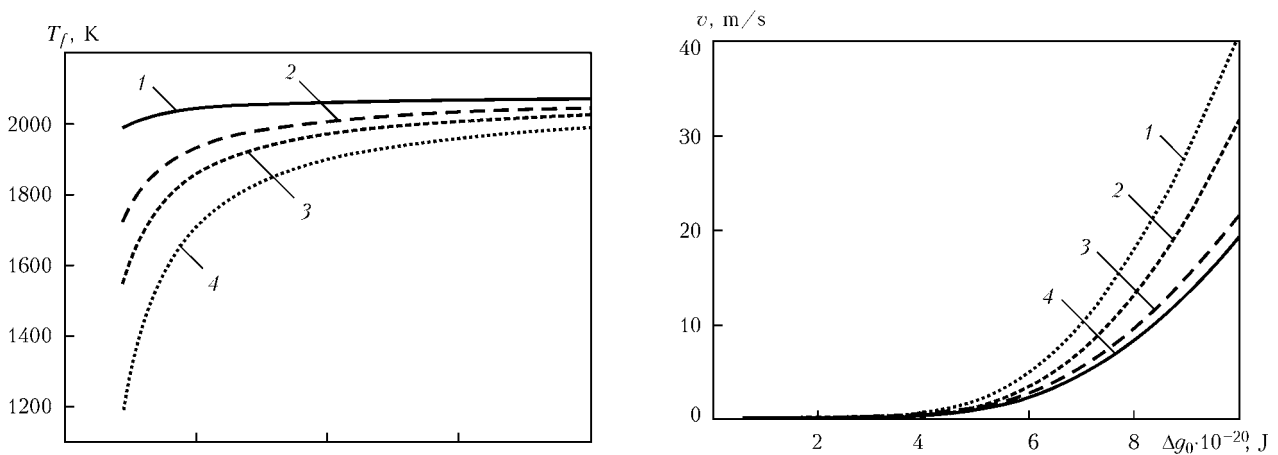
Figure 6. Dependence of reaction rate on thermodynamic stimulus for Ni/Al foil: *1* — λ = 50 nm, Δy_0 = 1 nm; *2* — λ = 50 nm, Δy_0 = 3 nm; *3* — λ = 100 nm, Δy_0 = 1 nm; *4* — λ = 100 nm, Δy_0 = 3 nm
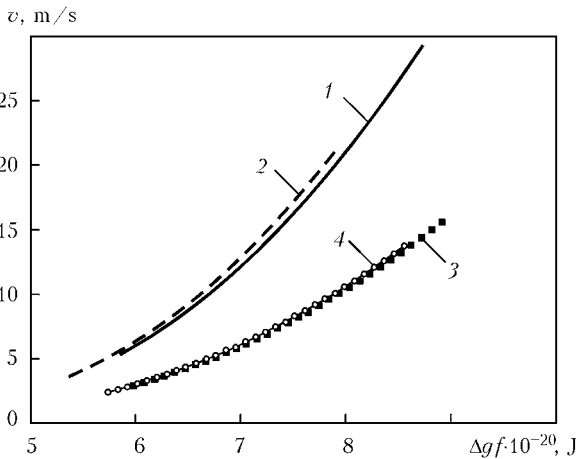
Figure 7. Dependence of reaction rate on thermodynamic coefficient of Ni/Al foil effectiveness: *1* — λ = 50 nm, Δy_0 = 1 nm; *2* — λ = 50 nm, Δy_0 = 3 nm; *3* — λ = 100 nm, Δy_0 = 1 nm; *4* — λ = 100 nm, Δy_0 = 3 nm
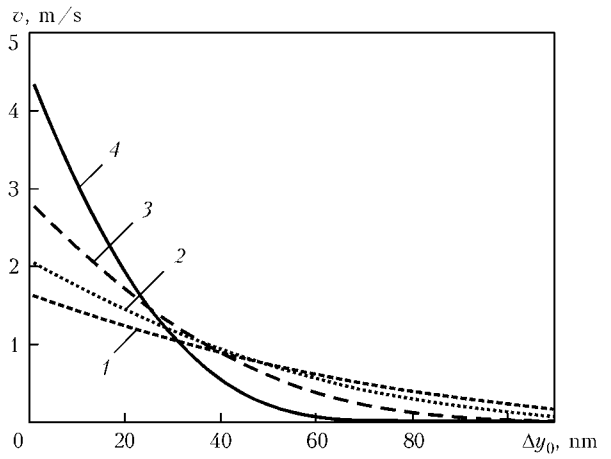
it does not seem possible to realize the SHS reaction.

If thermodynamic stimulus is greater than this critical value, then at increase of thermodynamic coefficient of foil effectiveness the velocity of SHS front propagation will rise parabolically. The rate of this increase depends on foil structural characteristics: the smaller the multilayer period and the thinner the intermediate layer, the greater the intensity of SHS propagation velocity rise at increase of thermodynamic stimulus.

As seen from Figure 7, however, dependence of SHS front propagation velocity on thermodynamic coefficient of effectiveness is almost independent on interlayer thickness, and is determined just by multilayer period.

When the influence of foil microstructure parameters was studied (at unchanged value of thermodynamic parameters), it turned out (Figure 8) that for 3—4 nm thickness of interlayer inversion of the dependence of SHS front propagation velocity on multilayer period takes place — at smaller values of interlayer thickness front propagation velocity rises significantly at reduction of multilayer period, and at larger values it decreases.

Non-monotonic dependence of front propagation velocity is observed also at the change of multilayer period (Figure 9). It is seen that at reduction of multilayer period, SHS reaction front velocity rises, but, having reached a certain critical value, it decreases.

Thus, performed calculations show that to ensure the maximum velocity of SHS front propagation, the multilayer period should be determined allowing for interlayer thickness. Considering that this parameter has a specific value, which is determined by foil preparation condi-

Figure 8. Dependence of reaction rate on interlayer thickness: *1* — λ = 480; *2* — 380; *3* — 280; *4* — 180 nm

tions, SHS front propagation velocity can be varied by changing the multilayer period.

To determine the range of parameter values of MF microstructure, at which it will be capable of intensive heating of the joint zone, let us define heat generation intensity (HGI) W in foil section of thickness d (cm), length l = 1 cm and width m = 1 cm at passage of SHS reaction front through it as

$$W = \frac{Q}{S\tau}, \qquad (4)$$

where Q is the quantity of heat evolving in a foil region, which can be determined from $Q = C(T_f - T_0)d\rho S$ relationship (here C is the heat capacity of foil; ρ is the foil specific weight; S is the foil region area); τ is the time of front passage through foil region, which is determined as $\tau = l/v$. After substitution into (4) of values, included in the expressions, we will obtain

$$W = \frac{C(T_f - T_0)d\rho v}{l} \qquad (5)$$

or allowing for (2)
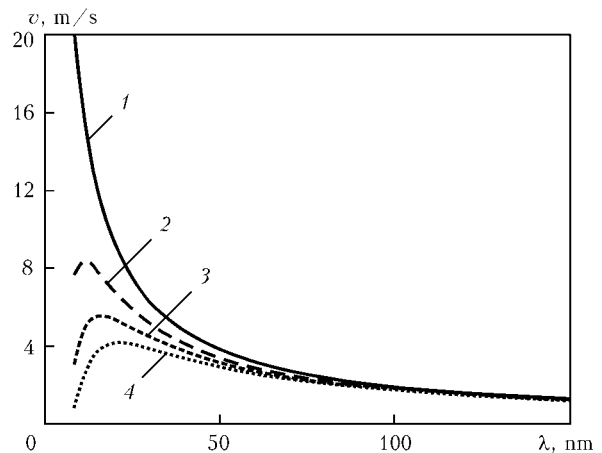
Figure 9. Dependence of combustion front propagation velocity on multilayer period: *1* — Δy_0 = 1; *2* — 4; *3* — 6; *4* — 8 nm

tal point with one of the curves in Figure 10
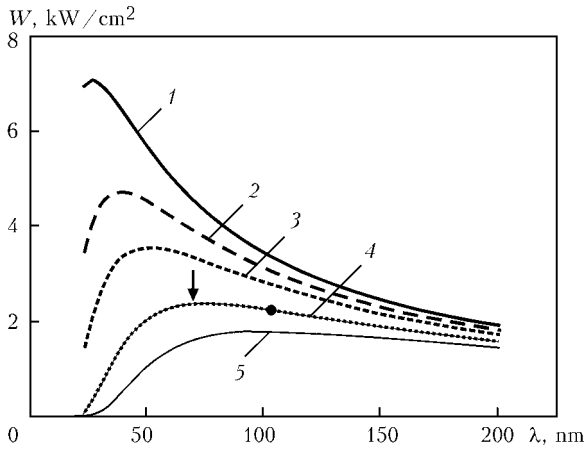
Figure 10. Dependence of HGI value during SHS reaction propagation in 26 μm Ni/AL foil on multilayer period at different interlayer thicknesses: $1 - \Delta y_0 = 2$; $2 - 3$; $3 - 4$; $4 - 6$; $5 - 8$ nm

Figure 11. Dependence of multilayer optimal period λ_{opt} on interlayer thickness Δy_0 in Ni/Al foil

$$W = \frac{Cd\rho}{3lk} \Delta g f v. \qquad (6)$$

It is seen from expression (6) that HGI value rises with increase of the coefficient of foil effectiveness f and SHS front propagation velocity v. Considering, however, that the velocity of front propagation shows a non-monotonic dependence on structural parameters, it is anticipated that HGI dependence on these parameters will also be non-monotonic.

Indeed, as is seen from Figure 10, HGI value at reduction of multilayer period first rises, and then, having reached a certain value, starts decreasing, irrespective of interlayer thickness. Comparing W dependencies on multilayer period λ, calculated at different values of interlayer thickness Δy_0, one can see that the maximum HGI value is the greater, the thinner the interlayer Δy_0.

Note the fact that the maximum position also depends on interlayer thickness: the thinner the interlayer, the smaller the multilayer period, at which maximum HGI value is reached.

It follows from the obtained results that if the thickness of interlayer formed under certain conditions of MF deposition, is known, then having plotted preliminary dependencies of W on multilayer period λ for different values of interlayer thickness, it is possible to find λ_{opt}, at which maximum HGI will be achieved.

Let us consider the possibility of λ_{opt} determination based on experimental study of MF with different multilayer periods, produced under similar conditions. For this purpose, two foils with different multilayer periods were produced (under similar conditions) by the process of layer-by-layer EB PVD [7] of nickel and aluminium. Foil characteristics and their deposition conditions are given in the Table, where d is the foil thickness; T_{substr} is the substrate temperature; v_{dep} is the deposition rate.

Measurement of SHS front temperature T_f and its propagation velocity v_f was performed by the method presented in [8].

Interlayer thickness was calculated from equation (3). It was equal to a value of the order of $\Delta y_0 = 6.5$ nm. Proceeding from calculated dependence of λ_{opt} on interlayer thickness Δy_0, given in Figure 11, one can see that under the given conditions of MF production, when $\Delta y_0 = 6.5$ nm, maximum HGI values can be equal to 2.3 kW/cm^2 under the condition that multilayer period $\lambda = \lambda_{opt}$ ($\lambda_{opt} \approx 72-80$ nm).

Condition for producing foil with maximum HGI can be also determined, if we use equation (5) to calculate HGI for foil with the smallest multilayer period (foil 1), and plot this value on the graph of W dependence on multilayer period λ (see Figure 10). One can see that the thus obtained experimental point can be correlated with one of W dependencies on multilayer period λ, earlier calculated for MF with different interlayer thicknesses. Coincidence of the experimental point with one of the curves in Figure 10

Foil characteristics and deposition conditions

Foil numder	d, μm	T_{substr}, °C	v_{dep}, μm/min	λ, nm	T_f, °C	v_f, m/s	W, kW/cm^2
1	25	220 ± 10	1.9	104	1160	1.23	2.21
2	30	225 ± 10	1.9	520	1290	0.49	0.70

allows determination of both the interlayer thickness, and W maximum position, which corresponds to multilayer period of 72−80 nm. Comparison of obtained λ_{opt} values determined by various methods shows their satisfactory agreement.

One can see from theoretical analysis and experimental assessment of multilayer optimum period that factors promoting increase of interlayer thickness lead to increase of multilayer optimum period and lowering of HGI value.

Conclusions

1. Within the phenomenological model of stationary propagation of SHS reaction front in multilayer structure based on reaction elements of equiatomic composition, a procedure was proposed for determination of thickness of the interlayer, which forms in the foil during its production, by determination of SHS front temperature in two multilayer foils with different multilayer periods, produced under the same conditions.

2. It is shown that SHS front temperature becomes essentially dependent on interlayer thickness for multilayer structures with multilayer period less than 50 nm.

3. It was confirmed that the temperature of SHS propagation front in the stationary mode is linearly dependent on thermodynamic coefficient of foil effectiveness.

4. It is shown that propagation of SHS front in the stationary mode is possible, if the thermodynamic coefficient of foil effectiveness exceeds a certain critical value, above which the velocity of SHS front propagation rises parabolically.

5. It is established that the maximum HGI level at SHS front propagation in multilayer foil is determined by interlayer thickness and multilayer period. At increase of interlayer thickness, multilayer period should be increased to provide maximum HGI.

1. (2003) *Concept of SHS development as a field of scientific-technical progress*. Ed. by A.G. Merzhanov. Chernogolovka: Territoriya.
2. Ustinov, A.I., Falchenko, Yu.V., Ishchenko, A.Ya. et al. (2008) Diffusion welding of TiAl alloys through nano-layered foil of Ti/Al system. *Intermetallic*, **16**, 1043−1045.
3. Rogachev, A.S., Grigoryan, A.E., Illarionova, E.V. et al. (2004) Gas-free burning of multilayer Ti/Al bimetallic nanofilms. *Fizika Goreniya i Vzryva*, 40(**2**), 45−51.
4. Zaporozhets, T.V., Gusak, A.M., Ustinov, A.I. (2010) Modeling of stationary mode of SHS reaction in nanolayered materials (phenomenological model). Pt 1: One-stage reaction. *Sovrem. Elektrometallurgiya*, **1**, 40−46.
5. Zaporozhets, T.V., Gusak, A.M., Ustinov, A.I. (2010) SHS reactions in nanosized multilayers — Analytic model versus numeric model. *Int. J. Self Propagating High Temperature Synthesis*, 19(**4**), 227−236.
6. Zaporozhets, T.V. (2010) Modeling of stationary mode of SHS reaction propagation in nano-layered materials (phenomenological model). Pt 2: Two-stage reaction. *Visnyk CherkGU*, **185**, 16−30.
7. Ustinov, A.I., Olikhovska, L.A., Melnichenko, T.V. et al. (2008) Effect of overall composition on thermally induced solid state transformations in thick EB PVD Al/Ni multilayers. *Surface and Coatings Techn.*, 202(**16**), 3832−3838.
8. Zaporozhets, T.V., Gusak, A.M., Korol, Ya.D. et al. (2013) Inverse problem for SHS in multilayer nanofoils: Prediction of process parameters for single-stage SHS reaction. *Int. J. Self Propagating High Temperature Synthesis*, 22(**4**), 217−225.

STRUCTURE AND PROPERTIES
OF EB- AND TIG-WELDED JOINTS
OF HIGH-STRENGTH TWO-PHASE TITANIUM ALLOYS

S.V. AKHONIN, V.Yu. BELOUS, R.V. SELIN, I.K. PETRICHENKO and **E.L. VRZHIZHEVSKY**

E.O. Paton Electric Welding Institute, NASU
11 Bozhenko Str., 03680, Kiev, Ukraine. E-mail: office@paton.kiev.ua

Modern two-phase high-alloyed alloys based on titanium are characterized by a high specific strength. The thermal cycle of welding results in change of structures of weld and HAZ metal and also in deterioration of mechanical characteristics of the joint. In the work the properties of welded joints of titanium alloys VT23, T110 and high-alloyed alloy Ti−6.5Al−3Mo−2.5V−4Nb−1Cr−1Fe−2.5Zr, produced using electron beam and argon arc welding, were evaluated. In weld and HAZ metal of the TIG-welded joints of alloy Ti−6.5Al−3Mo−2.5V−4Nb−1Cr−1Fe−2.5Zr, the structure is formed with a predominance of metastable β-phase and low values of strength and impact toughness, the joints require postweld high-temperature annealing at temperature of not less than 900 °C. The joints of VT23 alloy have high values of strength and impact toughness. High-strength titanium alloy T110 is characterized by good weldability in EBW and TIG welding, has high values of impact toughness of weld metal and HAZ after annealing, the strength of welded joints is at the level of 0.9 of base metal strength. 7 Ref., 2 Tables, 4 Figures.

Modern two-phase high-alloyed alloys based on titanium are characterized by a high specific strength, nowadays the growing attention is paid to widening the use of welded structures and assemblies of high-strength titanium alloys ($\sigma_t > 1100$ MPa) [1, 2]. The weldability of two-phase high-alloyed titanium alloys, the use of which may provide the greatest reduction in mass of the structure, is significantly worse than that of low-alloyed alloys, and according to this indicator they are inferior even to some high-strength steels, therefore, when developing new titanium alloys, a significant attention is paid to the possibility of producing welded joints with strength of not less than 0.90−0.95 of base material strength.

The aim of the work is to evaluate the properties of welded joints of both industrial and also new two-phase high-titanium alloys having $\sigma_t > 1000$ MPa (Table 1), developed at the E.O.

Paton Electric Welding Institute, as well as to study the influence of thermal cycle of welding and postweld heat treatment on structural and phase transformations in weld metal and HAZ.

In the course of investigations the properties of welded joints, produced by electron beam welding (EBW) and argon arc welding with tungsten electrode (TIG) without using filler metal were compared.

The joints of high-strength titanium alloy VT23 [3] were made of 10 mm thick plates, joints of titanium alloy of grade T110 were made of 7 mm thick plates. The high-grade alloy of T110 system Ti−5.5Al−1.2Mo−1.2V−4Nb−2Fe−0.5Zr was developed at the PWI together with the O.K. Antonov ASTC [4]. It contains the following alloying elements, wt.%: 5−6 Al, 3.5−4.8 Nb, 0.8−1.8 Mo, 0.8−2 V, 1.5−2.5 Fe, 0.3−0.8 Zr. Alloy T110, as compared to VT23, has a higher resistance to the formation of fatigue cracks and according to the number of service characteristics, such as fatigue life of base metal (BM), exceeds the values of VT23 alloy by 15−20 % [5].

Table 1. Mechanical properties of high-strength two-phase titanium alloys

Grade of alloy	Equivalent of molybdenum	Thickness of metal, mm	σ_t, MPa	$\sigma_{0.2}$, MPa	δ, %	KCV, J/cm^2
VT23	5.7−8.0	10	1030	980	13	35
T110	4.4−7.9	7	1190	1150	18	31
Ti−6.5Al−3Mo−2.5V−4Nb−1Cr−1Fe−2.5Zr	5.6−10.5	8	1195	1110	15	13

Also the properties of welded joints of pilot high-alloyed alloy of 8-component system Ti–6.5Al–3Mo–2.5V–4Nb–1Cr–1Fe–2.5Zr were evaluated. It contains more alloying elements as compared to alloy T110 and in the state after annealing it has tensile strength exceeding 1200 MPa. The joints of this alloy of 8 mm thickness were produced using EBW and TIG method.

TIG was performed on both sides using tungsten electrode of 5 mm diameter in argon without filler metal. The welding current was 300–350 A, welding speed — 10 m/h. EBW was conducted in installation UL-144, completed with power source ELA 60/60. The accelerating voltage was 60 kV, welding speed 25 m/h. The examples of produced welded joints are shown in Figure 1.

Immediately after welding VT23 weld metal produced using TIG welding represents the coarse primary β-grains, the intragranular structure of weld metal is characterized by martensite α″-phase [2]. In order to improve the ductile characteristics of VT23 welded joints the simplest way is postweld heat treatment — annealing [6]. After heat treatment the structure is characterized by presence of fine-dispersed decay products of metastable phases with formation of equilibrium α- and β-phases, however, the strength of welded joint after annealing decreases to level lower than 1000 MPa.

The metal of T110 welds, produced using EBW, consists of β-grains equiaxial and elongated in the direction of heat dissipation (Figure 2, a), inside which uniform decay of solid solution with precipitation of dispersed particles of martensitic α′-phase is observed [7]. In the near-weld area the grain of primary β-phase is finer.

The microstructure of TIG-welded joints of alloy T110 is not essentially differed from the microstructure of the joints made by EBW. The metal of welds and near-weld areas of joints produced using TIG method has a structure of β-transformed grain with precipitation of fine acicular martensite α′-phase. In the areas of HAZ metal adjacent to BM, except of the mentioned structural elements inside the grains, a primary coarse lamellar α-phase is observed. The joints made by TIG welding have also an identical structure. The joints made by EBW have a considerably smaller structurally modified fusion zone and HAZ as compared to the joints made using tungsten electrode. The strength of welds, produced using TIG method and EBW, is at the same level. For the joints in EBW, a typical place for fracture of rupture specimens is BM, and for TIG welding is weld. After welding, EB-
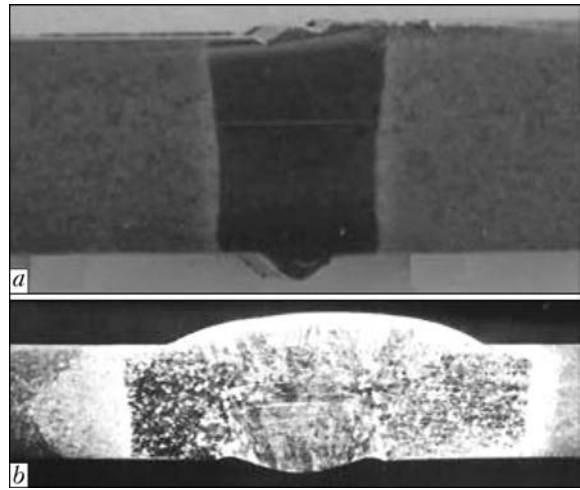
Figure 1. Transverse macrosection of EB- (*a*) and TIG-welded (*b*) joint of titanium alloy Ti–6.5Al–3Mo–2.5V–4Nb–1Cr–1Fe–2.5Zr of 8 mm thickness

welded joints have a strength equal or higher than that of BM, and the strength of TIG-welded joints is at the level of 0.9 % of the strength of alloy itself; annealing at 750 °C with subsequent furnace cooling results in a further decrease in strength of welded joints, but the values of impact toughness are increased to 30 J/cm^2 for the joints made by arc welding. In order to increase the impact toughness of joints made by EBW it is necessary to apply a higher-temperature annealing — at 850 °C. After this annealing the decay of metastable phases occurs with the predominance of lamellar α-phase (Figure 2, b), the
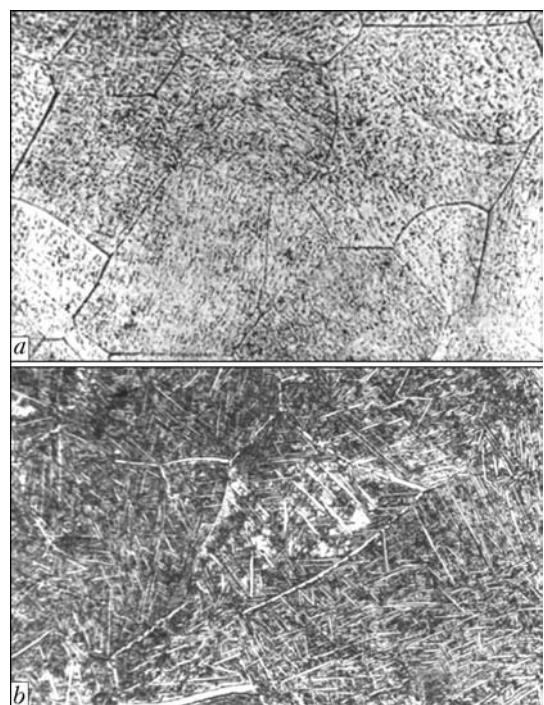
Figure 2. Microstructure (×400) of weld metal of EB-welded joint of titanium alloy T110: *a* — after welding; *b* — after annealing at 750 °C for 1 h
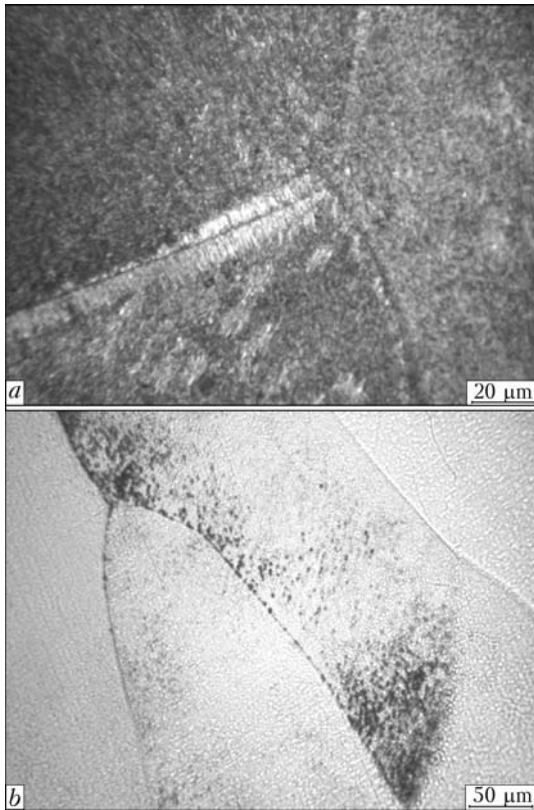
Figure 3. Microstructure of weld metal of titanium alloy Ti−6.5Al−3Mo−2.5V−4Nb−1Cr−1Fe−2.5Zr produced by EBW: *a* − BM; *b* − weld metal after welding

Figure 4. Microstructure of weld metal of alloy Ti−6.5Al−3Mo−2.5V−4Nb−1Cr−1Fe−2.5Zr produced by EBW after LHT (*a*) and annealing at 900 °C (*b*)

parameters of which contribute to increase of toughness at a high level of strength.

High-alloyed alloy Ti−6.5Al−3Mo−2.5V−4Nb−1Cr−1Fe−2.5Zr has stabilization factor of β-phase in the range of 0.96−1.07, and also, the same as the alloys considered above, is subjected to hardening as a result of influence of thermal cycle of welding.

After EBW in the weld metal and HAZ of alloy Ti−6.5Al−3Mo−2.5V−4Nb−1Cr−1Fe−2.5Zr the metastable β-phase (Figure 3, *a*) is observed with equiaxial grains, elongated in the direction of heat dissipation. Furthermore, both along the boundaries of β-grains and in the volume of grain the local accumulations of metastable α-phase are observed in form of very dispersed spot precipitates. To relieve the welding stresses and stabilize the structure of joint after EBW both annealing, as well as local electron beam heat treatment (LHT) was performed, which consisted in postweld heating of the welded joint zone by electron beam, temperature of heating zone was maintained at level of 850 °C during 5 min. The annealing at 800 °C with a delayed cooling resulted in decay of metastable α- and β-phases, observed in welding, with the formation of dispersed α- and β-particles, the values of impact toughness at that grow negligibly.

The study of mechanical properties of EB-welded joints of alloy Ti−6.5Al−3Mo−2.5V−4Nb−1Cr−1Fe−2.5Zr with the postweld LHT (Table 2) showed somewhat higher values of strength (σ_t = 1258 MPa) and lower values of impact toughness of weld metal (KCV = = 7 J/cm^2), as compared to the corresponding values for welded joints in the state after furnace annealing at 900 °C during 1 h. Evidently, this is explained by the partial decay of metastable structures in the weld metal as a result of effect of short-time LHT during 5 min and formation of fine acicular α-phase as a result.

The weld metal of alloy Ti−6.5Al−3Mo−2.5V−4Nb−1Cr−1Fe−2.5Zr after TIG welding in the as-welded state is also composed of grains, equiaxial and elongated in the direction of heat dissipation of metastable β-phase (Figure 3, *b*), observed at rapid cooling after welding. In the volume of β-grains and at their boundaries a small amount of dispersed precipitates of metastable α-phase is observed. As a result of thermal cycle of welding the metastable structures were formed in the weld with predomination of β-phase content. The precipitation of dispersed particles of metastable α-phase is observed along the boundaries of grains and subgrains, and is also observed in the body of grain both in weld as well as in HAZ metal. The metastable β-phase has a low

Table 2. Mechanical properties of welded joints of titanium alloys

Grade of alloy (welding method)	Thickness of metal, mm	State of joints	σ_t, MPa	Impact toughness KCV, J/cm^2	
				Weld metal	HAZ
VT23 (TIG)	10	As-welded	1030	27	23
VT23 (TIG)	10	Annealing at 750 °C, 1 h, air	970	30	28
T110 (EBW)	7	As-welded	1140	10	10
T110 (EBW)	7	Annealing at 750 °C, 1 h, air	1160	12	23
T110 (EBW)	7	Annealing at 850 °C, 1 h, air	1120	21	26
T110 (TIG)	7	As-welded	1118	11	10
T110 (TIG)	7	Annealing at 750 °C, 1 h, air	1078	29	30
Ti−6.5Al−3Mo−2.5V−4Nb−1Cr−1Fe−2.5Zr (TIG)	8	As-welded	960	5	5
Ti−6.5Al−3Mo−2.5V−4Nb−1Cr−1Fe−2.5Zr (EBW)	8	As-welded	1248	7	6
Ti−6.5Al−3Mo−2.5V−4Nb−1Cr−1Fe−2.5Zr (EBW)	8	LHT at 850 °C, 5 min	1258	7	14
Ti−6.5Al−3Mo−2.5V−4Nb−1Cr−1Fe−2.5Zr (EBW)	8	Annealing at 900 °C, 1 h, air	1131	12	13

strength, therefore, TIG-welded joints have low values of strength in as-welded state, moreover, due to the presence of a significant volume fraction of metastable α-phase, the weld and HAZ metal have also a low impact toughness (Table 2).

Thus, it is reasonable to carry out TIG welding of high-alloyed titanium alloy Ti−6.5Al−3Mo−2.5V−4Nb−1Cr−1Fe−2.5Zr with the use of filler materials that will reduce the degree of alloying of weld metal and provide higher values of strength, ductility and impact toughness.

Conclusions

1. High-strength titanium alloy VT23 is characterized by a good weldability, in as-welded state the metastable β- and α″-phases are present in the weld metal and HAZ, and though the values of impact toughness of weld metal are rather high ($KCV = 29$ J/cm^2 at $\sigma_t = 1128$ MPa), welded joints require the postweld heat treatment to stabilize their structure.

2. High-strength titanium alloy T110 is characterized by a good weldability in producing EB- and TIG-welded joints by through penetration, and after annealing it has high values of impact toughness of the weld metal and HAZ, and strength of welded joints is at level of 0.9 of the base metal strength.

3. The TIG-welded joints of high-alloyed titanium alloy Ti−6.5Al−3Mo−2.5V−4Nb−1Cr−1Fe−2.5Zr have low values of impact toughness in the weld and HAZ, where the structure is formed with a predominance of metastable β-phase, and welded joints require high temperature of postweld annealing at 900 °C, at which the impact toughness is twice increased.

4. The EB-welded joints of high-alloyed titanium alloy Ti−6.5Al−3Mo−2.5V−4Nb−1Cr−1Fe−2.5Zr with the highest ductility and impact toughness ($KCV = 12.4$ J/cm^2, $\delta_s = 12$ %) were produced after applying annealing at 900 °C during 1 h, with the subsequent cooling in furnace.

1. Kablov, E.N. (2012) Strategic trends in development of materials and technologies of their recycling for period up to 2030. *Aviats. Materialy i Tekhnologii*, **8**, 7−17.
2. Khorev, A.I. (2007) Theory and practice of development of titanium alloys for advanced structures. *Tekhnologiya Mashinostroeniya*, **12**, 5−13.
3. Khorev, A.I. (2008) High-strength titanium alloy VT 23 and its application in advanced welded structures. *Svarochn. Proizvodstvo*, **9**, 3−8.
4. Zamkov, V.M., Topolsky, V.P., Trygub, M.P. *High-strength titanium alloy*. Pat. 40087 Ukraine. Publ. 16.06.2003.
5. Antonyuk, S.L., Korol, V.N., Molyar, A.G. et al. (2003) Investigation of mechanical properties of forged semi-products of experimental titanium alloy T110. *Advances in Electrometallurgy*, **3**, 27−30.
6. Khorev, A.I., Joda, A.V., Krasnozhan, A.I. (1981) Mechanical properties and structure of EB-welded joints of VT23 titanium alloy. *Svarochn. Proizvodstvo*, **7**, 25−26.
7. Zamkov, V.N., Topolsky, V.F., Trofimov, V.A. et al. (2005) Hardening heat treatment, mechanical characteristics and structure of T110 high-strength titanium alloy to be weld. In: *Titanium-2005 in CIS*, 198−208.

STATE-OF-THE-ART
OF HYBRID LASER-PLASMA WELDING (Review)

A.I. BUSHMA

E.O. Paton Electric Welding Institute, NASU
11 Bozhenko Str., 03680, Kiev, Ukraine. E-mail: office@paton.kiev.ua

The paper presents brief retrospective of progress and state-of-the-art of hybrid laser-plasma welding. It is shown that the main objectives of HLPW include not only plasma-arc heating of item metal to increase its absorptivity, but also modification of welding thermal cycle to lower the rate of cooling after welding. This allows lowering the content of brittle structures prone to fracture in service. Moreover, presence of plasma-arc component of the process allows lowering the requirements to quality of fit-up of the butts to be welded, compared to laser welding. Prospects for introduction of HLPW into industry are related to its cost and technological advantages. Cost advantages consist in partial (up to 50 %) replacement of quite expensive laser power by much less expensive arc power, as well as reduction of process power input due to the possibility of filler wire replacement by the respective powder or complete elimination of filler material. Technological advantages consist in reduction of residual thermal deformations, lowering of requirements to preparation of edges to be welded (including the possibility of welding edges with a variable gap), obtaining the ability of cathode cleaning of aluminium alloys directly during welding, increase of penetration depth and process efficiency (several times compared to plasma welding and by approximately 40 % compared to laser welding). Introduction of laser-plasma welding can change the current ideas of technologists about the welding process and those of designers about welded structure design. Industrial application of laser-plasma technology is, primarily, associated with solving the problems of joining titanium and aluminium alloys, as well as stainless steels in the range of thicknesses of 0.3–15 mm. 50 Ref., 12 Figures.

Hybrid welding is a process which uses two heat sources, acting simultaneously on the item being welded (within a common heating zone). The main feature of this welding process is complementation and enhancement of the impact of each of the applied sources. In the case of hybrid laser-plasma welding (HLPW), the maximum impact is achieved at manifestation of the so-called synergic effect [1]. This effect consists in non-additivity of the results of impact of each of the heat sources, compared to the result of their joint action. In particular, the volume of metal, molten in hybrid welding, as a rule, exceeds the sum of metal volumes molten separately by each of the energy sources, making up the hybrid process. Otherwise, welding is usually regarded as combined, and not hybrid.

A paper published in 1979 on combining non-consumable electrode (TIG) arc with laser welding is taken to be one of the first works on hybrid welding [2]. A more detailed work by Prof. Steen (Great Britain) was published immediately after it in 1980 [3]. He already has several patents in

this field (for instance, [4]). After publications by W.M. Steen, hybrid laser processes began to be studied in the majority of industrialized countries of the world.

CO_2-lasers with 10.6 μm wave length were the first to be applied in hybrid welding processes, as they had high power and were easy to maintain. This type of lasers is still used [5, 6]. Then Nd:YAG-lasers began to be ever wider introduced [7]. One of the main advantages of this laser type is shorter wave length (1.06 μm), at which an increase of metal absorptivity and, therefore, of effective efficiency of the welding process, is observed. Recently introduced into mass production disc and fibre lasers are actively applied now in hybrid welding processes [8, 9]. Their application effectiveness is associated with a higher efficiency (25–35 %) of these systems that also promotes a higher effective efficiency of welding.

As a rule, in HLPW the focused laser beam is directed along a normal to the surface of item being welded (Figure 1) [10, 11], or at a small angle to it (up to 10°) (Figure 2) [12]. In terms of design, the laser-plasma welding head can consist of separate elements — laser focusing system and plasmatron, or it can be integrated into a common casing (Figure 3) [13]. Plasma torch is

inclined at a certain (minimum possible) angle to the axis of the focused laser beam (Figure 4) [14]. Filler wire can be fed co-axially with the plasma arc, towards it, or it may not be fed at all. Laser beam with a high power density and arc plasma with high energy efficiency interact simultaneously in the weld pool area. To enhance the effect of such interaction, they can be supplied to the parts being welded through a common nozzle (Figure 5) [15]. In all the cases the laser beam can be located relative to plasma behind or ahead along the welding direction.

Let us consider in greater detail the advantages and disadvantages of laser-plasma welding process schematics shown in Figures 1–5.

According to the method proposed in [16], material processing is performed by application of two heat sources, one of which is laser radiation. The other source can be electric arc or plasma. Here, the impact of each of the heat sources on the material being processed is of a pulsed nature, and the impact of these pulses is mutually synchronized. A number of technological operations (including welding, brazing, cutting, engraving, alloying, quenching, etc.) can be performed by the same process.

The disadvantage of this process is the need for pulse generators and their synchronizing device, whereas application of continuous impact of both the heat sources on the material being processed does not require such sophisticated additional equipment.

To eliminate the above drawback a torch is proposed in the patent [10], which combines the design elements of torches for laser and for plasma welding. Laser radiation is directed to the objective lens so that its axis coincides with that of plasma-arc torch. The laser beam passes through a flat (in the form of a washer) or conical
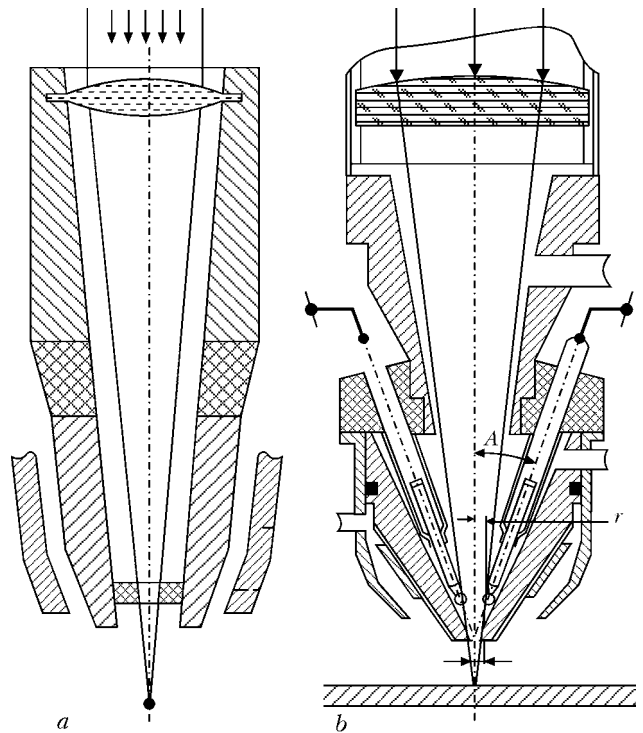
Figure 1. Design of plasma torches allowing laser radiation to be fed normal to the surface of item being welded: *a* — with hollow cathode [10]; *b* — with inclined cathodes located symmetrically relative to laser beam axis [11]

electrode (cathode) through a longitudinal co-axial hole made in it, with the diameter somewhat larger than that of a focused laser beam (see Figure 1, *a*). The plasma-forming nozzle is located under the cathode so that the laser beam passes through its axis. Similar to standard plasma-arc torch, the gas is passed through a chamber with cathode and nozzle in its lower part. Laser beam passing through such a cathode heats it to facilitate electron emission, and acts on the item being welded (anode), and also interacts with arc plasma, thus increasing the energy density on the item.
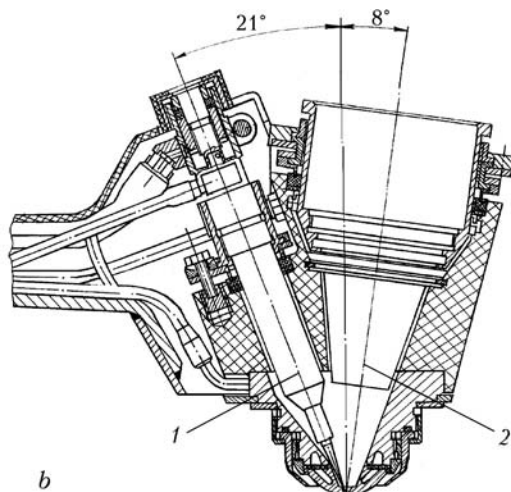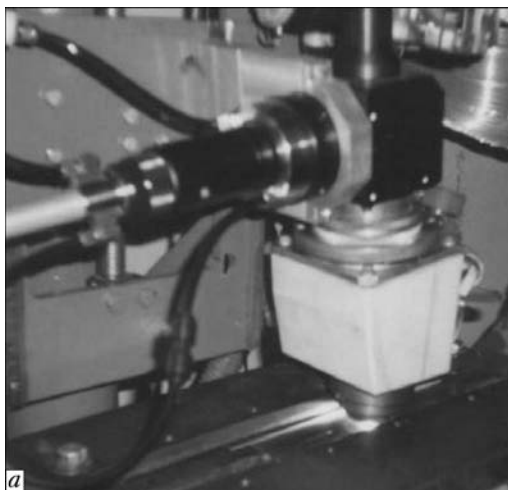
Figure 2. Appearance (*a*) and schematic (*b*) of integrated plasmatron for HLPW [12]: *1* — cathode axis; *2* — focused laser beam axis
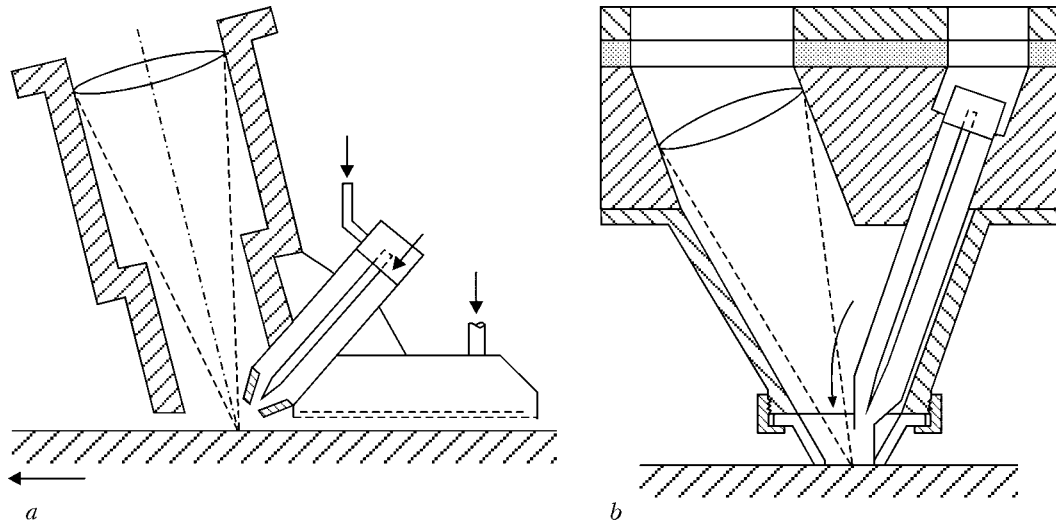
Figure 3. Design of HLPW heads, in which the laser focusing system and the laser torch are used separately (*a*) or are integrated in the common casing (*b*) [13]

A small design disadvantage of proposed in [10] torch for laser-plasma welding is presence of a tubular cathode, the outlet of which should be such that focused laser radiation flowed out of it. This increases the plasma arc transverse size, and lowers the resistance of the cathode proper because of its erosion in service. Its periodical sharpening becomes more difficult.

In laser-plasma torch of a better design, focused laser radiation passes by a group of electrodes located about its axis at a sharp angle to the torch central axis (see Figure 1, *b*) [11]. In this hybrid welding process, the focused laser radiation axis coincides with the torch axis, and is normal to the plane of parts being welded. Electrode axes are located on the generatrix of a cone, the vertex of which falls on the torch central axis near the edge of the nozzle, forming the plasma, and the cone proper is inverse relative to the torch outlet part. Laser-plasma welding occurs at running of electric arc between the elec-

trode (at least, one) and part being processed. Such a discharge forms the plasma by blowing gas through outlet nozzle. Plasma, leaving the nozzle, forms a hybrid laser-arc discharge together with laser radiation.

The disadvantage of the above design is the possibility of hitting the optical path along which the laser beam, reflected from weld pool, is fed. There is a high probability of failure of optical elements of the path. Particularly dangerous in this respect is the case of welding aluminium alloys, because of high values of their coefficient of laser radiation reflection.

Figures 3, *a* and 4 give the designs of HLPW heads, in which the radiation focusing system and plasma torch (plasmatron) are used separately. The main advantage of such structures is the possibility of hybrid welding realization with application of available welding equipment, i.e. without the need to create specialized integrated hybrid plasmatron (for instance, the one given
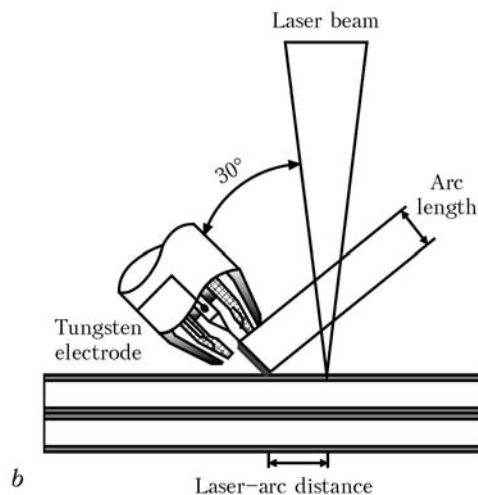

Figure 4. Process of HLPW with inclined position of plasma torch allowing the distance between the plasma and laser beam to be measured [14]: *a* — appearance of HLPW head; *b* — process technological schematic
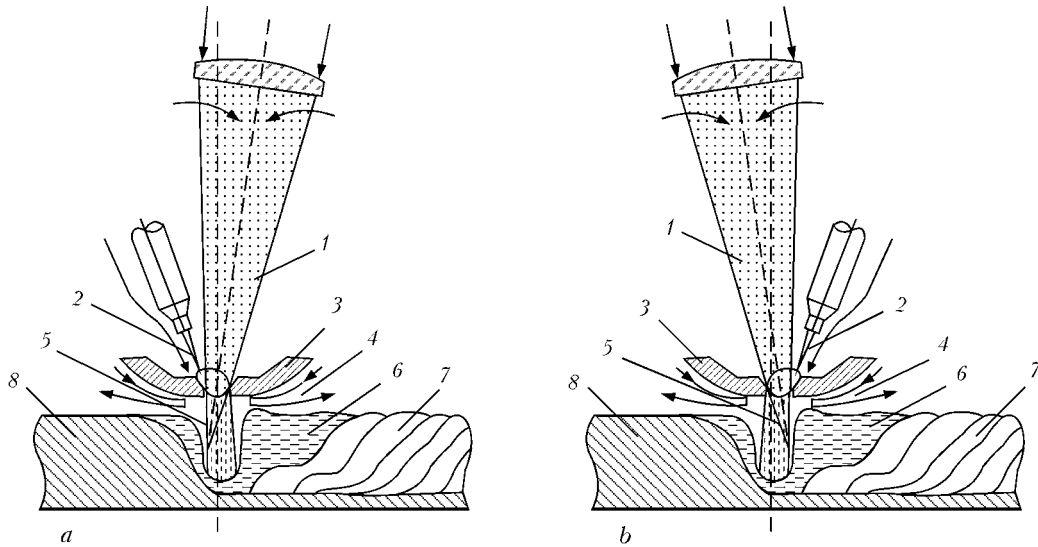
Figure 5. Schematics of the HLPW process with plasma torch location ahead of (*a*) and behind (*b*) the laser beam [15]: *1* — focused laser radiation; *2* — nonconsumable electrode; *3* — plasma-forming nozzle; *4* — shielding gas; *5* — plasma discharge; *6* — weld pool; *7* — weld metal; *8* — base metal

in Figures 2 and 3, *b*). The disadvantages of designs with separate components of hybrid process include rather high angles of inclination of plasmatron electrode axis that lowers its application effectiveness.

Therefore, an urgent task is application of such a method of laser-plasma welding, at which the electric arc, formed between the electrode (one as a minimum) and processed part, generates plasma due to gas blowing through the outlet nozzle, while laser radiation emitted through the same nozzle, promotes inducing laser-arc discharge. Here, the angle of inclination of focused laser radiation axis should be selected such as to eliminate the hazard of reflected radiation hitting the optical surfaces, and the angle between the axes of the electrode and focused radiation should be the minimum possible one. Summing-up the above-said, one can say that the best schemes of laser-plasma welding are those shown in Figure 5.

Another comparatively recent technological development is the hybrid laser-plasma process with powder filler material [17]. Schematic of such a process realization is given in Figure 6. Its main advantages are elimination of energy losses associated with heat removal into the filler (or electrode) wire, and improvement of the conditions of powder filler melting due to their low heat conductivity. These advantages enable raising the welding speed without increasing the heat input.

One of the most important features of laser-plasma welding is the possibility of removal of Al_2O_3 oxide film in aluminium alloy welding due to the so-called cathode cleaning. The cathodic cleaning process consists in breaking the refrac-

tory oxide film within the zone of the cathode spot, moving chaotically over the aluminium alloy surface without its melting. According to [18], the mechanism of such cleaning consists in the following. At ion bombardment kinetic energy is impacted to oxide film molecules, which is transformed into mechanical energy of vibrations. If this energy is greater than that of Al_2O_3 molecule dissociation, the latter decomposes into atoms which leave the surface.

In practice the above effect became widely applied in aluminium alloy welding. So, welding of external fuel tanks of the Space Shuttle, various beam structures, etc. was performed with application of cathode cleaning at plasma-arc welding by pulses of different polarity [19]. Attempts at removing the oxide film were also made in laser welding of aluminium-based alloys [20, 21]. This task is particularly urgent in laser weld-
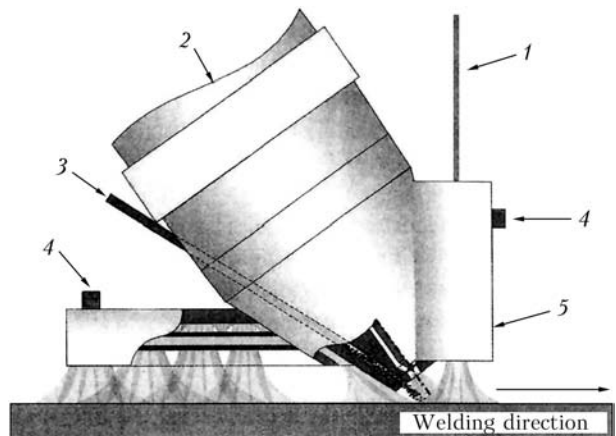

Figure 6. Schematic of HLPW with transferred plasma arc and powder filler [17]: *1* — laser radiation; *2* — plasma gas; *3* — powder with carrier gas; *4* — shielding gas; *5* — tube through which radiation is fed
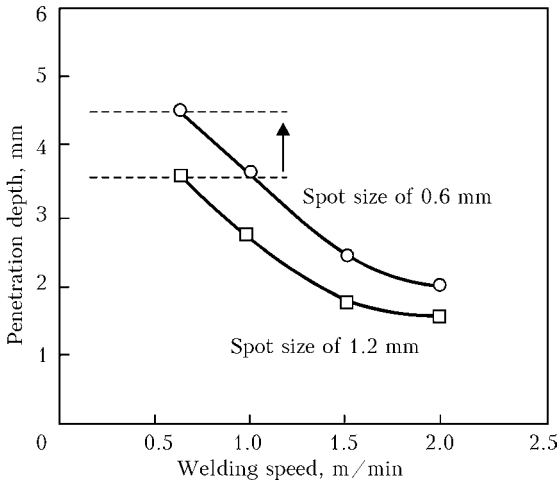
Figure 7. Influence of size of laser radiation focal spot on penetration depth of SUS304 steel plate (δ = 5 mm) [39] (2 kW power, shielding gas is argon)

ing of car bodies from aluminium alloys [22]. However, in the opinion of authors of [12, 23], HLPW is the most effective in welding these alloys with simultaneous cleaning of the edges being joined. It allows sound cleaning to be performed even at quite high (up to 300 m/h) welding speeds.

A number of studies devoted to comparison of the features of laser, arc (plasma) and hybrid welding should be noted. In [24] the prospects for application of plasma, consumable and non-consumable electrode arc in inert gas for hybrid welding are studied. In [25] the differences of hybrid laser-TIG welding processes at application of CO_2- and Yb:YAG-lasers in them, i.e. radiations with wave length of 10.6 and 1.03 µm, respectively, are analyzed. It is shown that with reduction of wave length, laser radiation absorption and refraction in arc plasma decreases. In [26] results of laser (with CO_2-laser radiation) and hybrid (CO_2-laser + TIG) welding of T-joints in fabrication of load-carrying stainless
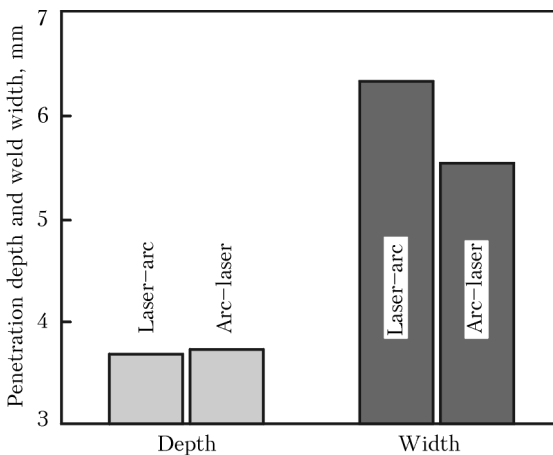

Figure 8. Influence of relative position of CO_2-laser beam or GMA arc on penetration depth and weld width in hybrid welding of HSLA-590 steel [41]

steel frames are compared. Here, the good prospects for the hybrid process are shown. Now, in welding of zinc-plated steel sheets for manufacture of car bodies preference is given to Nd:YAG-laser radiation [27].

Quite a lot of attention was given in many studies to metallographic features and strength characteristics of welded joints produced by laser, hybrid or other process (for instance, [28–30]). Residual stresses in weld metal were studied, that is particularly important in welding titanium alloys for aircraft industry applications [31]. New mechanisms of hybrid processes [32] and their technological features were investigated. Among the latter the following studies should be noted: studying the influence of shielding gas pressure on laser-MIG welding [33]; the results of laser-arc welding of titanium alloys [34]; hybrid welding by Nd:YAG laser radiation and MIG/MAG process [35]; laser-microplasma welding of metal filters using stainless filler wire [36]. New techniques were developed. In [37] hybrid laser-TIG welding of stainless steel 304 with application of rotating double-focus of the laser beam was proposed. In [38] the influence of relative position of laser radiation focus and consumable electrode arc on weld formation in hybrid welding was studied.

Of special interest are various technological and design recommendations given in the works on hybrid welding. For instance, to increase penetration depth it is recommended to use short-focus optics, which allows the size of the focal spot to be reduced (Figure 7) [39]. At application of fiber-optic lasers for hybrid welding, increase of radiation power and reduction of focal spot size increase the process effectiveness, similar to application of other laser types. In this case, increase of radiation power lowers the welding current, but it does not affect arc voltage [40]. Electric arc placing first along the welding direction in the hybrid process can lead to a certain increase of penetration depth and reduction of weld width (Figure 8). Influence of the distance between focused radiation and the arc on penetration depth was also established [41]. It is shown that the hybrid effect is lost if this distance is greater than 5–7 mm (Figure 9) [42].

An important aspect of hybrid welding is allowing for liquid metal pressure and arc pressure on weld pool (Figure 10). Balance of these pressures and surface tension forces prevents pool liquid metal flowing out and allows performance of «unsupported» hybrid welding, i.e. without application of process backing, which makes the processes of welding and subsequent treatment
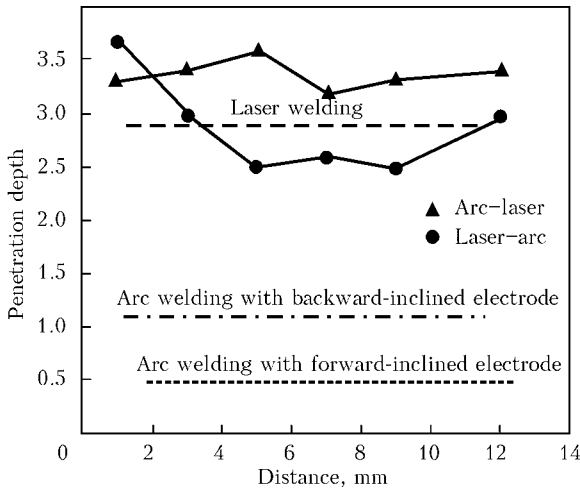
Figure 9. Influence of distance between Nd:YAG-laser beam and nonconsumable electrode arc, as well as their relative position, on penetration depth of stainless steel 304 [42]

Figure 10. Pressure balance in weld pool root part [6]

more complicated. Note that remelted metal volume in hybrid welding usually is greater than in laser welding (Figure 11). This circumstance can promote increase of penetration depth in welding butt joints with a gap (Figure 12) between the edges being welded due to this gap filling by liquid metal [43].

In HLPW the laser beam and the plasma arc should be positioned as close as possible to the item being welded. One of the variants of satisfying this condition is application of a tubular cathode, through which focused laser radiation is passed (see Figure 1, *a*) [1, 44]. Another vari-

ant is application of a cathode inclined at a certain angle (see Figure 4). This angle usually is rather large (for instance, about 45° [44, 45]) that weakens the effect of plasma. Works [46–48] demonstrate the urgency of reducing the angle of inclination of the cathode to item surface and the angle between the cathode and laser beam axis.

The main objectives of HLPW include not only arc heating of item metal to increase absorptivity, but also modifying the welding thermal cycle to lower the rate of cooling after welding [45]. This enables lowering the content of brittle structures prone to fracture in service. Moreover, presence of plasma component allows lowering the requirements to the quality of assembly of the butts being welded compared to laser welding. These requirements, however, are higher compared to laser-TIG welding [49].
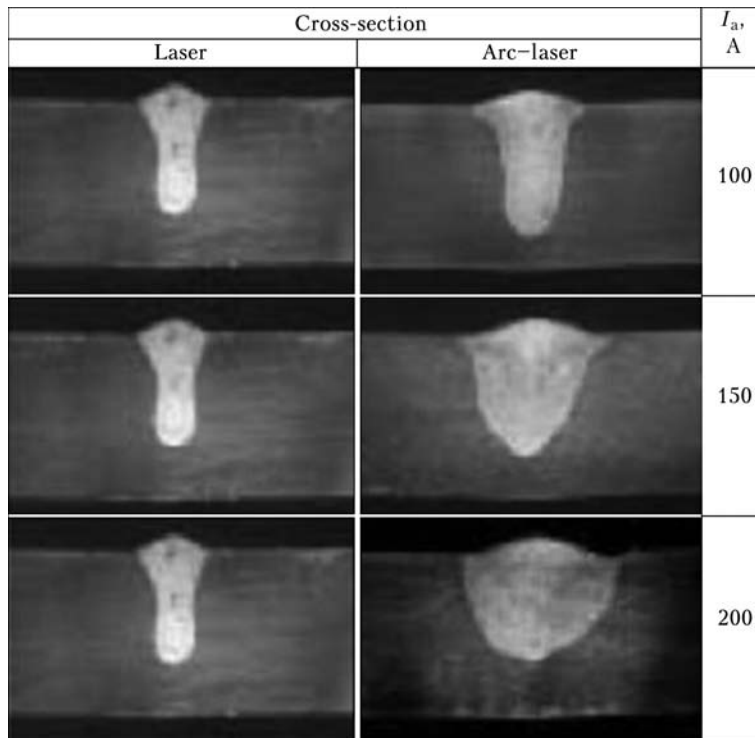
Figure 11. Comparison of penetrations in austenitic stainless steel AISI304 (δ = 5 mm) made by Nd:YAG laser (*P* = = 1.7 kW) and by hybrid process in combination of this laser with nonconsumable electrode arc at speed of 10 mm/s at different welding currents [42]
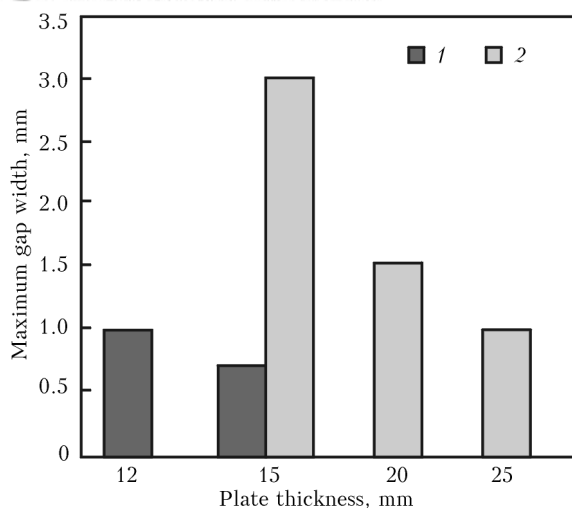
Figure 12. Dependence of maximum gap width between the edges of plates being welded on their thickness and position in space: *1* — downhand; *2* — horizontal welding [43]

In [47] experiments on laser-plasma welding of such materials as low-carbon and stainless steel, titanium and aluminium alloys 0.6–2.0 mm thick are described. Used for this purpose was radiation of CO_2-laser of up to 400 W power and up to 50 A welding current. It is established that laser-plasma process can prevent formation of «humps» in high-speed welding of thin sheets. Tolerances for the gap between the butt edges are equal from 0.15 up to 0.50 mm at welding speed of 2 m/min (~33 mm/s).

According to predictions given in [50], hybrid welding will allow increasing the efficiency by 300–500 % at cost reduction by 55 %. Here, the consumables cost will be reduced by approximately 2 times, that will allow lowering the welding process cost by approximately a quarter. Another important aspect is smaller width of welds produced by the hybrid process, compared to welds made by arc processes, that reduces the structure metal intensity.

Conclusions

This leads to the conclusion that the prospects for industrial application of hybrid laser-plasma welding are associated with its cost and process advantages. Cost advantages consist in partial (up to 50 %) replacement of quite expensive laser power by much less expensive plasma power, as well as in lowering of power inputs into the process due to the possibility of filler wire replacement by the respective powder or total elimination of filler material. Process advantages consist in reduction of residual thermal deformations, lowering of requirements to edge preparation (including the possibility of edge welding with a variable gap width), ability to perform cathodic cleaning of aluminium alloys directly during

their welding, increase of penetration depth, and increase of process efficiency several times compared to plasma welding and approximately by 40 %, compared to laser welding. Introduction of laser-plasma welding is capable of changing the modern attitudes of technologists to the welding process and those of designers — to welded structure design. Industrial application of laser-plasma welding is associated, primarily with solving the tasks of joining titanium and aluminium alloys, as well as stainless steels in the thickness range of 0.3–15.0 mm.

1. Krivtsun, I.V. (2002) *Combined laser-arc processes of treatment of materials and devices for their realization*: Syn. of Thesis for Dr. of Techn. Sci. Degree. Kiev: PWI.
2. Steen, W.M., Eboo, M. (1979) Arc augmented laser welding. *Metal Construction*, 11(**7**), 332–335.
3. Steen, W.M. (1980) Arc augmented laser processing of materials. *J. Appl. Physics*, 51(**11**), 5336–5641.
4. Steen, W.M. *Methods and apparatus for cutting, welding, drilling and surface treating*. Pat. 1547172 Great Britain. Int. Cl. B23 K 26/00, 9/00. Publ. 06.06.79.
5. Bagger, C., Olsen, F.O. (2005) Review of laser hybrid welding. *J. Laser Appl.*, 17(**1**), 2–14.
6. Petring, D., Fuhrmann, C., Wolf, N. et al. (2007) Progress in laser-MAG hybrid welding of high strength steels of up to 30 mm thickness. In: *Proc. of ICALEO* (Orlando, Fl, USA, 2007), 300–307.
7. Shibata, K., Sakamoto, H., Iwasa, T. (2006) Laser-MIG hybrid welding of aluminium alloys. *Welding in the World*, 50(**1/2**), 27–34.
8. Laser technology of Trumpf company. *http://www.trumpf-laser.com*
9. Products of STA IRE-Polus. *http://www.ntoire-polus.ru*
10. Dykhno, I.S., Krivtsun, I.V., Ignatchenko, G.N. *Combined laser and plasma arc welding torch*. Pat. 5700989 USA. Int. Cl. B23K 26/00, 10/00. Publ. 23.12.97.
11. Dykhno, I., Ignatchenko, G., Bogachenkov, E. *Combined laser and plasma-arc processing torch and method*. Pat. 6388227 B1 USA. Publ. 14.05.2002.
12. Krivtsun, I.V., Shelyagin, V.D., Khaskin, V.Yu. et al. (2007) Hybrid laser-plasma welding of aluminium alloys. *The Paton Welding J.*, **5**, 36–40.
13. Walduck, R.P. *Enhanced laser beam welding*. Pat. 5866870 USA. Int. Cl. B23 K 10/00, 26/00. Publ. 02.02.99.
14. Kim, C.H., Ahn, Y.H., Kim, J.H. (2011) CO2 laser-microplasma arc hybrid welding for galvanized steel sheets. *Transact. of Nonferrous Metals Society of China*, Vol. 21, Suppl. 1, 47–53.
15. Krivtsun, I.V., Bushma, A.I., Khaskin, V.Yu. (2013) Hybrid laser-plasma welding of stainless steels. *The Paton Welding J.*, **3**, 46–50.
16. Petring, D. *Laser material machining using hybrid processes*. Pat. WO2003089185 A1 USA. Publ. 30.10.2003.
17. Stelling, K., Lammers, M., Schobbert, H. et al. (2006) Qualification of Nd:YAG and CO2 laser plasma hybrid welding with filler material powder. *Welding and Cutting*, 5(**6**), 330–334.
18. Paton, B.E., Gvozdetsky, V.S., Dudko, D.A. et al. (1979) *Microplasma welding*. Kiev: Naukova Dumka.
19. Kexuan, Ch., Heqi, L., Chunxu, L. (2003) Cathodic cleaning in variable polarity plasma arc welding of aluminum alloys. *China Welding*, **2**, 168–170.
20. Bingkun, Z. (2000) Study of processing parameters of CO2-laser welding on aluminum alloys. *Chinese J. Lasers*, **2**, 183–186.

21. Junfeng, Q., Dongyun, Z., Rongshi, X. et al. (2007) Joint performance of CO₂ laser beam welding 5083-h321 aluminum alloy. *China Welding*, **2**, 40−45.
22. Shu-rong, Y., Ding, F., Jin-hui, X. et al. (2006) CO₂-laser welding of 5a06 aluminum alloy plates with different thicknesses. *Transact. of Nonferrous Metals Society of China*, **3**, 1407−1410.
23. Khaskin, V.Yu. (2013) Development of laser welding of aluminium alloys at the E.O. Paton Electric Welding Institute (Review). *The Paton Welding J.*, **5**, 51−55.
24. Bagger, C., Olsen, F.O. (2003) Comparison of plasma, metal inactive gas (MIG), tungsten inactive gas (TIG) processes for laser hybrid welding. In: *Proc. of 22nd ICALEO* (Jacksonville, Fl, USA, 13−16 Oct. 2003), 11−20.
25. Shikai, W., Rongshi, X., Wuxiong, Y. et al. (2010) Characteristics comparison of laser-TIG arc interaction using high power CO₂ and Yb:YAG laser. *Chinese J. Lasers*, **10**, 2667−2671,
26. Shikai, W., Rongshi, X., Kai, C. (2009) CO₂-laser welding and CO₂-laser-TIG hybrid welding of thin walled stainless steel butt joint from the base plate side. *Electromachining & Mould*, **6**, 29−33.
27. Katayama, S., Mizutani, M., Tarui, T. et al. (2004) Monitoring and phenomena observation during YAG-laser lap welding of Zn-coated steel sheets. *J. Lanzhou University of Technology*, **4**, 31−36.
28. Liming, L., Gang, S., Jifeng, W. et al. (2004) Microstructure and mechanical properties of wrought magnesium alloy AZ31B welded by laser-TIG hybrid. *Transact. of Nonferrous Metals Society of China*, **14**(**3**), 550−555.
29. Zhang, X., Chen, W., Wang, C. et al. (2004) Microstructures and toughness of weld metal of ultrafine grained ferritic steel by laser welding. *J. Materials Sci. & Techn.*, **6**, 755−759.
30. Wenquan, W., Daqian, S., Chungyan, K. (2008) Macrostructural and microstructural features of 1000 MPa grade TRIP steel joint by CO₂-laser welding. *China Welding*, **2**, 1−7.
31. Xiaodong, H., Jianxun, Z., Zuo, P. et al. (2003) Test of residual stress in laser beam welding and TIG welding joints of aeronautical titanium alloy plate. *Welding & Joining*, **10**, 26−29.
32. Yuan, X., Yonglun, S., Kunping, H. (2008) New development of mechanisms of laser-TIG arc hybrid welding. *Ibid.*, **12**, 21.
33. Chen, Y., Lei, Z., Li, L. et al. (2006) Influence of shielding gas pressure on welding characteristics in CO₂-laser-MIG hybrid welding process. *Chinese Optics of Letters*, **1**, 33−35.
34. Li, C., Xiaoyan, L., Dingyong, H. et al. (2009) Laser-arc hybrid welding of titanium alloy. *Welding & Joining*, **7**, 60−64.
35. Zhen, L., Guoliang, Q., Shangyang, L. (2005) Development of YAG laser-MIG/MAG arc hybrid welding technology. *Ibid.*, **9**, 9−12.
36. Fuzuo, W., Jianping, H., Feng, X. (2010) Study on stainless steel screen mesh welding using microplasma arc welding. *Hot Working Techn.*, **1**, 128−130, 133.
37. Xiaohui, L., Su, W., Caiyun, X. (2008) 304 stainless steel rotary twin-focus laser-TIG hybrid welding. *J. Beijing University of Aeronautics and Astronautics*, **4**, 431−434.
38. Gao, Zh., Huang, J., Li, Y. (2008) Effect of relative position of laser beam and arc on formation of weld in laser-MIG hybrid welding. *Transact. of China Welding Inst.*, **12**, 69−73.
39. Ishide, T., Tsubota, S., Watanabe, M. (2002) Latest MIG, TIG arc-YAG laser hybrid welding systems for various welding products. In: *Proc. of 1st Int. Symp. on High-Power Laser Macro* (Osaka, 2002), 347−352.
40. Roepke, C., Liu, S., Kelly, S. et al. (2010) Process monitoring and macrostructure examination of low laser power hybrid gas metal arc welding on A36 steel: *IIW Doc. IV-1030−10*.
41. Liu, Z., Kutsuna, M. (2005) Metallurgical study on laser-MAG hybrid welding of HSLA-590 steel. In: *Proc. of Laser Materials Processing Conf.* (Miami, Fl, USA, 2005), 127−133.
42. Naito, Y., Mizutani, M., Katayama, S. (2003) Observation of keyhole behavior and melt flows during laser-arc hybrid welding. In: *Proc. of ICALEO* (Jacksonville, USA, 2003), Sect. A, 159−167.
43. Yuan, Y., Wouters, M., Powell, J. et al. (2008) Optimization research on laser-MIG composite welding for rear axle steel plate. *Automobile Techn.*, **1**, 54−57.
44. Krivtsun, I.V., Chizenko, M.I. (1997) Principles of calculation of laser-arc plasmatrons. *Avtomatich. Svarka*, **1**, 16−23.
45. Kah, P., Salminen, A., Martikainen, J. (2010) Laser-arc hybrid welding processes (Review). *The Paton Welding J.*, **6**, 32−40.
46. Krivtsun, I.V., Bushma, A.I., Khaskin, V.Yu. (2013) Laser-plasma welding of stainless steels and aluminium alloys. *Dopovidi NANU*, **3**, 76−82.
47. Sidorets, V.N., Bushma, A.I., Khaskin, V.Yu. (2012) Prospects of application of hybrid laser-plasma welding of stainless steels in machine-building. *Visnyk DDMBA*, 28(**3**), 244−246.
48. Shelyagin, V.D., Orishich, A.M., Khaskin, V.Yu. et al. (2014) Technological peculiarities of laser micro-plasma and hybrid laser-microplasma welding of aluminium alloys. *The Paton Welding J.*, **5**, 33−39.
49. Walduck, R.P., Biffin, J. (1994) Plasma arc augmented laser welding. *Welding and Metal Fabr.*, **4**, 172−176.
50. Paul, K., Ridel, F. (2009) Hybrid laser welding — joining the efforts. *Fotonika*, **1**, 2−5.

ANALYSIS OF THE COPPER-CHROMIUM BASED ELECTRODE DEFORMATION DURING RESISTANCE SPOT WELDING PROCESS

C. NACHIMANI

Department of Mechanical Engineering, Faculty of Engineering, University of Malaya
50603, Kuala Lumpur, Malaysia. E-mail: nachicharde@yahoo.com

This research presents an experimental investigation of the RMWA class two (Cu–Cr) electrode caps in resistance spot welding of carbon and stainless steels. A pair of equal-size circled-electrode caps 5 mm diameter is committed to weld up to 900 welding processes. The electrode caps are sharpened once in the meantime and are replaced using electrode dresser after underwent approximately 400 weld attempts. The degrading factors of Cu–Cr electrodes have directly influenced the weld geometries on carbon and stainless steels while affected the bonding strength implicitly. The electrode caps that performed up to 900 weld attempts have been underwent the microstructural analytical observation, and several cracks in its internal structure were found. The internal cracks are only appeared in the movable-upper electrode cap due to continuous heating and hitting effects by pneumatic pressures, to compared with static-lower electrode in the 75 kV·A spot welder. Mushroom growth of electrode cap tips is another threat to weld surfaces as it reduces the process resistances during welding. In this experiment, the mushroom growth is seemed to be higher on upper side electrode than the lower side one. With increased diameter of electrode tip areas due to mushrooming effect, the weld geometries become odds which lead to inconsistency in its appearances and pave the way for expulsions. 21 Ref., 9 Figures.

Joining the carbon and stainless steels by spot welding is widely recommended by using class two alloys of Resistance Welder Manufacturers Association (RMWA) [1]. The ground for this sort of recommendations is their superior resistance, heat toleration and high corrosive opponent [2]. Without the mixture of substances, a pure copper is intrinsically soft and fails prematurely in demanding applications [3]. Mixture of substances is, therefore, a good choice for the manufacturing of electrode caps as to produce superior qualities, specifically for the mechanical and electrical properties. So, with this consideration in mind, Cu–Cr-based electrode caps are practically tested in welding approximately 900 weld pairs on carbon and stainless steels sheets in this experimental work.

Figure 1 shows the Cu–Cr phase diagram for Cu-based alloys [4]. It shows that chromium is easily soluble in the liquidus of copper when heated above 1076 and below 1860 °C. Once the compound is solidified, it requires equal amount of heat to remelt it again [5]. This factor, now, creates significance in welding of carbon and stainless steels because the carbon steel melting point falls between 1426 to 1540 °C, and that of stainless steel is 1400–1450 °C. Copper and chromium solubility phases are actually of the eutectic type. The face-centered cubic (FCC) lattice will be formed in copper while body-centered cubic (BCC) one will be formed in chromium, when solidification process is concerned in Cu–Cr alloy.

Fundamentally the welding process is varied by its process parameters (welding current, welding time, electrode tip diameters and electrode force) [6]. These parameter variations establish the corresponding heat growth for any materials as for which the bonding strengths are mainly anticipated. By doing so, the amount of heat that produce in an enclosed areas of electrode tips will cause the electrode tip deteriorations. Another factor that obviously affecting the electrode tip deteriorations is the electrode pressing forces, which is primarily supplied by the pneumatic pressure in this research. Thus, every time when electrodes are pressed to hold the materials being welded together, the hitting effect of electrode tips towards the base metal results metal hitting effect or simply the hitting effect, subjected to its fatigue at last. So in this experiment the mushroom growth, degradation as well as deterioration is what examined for the Cu–Cr electrode caps using 75 kV·A spot welder. Part of this research works have been previously published for the simulation, tensile shear strength, hardness distribution and metallurgical analysis, and

therefore, such information is excluded in this paper but relevant references are given by [7].

Experimental. The base metals were prepared in rectangular shape with length of 200 mm, width 25 mm and thickness 2 mm. Chemical elements in stainless steel sheets were, wt.%: 0.046C, 18.14Cr, 8.13Ni, 1.205Mn, 0.506Si, 0.004S, 0.051N and 0.03P. Carbon steel sheets have the following chemical composition, wt.%: 0.23C, 0.095Mn, 0.006Si, 0.05S and 0.04P. Hardness of austenitic stainless steels was HRB 86.2, for the carbon steel it was about HRB 65. A pair of water-cooled (4 l/min) truncated-cone electrodes with 5 mm of round diameter was applied to join these base metals (Figure 2).

Properties of Cu–Cr electrodes

CMW alloy (class 2)	C18200
Chemical elements, wt.%	99.1Cu, 0.1Fe,
	0.05Pb, 0.6Cr, 0.1Si
Rockwell hardness HRB	70
Electrical conductivity, %	80
Tensile strength, KSI	70
Yield strength, KSI	55
Elongation, % in 2 inch	21
Thermal conductivity, W/m·K (min)	187
Thermal expansion, /K	$9.8 \cdot 10^{-6}$

Approximately 900 welding attempts were made, and the electrode caps were sharpened once to remove the mushrooms after completed about 400 welding attempts. The electrode caps are then removed from the holder and cut at the line of its diameter (middle) using abrasive cutter to form flat surfaces. Once it has been cut across the diameter, it was mounted using resin powder on hot press mount-machine, such as way that it shows the cross sectional view of the electrode caps. The mounted samples were thereafter polished well using silicon papers, graded as 1200/800p and 600/200p, and also continuously polished using Metadi polishing cloth. This polishing process has been conducted about 30 min to 1 h on each sample until the shining (mirror-like) surfaces are seen. The V2A etchant that consists of 100 ml water, 100 ml hydrochloric acid and 10 ml nitric acid is used to etch the polished samples. It was immersed into a box for about 45–60 min. After that the samples were well-rinsed off using plain water; dried using air blower; applied anti-corrosion liquid and kept in vacuum chamber for SEM observation. These preparatory steps and the above listed polishing materials are good enough to get reasonable micro- and macrographs for analytical purpose.

Results and discussion. *Weld nuggets for carbon, stainless and mixed steels.* Classical concerns about spot welding of carbon and stainless steels are, of course, rely on the dissimilarity of
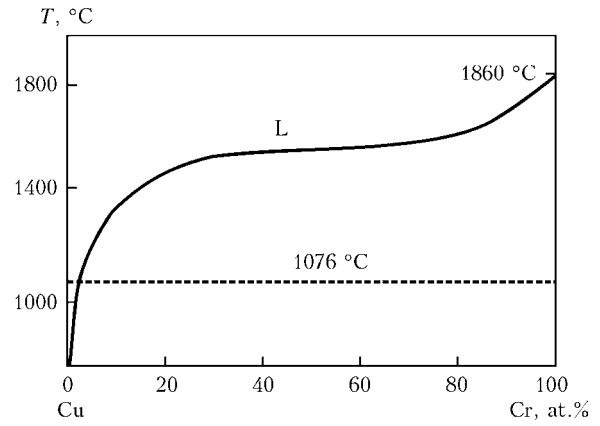
Figure 1. Cu–Cr phase diagram

melting points in individual weld joints and also the heat imbalances in the dissimilar weld joints [7]. In this experiment, both issues have been observed for several combinations of process parameters, for example, variations of welding current levels against variations of welding time cycles have been monitored [7]. Figures 3–5 show the carbon, stainless and both steels mixed welds made using Cu–Cr electrode caps, respectively. Right sides in Figures represent the corresponding SORPAS simulations, in which the maximized temperatures are clearly shown before the solidification processes started, where as the left sides show the real welds after solidification processes are utterly done. Color representations are
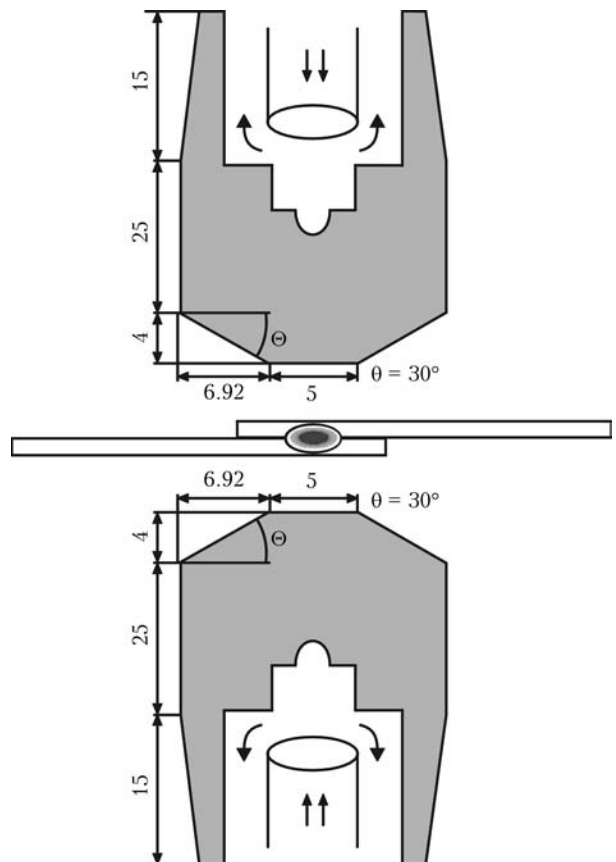
Figure 2. Dimension of electrodes on materials to be welded

$$1.740 \cdot 10^2 \quad 4.820 \cdot 10^2 \quad 7.900 \cdot 10^2 \quad 1.098 \cdot 10^3 \quad 1.406 \cdot 10^3$$

← Melting point

1   2   3   4
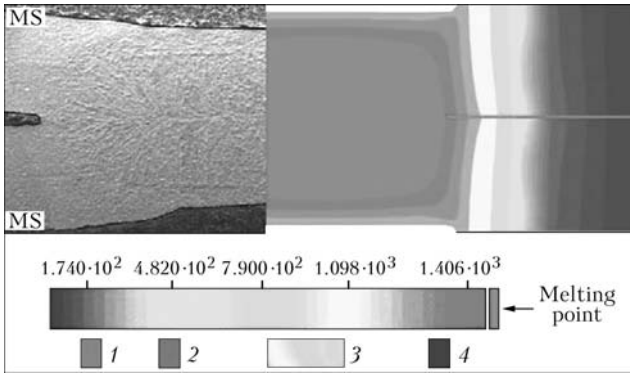
Figure 3. Temperature distribution in carbon steel weld (real vs simulation) (here and Figures 4, 5: *1* — fusion zone; *2* — HAZ; *3* — HEZ; *4* — base metal)

used to interpret the molten zones and also its vacinities, as to distinguish the heat-affected and also the heat-extended zones vividly. General point is that the Cu–Cr electrode caps have significantly contributed for the formation of sound welds in carbon, stainless and mixed materials but in long run, it deteriorates itself.

Electrode mushrooming effect and chemical changes. The class two spot welding electrode caps are primarily made of copper and chromium materials as major components according to RMWA clasiffication [8]. It has dual phase mixture of chromium and alpha-copper as major chemical elements although it has other minor ones. The changes in properties happen at the rise of temperature ($Q = I^2Rt$) due to precipitation of chromium out of the solid solution. Literally, when the electrode is heated together with metals, it has high tendency of forming new kind of alloys [9, 10]. This is where the precipitation of chromium out of the solid solution is easily noticed [11, 12]. This has also been confirmed in the microstructural view of electrode caps (Figure 6). As welding processes are repeatedly being carried out on carbon and stainless steels, the mushrooming effect are growing due to heat exposure at the electrode tip surfaces. It is nothing but simply enlarging the areas A of the cap tips, on the other end, causing the drop of contact resistance ($R = pl/A$) adverse to efficient welding processes [13, 14]. In this research, the electrode tip of both sides was originally 5 mm in
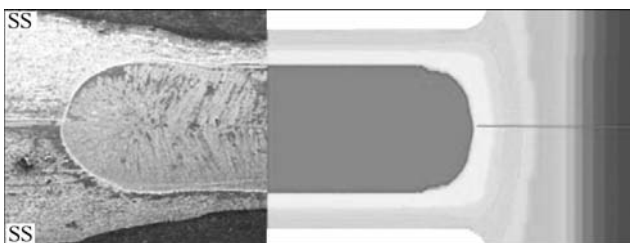
Figure 4. Temperature distribution in stainless steel weld (real vs simulation)
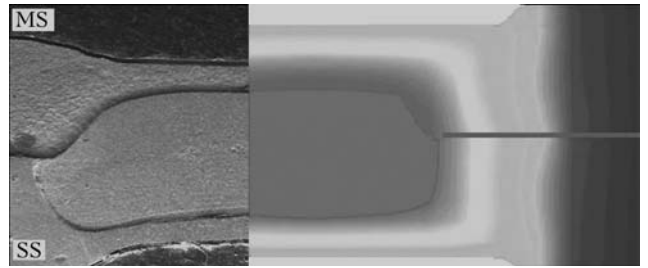
Figure 5. Temperature distribution in carbon and stainless steel dissimilar weld (real vs simulation)

diameter and it was partially-mushroomed. Literally the upper electrode tip diameter was enlarged up to 7.458 mm whereas the lower electrode tip diameter was enlarged up to 7.238 mm. Figure 7 shows the deterioration of electrode tips which were engaged to weld about 900 times.

Having considered the deterioration that happen on the electrode caps after underwent 900 welding attempts, it was scanned for the profound structural changes. Point A in Figure 6 represents the cap tip, at which the base metal molten heat (max ≈ 1600 °C) was directly exposed. Points B and C are the following points
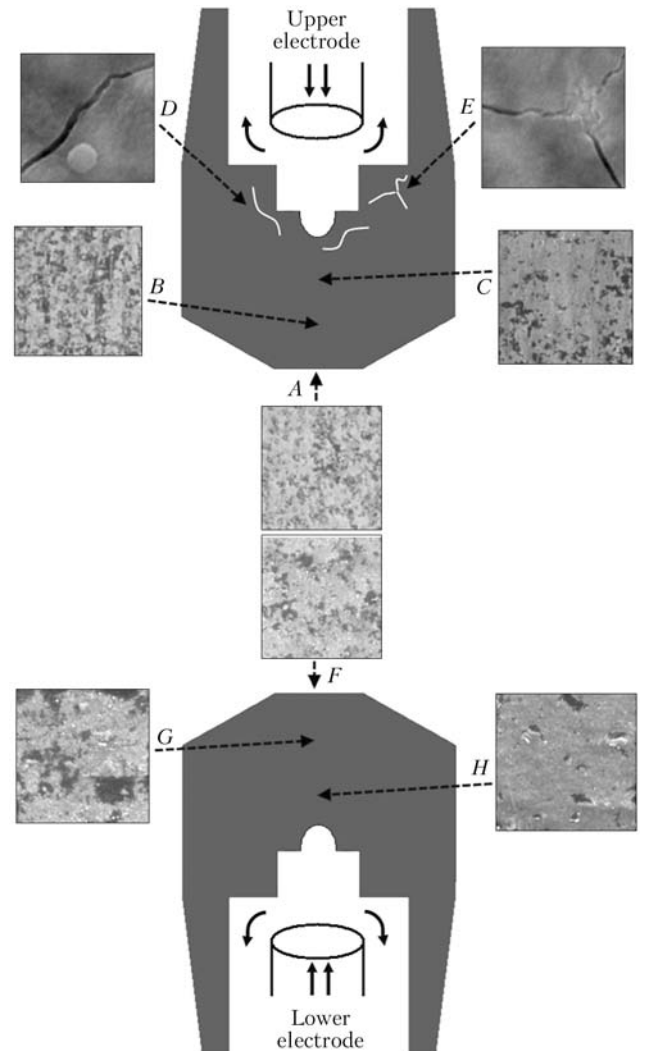
Figure 6. Electrode microstructural view

lead to the way to electrode holder, which are also exposed to thermal flow but cooled by internal water flowing. Thus, chromium-to-copper ratio is gradually diminished from point A to point C. The microstructural views reveal that the chromium precipitation is higher at the cap tip (point A) due to direct exposure of heat, which is above the threshold of melting points of Cu−Cr alloys (see Figure 1). Point B was, somehow, balanced of chromium-to-copper ratio, which is located between points A and C. However, the difference of cooling rates at point C due to water coolant (4 l/min) that flowing inside the electrode holders prevents chromium precipitation but resulted in internal cracks on the upper electrode cap. Lower electrode cap has similar effects (points F, G and H in Figure 6) that of the upper electrode cap had in terms of chemical properties changes but no internal crack is found because of its position as static during the welding process. Theoretically, the heated and cooled tip surfaces encounter the similar experiences that of annealing and quenching process caused in metal processing [15]. Annealing in Cu−Cr alloy can induce ductility over time [16]. Chemical distribution for Cu−Cr alloy has been graphically compared for both electrode caps and found similar patent of gradual precipitation of chromium out of the solid solution.

The electrode tip diameter was measured for every 100 weld attempts and it has been shown in Figure 8 to visualize the tip enlargement. The upper electrode cap mushrooming effect is slightly higher than the lower one because it has to bear the pressing forces (impact) while the squeezing process takes place every time. The severe deformation of electrode tips was noticed after underwent the first mushroom cleaning process. The diameter of tip was increased beyond 7 mm after underwent 900 welding attemps for which it requires the increments of the combination of process controlling parameters (i.e. welding current, welding time and electrode force) [17].

Hardness distribution. Spot welding process reduces the hardness of the Cu−Cr electrode caps over time, particularly at the tip areas. This is possible because both the electrode tips are always working on the encapsulation of heat generation as for the weld formation [18]. Once the faying surfaces of metals are fused together and formed new composite of phases or so, the electrode caps ensure that the holding force is enough to avoid any escape of molten metals or to avoid over pressure at the molten areas [19]. So this behaviour is clearly subjected to the closed contact with metals being welded without producing
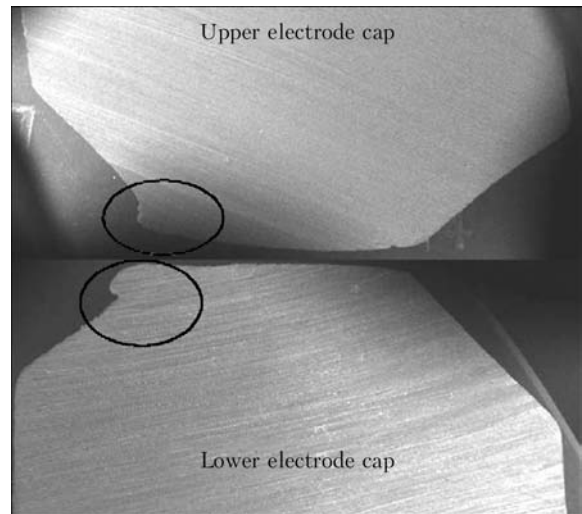
Figure 7. Macrograph view of electrode caps after underwent one-sided detoriaration

asperity [20]. Here, the hardness is what matters for, and hence both, the upper and lower electrode caps are measured for hardness distributive patterns. Hardness distribution is shown in Figure 9 as 10 measuring points are considered for each of the electrode caps separately. The 30°-truncated electrode caps are then measured along the cone areas approximately for the first 4 mm of distance (see a and b in Figure 9). Meanwhile the letter A and B represent the vanished portions and thereby no results found for these portions. It should be certainly noted once again here that the average hardness of brand new, class two Cu−Cr alloy is around HRB 70. This value is significantly reduced at the tip areas and ascending gradually with increase of distance from tips towards its rear portions. This pattern (see Figure 9) supports the previous findings that the chromium precipitation is higher at the tips, as long as the rear portions are compared regardless of upper or lower position of electrode place-
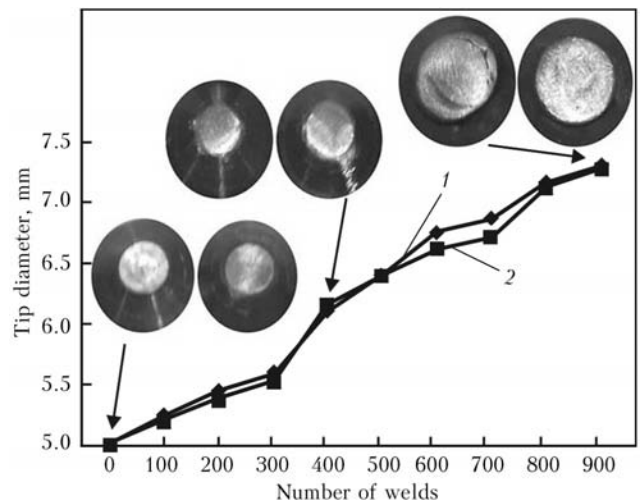
Figure 8. Electrode cap physical changes due to mushroom cleaning process: *1* — upper tip; *2* — lower tip
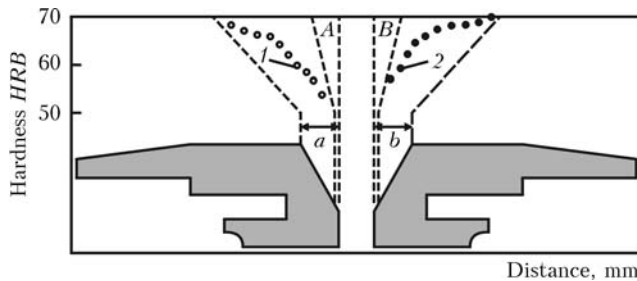
Figure 9. Electrode cap hardness distribution after 900 weld attempts: *1, 2* — points of hardness measurement of upper and lower electrode cap, respectively; $A \approx 0.22$; $B \approx 0.21$; $a, b = 4$ mm

ments. However, the hardness reduction is still slightly higher in upper electrode cap as compared to lower one. So, with this magnitude of analysis, a conclusion is drawn that the hardness of electrode cap tips (Cu–Cr alloy) reduce and deform themselves over number of repetitive welding processes in welding carbon, stainless and mixed steels [21].

Conclusions

1. Precipitation of chromium out of the solid solution is higher at the electrode cap tips, as compared to its rear portions. This happens due to the frequent encapsulation of heat generation for the spot weld formation.

2. Precipitation of chromium out of the solid solution leads to deterioration of tip surfaces as well as degrading themselves.

3. Initial welding processes up to 400 times increases the electrode tip diameter about 23 % of its original value due to mushrooming effects.

4. Further welding processes up to 500 times more (after the initial 400 times) increase the electrode tip diameter to another 26 % of altered value, even after the accomplishement of sharpening of electrodes are done.

5. In overall, 49 % of its original value (5 mm) of upper electrode tip diameter increment is noticed whereas the lower electrode tip diameter increment is about 44 %.

6. Hardness of the upper electrode cap tip is reduced to approximately *HRB* 54 as compared to its original value of *HRB* 70.

7. Hardness of the lower electrode cap tip is reduced to approximately *HRB* 57 as compared to its original value of *HRB* 70.

1. Bower, R.J., Sorensen, C.D., Eager, T.W. (1990) Electrode geometry in resistance spot welding. *Welding J.*, **2**, 45–51.
2. Babu, S.S., Santella, M.L., Peterson, W (2000) *Modelling resistance spot welding electrode life*. ORNL.
3. Yeung, K.S., Thornton, P.H. (1999) Transient thermal analysis of spot welding electrodes. *Welding J.*, 1–6.
4. Chakrabarti, D.J., Laughlin, D.E. (1984) The chromium–copper (Cu–Cr) system. *Bull. of Alloy Phase Diagrams*, 5(**1**).
5. Chen, Z., Zhou, Y., Scotchmer, N. (2005) Coatings on resistance welding electrodes to extend life. *SAE Int.*, 1–4.
6. Nachimani, C. (2012) Effect of spot welding variables on nugget size and bond strength of 304 austenitic stainless steel (2 mm). *Australasian Welding J.*, **57**, 39–44
7. Nachimani, C., Farazila, Y., Rajprasad, R. (2014) Material characterizations of mild steels, stainless steels, and both steel mixed joints under resistance spot welding (2-mm sheets). *Int. J. Advanced Manufact. Techn.*, 75(**1–4**), 373.
8. Rao, Z.H., Liao, S.M., Tsai, H.L. et al. (2009) Mathematical modeling of electrode cooling in resistance spot welding. *Welding J.*, 111–119.
9. Elise, G., Denis, C., Philippe, R. et al. (2014) Numerical modelling of electrode degradation during resistance spot welding using CuCrZr electrodes. *J. Materials Eng. and Perform.*, 23(**5**), 1593–1599.
10. Chang, B.H., Zhou, Y. (2003) Numerical study on the effect of electrode force in small scale resistance spot welding. *J. Materials Proc. Techn.*, **139**, 635–641.
11. Babu, S.S., Joseph, A. (2010) Carpenter long-life electrodes for resistance spot welding of aluminum sheet alloys and coated high-strength steel sheet. *Automotive Lightweighting Materials*, 229–236.
12. Luo, P., Dong, S., Xie, Z. et al. (2014) The effects of coating parameters on the quality of TiB–TiC composite phase coating on the surface of Cu–Cr–Zr alloy electrode. *Surface and Coatings Techn.*, **253**, 132–138.
13. Li, Y.B., Wei, Z.Y., Li, Y.T. et al. (2013) Effects of cone angle of truncated electrode on heat and mass transfer in resistance spot welding. *Int. J. Heat and Mass Transfer*, **65**, 400–408.
14. Bayraktar, E., Moiron, J., Kaplan, D. (2006) Effect of welding conditions on the formability characteristics of thin sheet steels: Mechanical and metallurgical effects. *J. Materials Proc. Techn.*, **175**, 20–26.
15. Primoz Podrzaj, Samo Simoncic (2014) A machine vision-based electrode displacement measurement. *Welding in the World*, **58**, 93–99.
16. Wei, P.S., Wu, T.H. (2014) Effects of electrode contact condition on electrical dynamic resistance during resistance spot welding. *Sci. and Techn. of Welding and Joining*, 19(**2**), 173–180.
17. Wei, P.-Sh., Wu, T.-H., Chen, L.-J. (2013) Joint quality affected by electrode contact condition during resistance spot welding. *IEEE Transact. on Components, Packaging and Manufact. Techn.*, 3(**12**), 2164–2173.
18. Aravinthan, A., Nachimani, C. (2011) Analysis of spot weld growth on mild and stainless steel (1 mm). *Welding J.*, **Aug.**, 143–147.
19. Pouranvari, M., Marashib, S.P.H. (2010) Failure mode transition in AHSS resistance spot welds. Pt 1: Controlling factors. *Materials Sci. and Eng. A*, **528**, 8337–8343.
20. Feramuz, K. (2009) The effect of process parameter on the properties of spot welded cold deformed AISI 304 grade austenitic stainless steel. *J. Materials Proc. Techn.*, **209**, 4011–4019.
21. Dursun, O. (2008) An effect of weld current and weld atmosphere on the resistance spot weld ability of 304L austenitic stainless steel. *Materials and Design*, **29**, 597–603.

CALCULATION OF SIZE
OF STRUCTURAL CONSTITUENTS OF METAL
DEPOSITED BY INDUCTION METHOD
WITH APPLICATION OF MECHANICAL VIBRATION

V.S. SENCHISHIN and **Ch.V. PULKA**

Ternopol Ivan Puluj National Technical University, MSEU
56 Russkaya Str., 46001, Ternopol, Ukraine. E-mail: Viktor_Synchyshyn@i.ua

Possibility of regulation of structure of deposited metal allows improving service properties of the parts. Present work studies the processes of refining of structure of deposited metal at application of horizontal mechanical vibration. Calculation model for determination of parameters of metal structure of PG-S1 type alloy, deposited by induction method applying mechanical vibration, was developed. Graphic dependencies of carbide constituents in the deposited metal on vibration amplitude and frequency were plotted based on received relationships. 9 Ref., 5 Figures.

Works [1–3] tried to develop a quantitative theory of effect of parameters of mechanical vibration on solidification of metal melts. The calculations were based on ideas of authors of work [4] on evaluation of breaking of coagulation structures in electrolytes by vibration field. Present work also uses data of these investigations [4] in development of mathematical model for refining of structure of deposited metal of high-carbon chromium PG-S1 type alloy (sormite 1) by vibration field.

Calculation model for evaluation of effect of vibration parameters on structure of deposited metal. Work [5] based on results of experimental investigations showed that application of mechanical vibrations during surfacing can have ambiguous effect on characteristics of deposited metal. Aim of the present work is development of mathematical model, which allows determining optimum values of vibration amplitude and frequency using calculation method. They will provide the best service characteristics of deposited metal. Size of carbide inclusions in deposited metal is taken as optimality criterion.

Let us consider (Figure 1) substrate–metal melt on substrate system, which vibrates along the deposit surface with frequency ω and amplitude *a*. The thickness of metal melt is regarded as relatively small [5].

Groups of metal particles joined in clusters as a result of coagulation, i.e. adhesion of these particles (see Figure 1), are formed in molten metal in surfacing. Particles, representing themselves small clusters (≥0.1 μm), are joined in larger on size (≤100 μm). This process takes place in the following way [6]. Molten metal is considered as electrolyte. Forces of different nature (Figure 2) act between the particles of molten metal. Approaching of disperse phase particles promotes for disjoining pressure of metal liquid which is between them. This pressure is determined by molecular attracting forces and electrostatic repulsive forces. Attracting forces are Van der Waals forces, which consist of forces of orientation, induction and dispersion interaction. Repulsive forces appear in overlapping of particle diffusion layers.

Condition of the system is determined by balance of attraction and repulsive energies, which is determined by equation

$$U = Be^{-kh} - Ah^{-2}, \qquad (1)$$

where *U* is the sum energy of particle interaction; *B* is the multiplier depending on value of electric
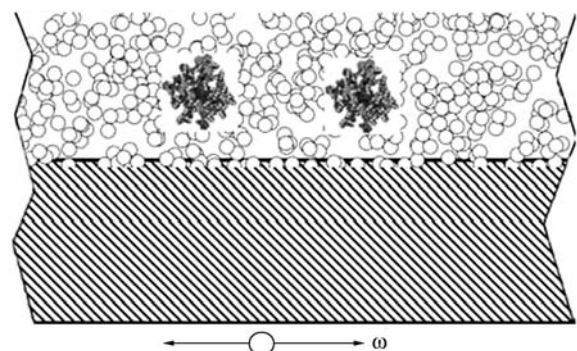

**Figure 1.** Scheme of formation of clusters in surfacing with vibration
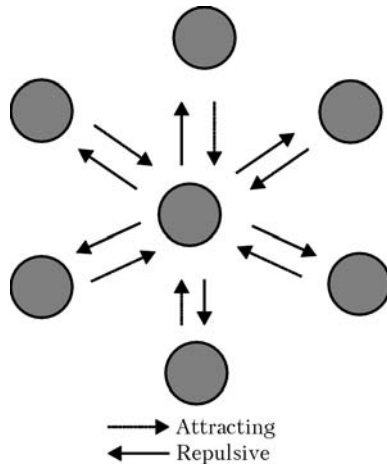
Figure 2. Force action between the particles in metal melt

potentials, properties of environment, and temperature; k is the value inverse to diffusion layer thickness; h is the distance between particles; A is the constant of molecular attracting forces (Hamaker constant). Sum energy U will be negative (secondary potential minimum) at large distances between the particles. Energy U at average distances (around 100 μm) will be positive, that means formation of energy barrier, i.e. electrostatic repulsive forces prevail at this distance. At close distances with prevailing attractive forces, sum energy U of interaction of particles will be positive (primary potential minimum). If energy, which corresponds to potential barrier, is lower than kinetic energy of particles, then they can overcome electrostatic repulsive forces and approach to very small distance (overlapping of double electric layers take place), at which molecular attractive forces prevailing.

Particles are stuck together as a result (i.e. fall in the closest potential well) (Figure 3). This deep potential well explains mechanical strength of coagulate. The particles at close distances are bonded due to Van der Waals forces, and formed aggregates acquire some properties of solid body. If energy barrier is high, the particles can not overcome it and develop aggregates.
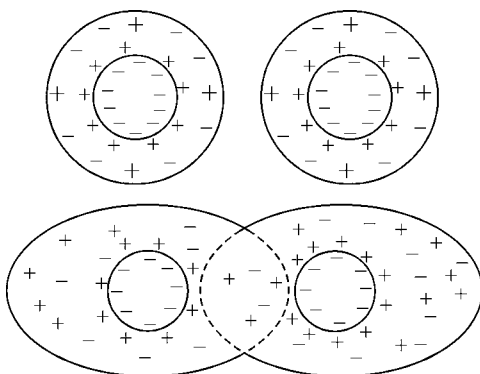
Figure 3. Overlapping of double electric layers and adhesion of particles in melt

Reduction of energy barrier decreases aggregate resistance of the system. For example, adding of electrolyte can reduce thickness of diffusion layer and, thus, decreasing repulsive forces so that energy barrier will escape and particles stick to each other at approaching.

Thus, there are primary and secondary potential wells, depth of which is marked by potential constituents E_1, E_2 and width by h_1 and h_2, respectively. Movement of particles of diameter D in the vicinity of each potential maximum is represented as oscillations of harmonic oscillator respectively to own frequencies f_1, f_2, which are found based on solution of Schroedinger equation [4, 7] approximated in the following way:

$$f_1 \approx \sqrt{E_1 h_1^{-2} m^{-1}}, \quad f_2 \approx \sqrt{E_2 h_2^{-2} m^{-1}}, \qquad (2)$$

where E_1, E_2 values are determined based on [4] in such a way:

$$E_1 = nBD[0.04 h_1^{-1} - 0.5 A_0(1 - \ln(12 A_0 h_1 A^{-1}))],$$
$$E_2 = nBD h_2^{-2}(0.5 - \lambda^{-1} h_2^{-1}), \qquad (3)$$
$$\lambda = \sqrt{8\pi q^2 N \varepsilon^{-1} T^{-1}}.$$

In this case A_0, A, B are the constants which depend on system properties [4]; n is the number of particles in structure which are close to the considered; N is the electrolyte concentration (molten metal); T is the temperature in energy units; q is the charge of electrolyte ions; ε is the dielectric constant; m is the particle mass.

Under static conditions criterion of structure stability will be determined [4] by such inequality:

$$E_1 > 0.5(\rho_0 - \rho)D^3 g h_1,$$
$$E_2 > 0.5(\rho_0 - \rho)D^3 g h_2, \qquad (4)$$

$$E_1 > \beta T, \quad E_2 > \beta T. \qquad (5)$$

Here ρ_0, ρ are the density of dendrite and molten metal, respectively; g is the gravitation acceleration; $\beta \approx 1$.

Let us consider effect of vibration on structure of molten metal, when dendrites of larger size H are formed in it from average size clusters, that in given case corresponds to inequality

$$H^2 >> \eta \omega^{-1} \rho^{-1}, \qquad (6)$$

where η is the average dynamic toughness of molten metal.

Such big aggregates are not going to oscillate in molten metal. Further, oscillations of melt with amplitude a and frequency ω are recoded. At that, rate $\dot{x}(t)$ of oscillation of melt along the deposit surface on coordinate x can be written in the following way:

$$\dot{x}(t) = a\omega \sin \omega t. \qquad (7)$$

Then power P, acting on such moving particle of diameter D, will be determined according to [4, 8] in such a way:

$$P \approx \eta D^2 h_i^{-1} a\omega. \qquad (8)$$

Taking into account mentioned above, equation of forced vibrations of studied dendrite particle is written respectively in the primary potential well (primary coagulation) under effect of vibration and external force in such a form [4, 7]:

$$\ddot{x} + 2\xi\dot{x} + f_1^2 x = Pm^{-1} \sin \omega t. \qquad (9)$$

In this case $\xi \approx n\eta D^2 m^{-1} h_1^{-1}$.

Linear differential equation of the second order with constant coefficients (9) is solved via representation of the required function $x(t)$ in trigonometric form. As a result the next law of particle oscillation in dendrite volume is received:

$$x(t) = V_0 \sin (\omega t + \alpha_0), \qquad (10)$$

where it is formally taken that initial phase α_0 equals zero and amplitude V_0 of forced oscillations of the particle equals

$$V_0^2 = P^2 m^{-2}[\omega^2 - f_1^2)^2 + 4\xi^2\omega^2]^{-1}. \qquad (11)$$

If particle of diameter D jumps out from the potential well in vibration, than physically it means that dendrite consisting of such particles will start to collapse. It is possible only if amplitude V_0 of its oscillations is larger than width of the primary potential well h_1, i.e. it comes out of the limits of effect of surface force, or receive such energy, which exceeds depth of potential well E_1, and moves as in absence of surface forces. Based on relationships (3), (8) and (11) these conditions can be written mathematically in such a form:

$$V_0 \geq h_1, \qquad (12)$$

$$mV_0^2\omega^2 \geq E_1. \qquad (13)$$

P and V_0 are represented according to (8), (11) in (12), (13), as a result of what the following is received:

$$\omega^4 - \omega^2(2f_1^2 - 4\xi^2 + \eta^2 D^4 m^{-2} a^2 h_1^{-4}) + f_1^4 \leq 0, \qquad (14)$$

$$(E_1^{-1}\eta^2 m^{-1} D^4 h_1^{-2} a^2 - 1)\omega^4 + \\ + (2f_1^2 - 4\xi^2)\omega^2 - f_1^4 \geq 0. \qquad (15)$$

Solution of inequality (14), (15), taking into account (2) and assuming that $m \approx 0.5\rho D^3$ and

ω is always constant, promotes receiving of the following relationships for evaluation of vibration parameters for earlier selected values of diameter D of the particles for which dendrite is decomposed:

$$\omega^2 \leq 0.5(2f_1^2 - 4\xi^2 + 4\rho^{-2}D^{-2}\eta^2 a^2 h_1^{-4}) + \\ + \sqrt{0.25(2f_1^2 - 4\xi^2 + 4\rho^{-2}D^{-2}\eta^2 a^2 h_1^{-4})^2 - f_1^4}; \qquad (16)$$

$$a^2 \geq \frac{f_1\rho^2 D^2 h_1^4[\omega^4 - (2f_1^2 - 4\xi^2)\omega^2 + f_1^4]}{4\eta\omega^4}.$$

Thus, if characteristics of molten metal f_1, g, ρ, η, h_1 are set, than corresponding parameters of vibration ω and a based on relationships (16) can be found for set grain size D of structure of deposited metal.

Calculation of parameters of structure of deposited metal. Investigations of structure of metal deposited by induction method without and with application of vibrations [5] were carried out for verification of correctness of stated model.

Flat specimens from steel St3 were deposited (Figure 4) with horizontal vibration and without it for performance of investigations by induction method using charge containing powder of PG-S1 alloy. The surfacing was carried out using high-frequency generator of VChG-60/0.44 type at constant specific power W and time of surfacing t. The modes were similar for two surfacing variants, i.e. anode voltage 10 kV; circuit voltage 5.4 kV; current of lamp grid 2.2 A; lamp anode current 2 A; surfacing time 35 s; oscillating amplitude 0.2 mm at 50 Hz frequency.

Electrolytic method (etching in 20 % solution of chromium acid, voltage 20 V and holding time 10 s) was used for determination of structure of deposited metal. Structure of the base metal was discovered by chemical etching in 4 % solution of nitrogen acid. It is determined that carbides in metal deposited without vibration have 10−
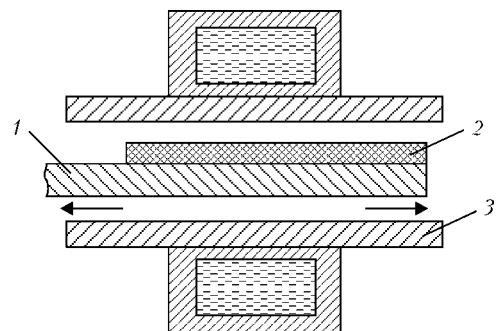

Figure 4. Scheme of induction surfacing: *1* — deposited part; *2* — powdered charge; *3* — inductor (arrows show direction of horizontal vibration)
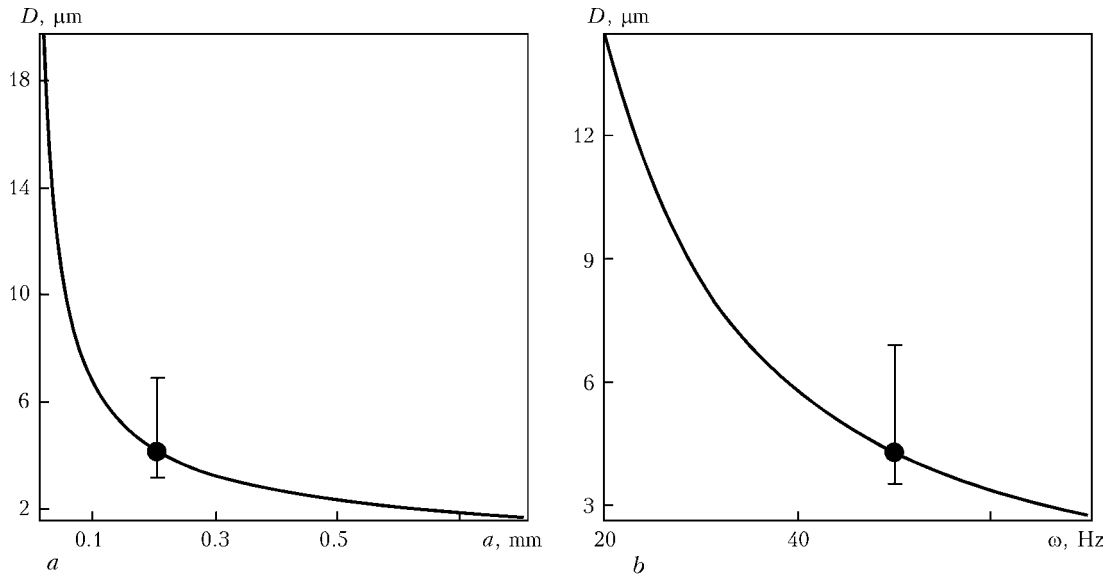
Figure 5. Dependencies of carbide size D on amplitude a (a) and frequency ω (b) of vibration

12 μm size, and if horizontal vibrations are applied they are refined to 3.5–7.0 μm size.

The results were compared with calculation ones by model given above. The following approximated averaged values of characteristics in relationships (16) are given for this purpose for high-chromium alloy based on reference data [4, 9]:

$$\rho = 7.8{\cdot}10^{-6}\ \frac{kg}{mm^3}; \quad \eta \approx 7{\cdot}10^{-6}\ \frac{kg}{mm{\cdot}s}; \quad (17)$$

$$\omega = 60\ Hz; \quad f_1 \approx 2{\cdot}10^3 D^{-1}\ Hz;$$

$$\xi \approx 2{\cdot}10^6 D^{-1}\ Hz; \quad h_1 = 2{\cdot}10^{-6}\ mm.$$

Dependencies D–a and D–ω are plotted for more obvious representation of dependence of size D of carbide inclusions on vibration parameters a and ω. Only second relationship (16) was used for that. Considering that $f_1^4 > \omega^4 - (2f_1^2 - 4\xi^2)\omega^2$, the second relationship can be represented approximately as

$$D^3 \geq \frac{8{\cdot}10^{15}\rho^2 h_1^4}{a^2\eta^2\omega^4}. \quad (18)$$

Equation of dependencies D–a ($\omega = 50$ Hz) and D–ω ($a = 0.2$ mm) based on relationship (18) is written in such a form:

$$D \approx 1.45 a^{-2/3}\ \mu m, \quad D \approx 785\omega^{-4/3}\ \mu m. \quad (19)$$

Graphical dependencies D–a and D–ω are plotted based on relationships (19) (Figure 5). The circle on diagrams mark coordinates, where matching of calculation and received in work [5] values of size of carbides on set vibration parameters is observed. This indicates correctness and sufficient accuracy of proposed calculation model. Figure 5 shows that increase of vibration parameters a and ω promotes for significant reduction of carbide size D.

Thus, applying relationships (16) and (17) the previously set values of vibrations parameters a and ω can be chosen, using which desired structure of deposited metal layer can be produced.

1. Bugaj, Yu.M., Pitulej, L.D., Fedenchuk, D.I. (2000) Mathematical model of sedimentation-vibration equilibrium of armitors of composite picks of roller bit. *Metody ta Prylady Kontrolyu Yakosti*, **6**, 100–102.
2. Kryzhanivsky, E.I., Pitulej, L.D., Fedenchuk, D.I. (2005) Influence of vibration on crystalline structure of bit steel. *Nauk. Visnyk NTUNG*, 12(**3**), 26–30.
3. Petryna, Yu.D., Pitulej, L.D., Fedenchuk, D.I. (2005) Influence of reinforced melt vibration on crystalline structure of matrix bit steel. *Rozvidka ta Rozrobka Naft. i Gaz. Rodovyshch*, 16(**3**), 15–19.
4. Potanin, A.A., Uriev, N.B. (1988) Condition of fracture of coagulation structure by vibration field and aggregability criterion. *Teoret. Osnovy Khim. Tekhnologii*, **4**, 528–534.
5. Pulka, Ch.V., Shably, O.N., Senchishin, V.S. et al. (2012) Influence of vibration of parts on structure and properties of metal in surfacing. *The Paton Welding J.*, **1**, 23–25.
6. Tutorsky, I.A. (2008) *Introduction to colloid chemistry*. Pt 4: Electric surface properties of dispersion systems. Stability and coagulation of colloid systems. Moscow: MITKhT.
7. Landau, L.D., Lifshits, E.M. (1965) *Mechanics*. Moscow: Nauka.
8. Deryagin, B.V., Churaev, N.V., Muller, V.M. (1985) *Surface forces*. Moscow: Nauka.
9. Kabachny, V.I., Osypenko, L.K., Grytsan, L.D. et al. (1999) *Physical and colloid chemistry*. Kharkiv: Prapor.

APPLICATION OF PULSE WELDING POWER SOURCES IN ELECTROCHEMICAL PROCESSES

A.M. ZHERNOSEKOV and **V.M. KISLITSYN**

E.O. Paton Electric Welding Institute, NASU

11 Bozhenko Str., 03680, Kiev, Ukraine. E-mail: office@paton.kiev.ua

It was determined that area of application of pulse welding power sources for processes of metal flame treatment can be expended. At that continuously rising in price natural gas is substituted by hydrogen-oxygen mixtures or hydrogen. Application of nickel instead of low-carbon steel as electrodes at water electrolysis allowed reducing process voltage to 2.1 V. Dependence of increase of percent content of finer powder fractions (1–50 μm and 1 μm, and less) at increase of frequency of current of anode dissolution was determined. Received results indicate perspectives of investigations in this direction for increase of efficiency of electrochemical processes of hydrogen production as well as micro- and nanopowders for manufacture of welding and brazing powder consumables. 12 Ref., 3 Figures.

Pulse power sources for gas-shielded metal arc welding are widely used in such branches of industry as shipbuilding, chemical-machine building, rocket production, car industry, pipeline construction and many others [1, 2]. Frequency of transfer of electrode metal droplets is an important parameter among the different parameters for regulation of process of pulse-arc welding and it usually lies in 30–300 (500) Hz range. Smooth regulation of frequency of welding current pulses allows electrode metal transfer by principle «1 pulse-1 droplet». The E.O. Paton Electric Welding Institute works on development of equipment and technology of pulse-arc processes for a long time. Different types of welding equipment were developed including power sources for pulse-arc welding. They showed themselves good in welding of critical designation structures [3, 4]. The main peculiarities of such sources are possibility of smooth regulation of frequency of current pulses from 30 to 300 Hz, duration of pulses 0.5–5.0 ms and amplitude to 850 A.

Power sources are used in related technologies, for example, in production of hydrogen-oxygen mixtures for processes of welding, brazing, welding-brazing and operations of flame treatment of metals. Gas generators in indicated processes consist of direct current welding source and electrolytic cell. Possibility of dramatic reduction of consumption of continuously rising in price natural gas and decrease of environment pollution are the advantages of application of

hydrogen and hydrogen-oxygen mixtures in flame treatment processes.

Besides, one of the variants of significant reduction of costs for welding and brazing consumables are the possibility of in-situ production, for example, of braze pastes of necessary composition with guaranteed quality, by methods of electrochemical dispersion of ferrous, nonferrous and noble metals. Therefore, it is relevant to carry out experimental investigations on increase of efficiency of electrochemical processes due to regulation (increase) of current frequency.

The most repeatable in final result processes were selected for performance of experimental investigations of effect of current frequency on some electrochemical processes. First of all, these are the processes essential for power engineering of future, for example, production of hydrogen by water electrolysis. Secondly, the processes of micropowder production, including nanopowders, can be referred to them. The latter proved their perspectives in area of metallurgy as well as many other areas of technology and medicine.

Regardless apparent versatile of considered processes, they are combined by similar conditions for realizing electrochemical reactions taking place in aquatic environment on the surface of electrodes being connected to DC sources.

Among the significant differences of these processes are the parameters of their performance, for example, composition of aquatic environments, electrode materials, parameters of power sources (voltage, current and frequency), and final products, obtained as a result of these processes.

Currently, around 95 % of hydrogen in all countries of the world are produced with the help of catalytic conversion of water steam or methane reforming. However, hydrogen produced by

these methods, is not suitable for supplying fuel cells transforming chemical energy in electric one, for example, in vehicle motor drive. Fuel cells require hydrogen of high purity, for example, produced from water via electrolysis.

Electrolytic hydrogen is more expensive than catalytic one due to high expenses for providing explosive and electric safety at its production as well as significant specific expenses for electric energy.

Development of new type of electolyzers allowed eliminating one of the main obstacles to wide application of hydrogen. They provide high level of explosive and electric safety in production of hydrogen as well as hydrogen-oxygen mixture [5, 6]. A problem of reduction of power consumption necessary for production of electrolytic hydrogen is still unsolved.

The most widespread methods of production of micro- and nanopowders of metals or their oxides are spark and electro-explosive dispersion [7], spraying of liquid metal by water and gas jet or condensing of metal vapors in its heating using electron beam, high-frequency plasma [8], or laser.

These processes are characterized by high power consumption related with necessity of metal heating well above than its melting temperature. In this connection application of micro- and nanopowders, produced by these methods, can be economically sound only in special cases, for example, in research projects and in medicine, where necessity in micro- and nanopowders is measured in grams, but not in widely used technological processes, for example, welding and brazing, requiring hundred of kilograms. Moreover, application of mentioned above processes for production of micro- and nanopowders is justified only under condition of efficient solution of the problem of their production in monodisperced form, that allowed eliminating laborious operation on dispersion of produced product by fractions.

Aim of the present work is an investigation of effect of frequency of electrolysis current on

efficiency of electrochemical processes mentioned above.

Existing equipment used for realizing electrolytic method of hydrogen production has a coefficient of transformation of electric current energy into chemical one at 70 % level. Currently, there is a possibility of improvement of this index to 80 % and more not only due to increase of pressure and application of low-wear anodes with coatings from metals of platinum group, but as a result of application of modern power sources for electrolysis processes. This allows reducing prime cost of electrolytic hydrogen.

Experimental verification of idea of electrolysis using increased frequencies was carried out with the help of power sources for pulse-arc welding developed at the PWI.

A research bench in addition to measurement and controlling equipment included pulse power supply providing electrolysis current up to 300 A and electrolyzer consisting of 10–12 series electrolytic cells.

Experiments on determination of effect of frequency of current pulses on process of water electrolysis carried at the PWI more than 10 years ago showed the possibility of efficiency increase due to reduction of electrolysis voltage from 2.4 to 2.16 V [9]. These results were received on electrolytic cell using low-carbon steel electrodes. Water electrolysis at increased frequency using more expensive metals, for example, nickel as the electrodes, allowed reducing electrolysis voltage to 2.1 V (Figure 1).

Based on diagram given, insignificant, from first point of view, reduction of electrolysis voltage can promote notable economy of electric energy in processes of receiving of electrolytic hydrogen, due to volumes of its production measured as million of tons per year.

In the case of application of direct current with pulsation, typical for power sources with simple rectification circuits (Larionov connection and bridge connection), process of anode dissolution of the most projecting electrode areas, i.e. some kind of polishing of electrode working surface, is observed, in addition to products of electrolysis appearing on the surface of electrodes. At that, its passivation takes place due to formation on it of oxide films, dissolved gases and chemical compounds increasing electric resistance of electrode surface. Compensation of gradual increase of electrolytic cell voltage requires periodic switching-off of electrolyzers and depolarizing of the electrodes by means of change of voltage polarity on cell.

Analysis of the processes taking place in our case on the surface of electrode at water electrolysis allowed noting inevitable appearance of electric current streamers (lines of the most probable break-
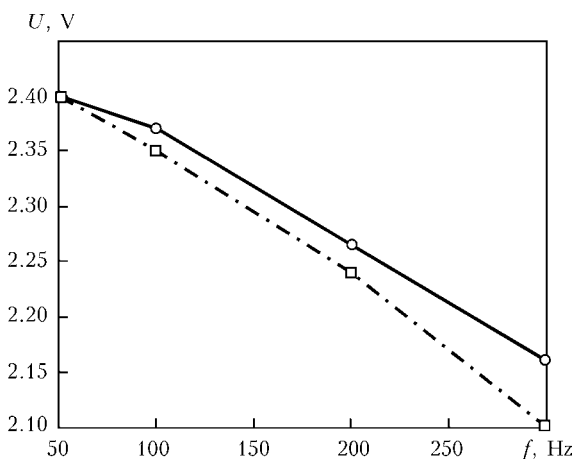

Figure 1. Electrolytic cell voltage versus frequency of current pulses for low-carbon steel (*solid*) and nickel (*dashed line*)

down of dielectric environment, to which water and aqueous solutions of salt are referred) in the zone of double electric layer (DEL) in addition to oxidation-reduction reactions tacking place close to the surface of electrode.

Highly possible that experimentally determined advantages of application of HF currents in processes of electrolysis and anode dissolution of metals can be explained based on proposed model of electrolysis process (Figure 2).

Arrows in Figure indicate the lines of desirable movement of electric current directed to projections of electrode rough surface. Similar processes to be place on projections of cathode surface, where dissolution of hydrogen in metal and increase of thickness of layer of adsorbed hydrogen occur. The level of electric field of applied voltage is not always enough for breakdown of the latter. In this case DEL thickness is risen, where the main drop of voltage on electrolytic cell takes place. Further screening of deepened places of electrode surface by layer of adsorbed gases provokes the necessity of additional increase of electric field voltage.

Rapid increase of temperature in microzones of electrode, in which current density rises, is accompanied by local heating of the surface, that results in appearance of impact mechanical waves in electrolyte and intensive detachment of hydrogen molecules from cathode and revealing of its working surface as well as films of metal oxides forming on anode surface.

Pauses between the pulses of current in the case of electrolysis using pulses of current of increased frequency results in the fact that average value of voltage on electrolytic cell is lower in application of increased frequency (50–100 Hz) regardless the increased voltage of each separate pulse.

Investigations of processes of oxygen emission on anode surface always had more attention than processes of hydrogen emission due to preferred anode electrochemical dissolution. At that, known fact of more intensive heat emission on cathode than on anode was not taken into account, that indicates the necessity of more detailed consideration of processes taking place particularly on cathode.

Reference data [10, 11] show that value of hydrogen overpotenial at electrolysis of water solutions mainly depends on cathode material and electrolysis current density. Increase of current density results in cathode covering by layer of adsorbed hydrogen for several tens of seconds in process of electrolysis. Its is accompanied by increase of electrolysis voltage due to rise of transition resistance on metal–electrolyte boundary. Parallel processes of increase of oxide film thickness take place on anode.
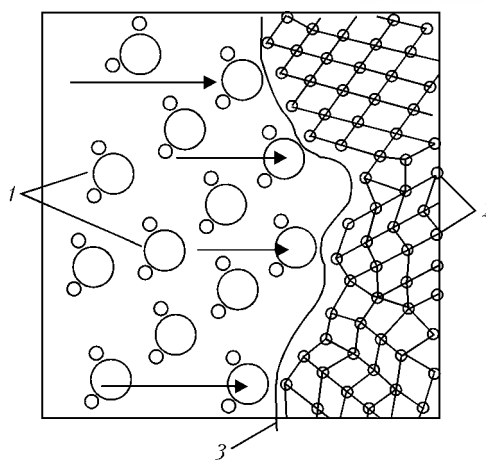
Figure 2. Scheme of processes taking place on surface of electrode in water electrolysis: *1* — water molecules; *2* — atoms of metal electrode; *3* — DEL boundary

Experiments showed that using pulse current with inverted pulses at zero-crossing provokes cathode potential jump. Probably, this is the fact resulting in formation of new adsorption centers and redistribution of adsorbed gas bubbles. At that the largest hydrogen bubbles, which are removed from electrolyte volume, are detached from the cathode surface. Emission of hydrogen at the next electrolysis current pulse will be the most intensive in the new zones on cathode surface, generated in process of depolarization, moreover at lower value of power source voltage.

Primary importance in this case is not in reduction of voltage, promoted by pulsation, typical for simple rectifiers with supply from alternating current main, but complete stop of electrolysis current achieved at voltage drop to zero. Obviously that presence of insignificant peak of negative voltage will also promote removal of gaseous sublayer on cathode surface that provides for reduction of overpotential level.

Technological experiments on brazing of samples from copper and brass [12] showed the perspectives of application of braze pastes based on micropowders for production of joints from metals of 40–1000 μm thickness range.

Results of further experiments indicate that braze pastes based on micropowders, in comparison with pastes based on powders with particles of 40 μm size and more produced by conventional methods, have series of advantages, namely, possibility of reduction of heating temperature in brazing for 50–70 degrees and decrease of brazing time, that is relevant for joining of materials critical by heating temperature; shortening of consumption of braze alloy and flux not less than by 20 %; expansion of range of thickness of materials being joined to 40 μm and less.

Advantages of application of increased frequency current were also found in processes of electrolytic dissolution of anode metal in aqueous
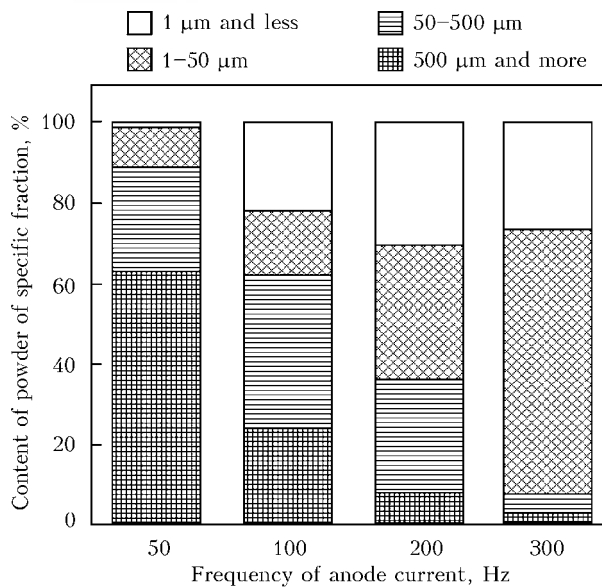
Figure 3. Effect of current frequency in dissolution of nickel anode on micropowder size

environment and alcohol solution. First of all, they include possibility of increase of level of powder monodispersity, secondly, it is the possibility of reduction of energy consumption of dispersion processes, in comparison with methods characterized by heating of metal above its melting point.

Copper M1, nickel NP2 and silver of 99.9 purity (precious metal) were used in dispersion. Moreover, each of dispersion variants were carried out in 50–300 Hz frequency range as well as 10 kHz frequency (at silver dispersion).

It was determined in course of experiments that electrolytic (anode) dissolution of metals result in formation of microparticles of different size, which are conditionally divided on following groups: a — 500 μm and larger; b — 500–50 μm; c — 1–50 μm; d — 1 μm and less.

Mass of powders of grain size up to 50 μm was determined using the method of sampling of powder with corresponding grain size on sieving machine having set of control grading screens. Procedure based on calculation of number of grains at visual measurement of their sizes by hair lines of microscope graticules at 1800 magnification (in immersion liquid), respectively, was used for finer fraction powders. This procedure is used at determination of grain size of diamond powders.

Results of carried experiments were used for plotting the histogram of different fractions of micropowders depending on current frequency at anode dissolution of metal (Figure 3).

Dependence of increase of percent content of powder finer fractions at increase of current frequency of anode dissolution can be seen from histogram given.

Carried experiments on silver anode dissolution showed possibility of production of micro-

powder suspension of its oxides of less 1 μm dispersion. However, one of significant disadvantages of process of silver dispersion in aqueous environment is susceptibility of received micro-powder to coagulation with further growth of separate crystallites of up to 2 μm length and around 2–5 μm width.

To eliminate indicated disadvantage a storage time of micropowders should not exceed one-two tens of hours from the moment of receiving to production of braze paste and its application in brazing process.

Conclusions

1. Using current increased frequency promotes rise of efficiency in process of electrolytic production of hydrogen-oxygen mixtures and hydrogen as well as increase of output of finer fraction metal powders for production of braze pastes.

2. Production of micropowders directly before brazing allows using them in active condition in form of monocomponent as well as mixtures of different metals.

3. Set of equipment consisting of power source of welding current of increased frequency and generator of hydrogen-oxygen mixture allows expanding its application range in flame treatment of metals as well as for processes of electrolytic dispersion of metals.

1. Zhernosekov, A.M., Andreev, V.V. (2007) Pulsed metal arc welding (Review). *The Paton Welding J.*, **10**, 40–43.
2. Zhernosekov, A.M. (2012) Tendencies in development of control of metal transfer processes in shielding gases (Review). *Ibid.*, **1**, 29–33.
3. Shejko, P.P., Pavshuk, V.M., Zhernosekov, A.M. et al. (2003) Power sources for pulsed metal-arc welding with automatic stabilizing of welding parameters. *Svarshchik*, **4**, 4.
4. Kudryashov, O.N., Novikov, O.M., Alekseev, I.V. et al. (2001) Welding of structures of aircrafts from thick aluminium alloys. *Svarochn. Proizvodstvo*, **12**, 31–33.
5. Lebedev, V.K., Rossoshinsky, A.A., Kislitsyn, V.M. et al. *Electrolytic tank for producing of oxyhydrogen gases from water and water solutions*. USSR author's cert. 507668. Publ. 27.04.76.
6. Pismenny, A.S., Kislitsyn, V.M. (1995) Prospects of development of flame treatment of materials by hydrogen-oxygen mixtures. *Avtomatich. Svarka*, **2**, 39–42.
7. Shcherba, A.A., Podoltsev, A.D., Kucheryavaya, L.N. et al. (2005) Spark-eroded particles: Size analysis, cooling rate, microstructure. *Tekhnich. Elektrodynamika*, **5**, 3–8.
8. (2014) Technology using microwave heating may impact electronics manufacture. *http://www.technology.org/2014/06/11/technology-using-microwave-heating-may-impact-electronicsmanufacture/*
9. Zhernosekov, A.M., Kislitsyn, V.M. (2007) Efficiency enhancement of gas generators of hydrogen-oxygen mixture. *The Paton Welding J.*, **4**, 51–52.
10. Lebedev, V.V. (1969) *Physical-chemical principles of producing of hydrogen from water*. Moscow: Nauka.
11. Fioshin, M.Ya., Pavlov, V.V. (1976) *Electrolysis in inorganic chemistry*. Moscow: Nauka.
12. Pismenny, A.S., Shvets, V.I., Kuchuk-Yatsenko, V.S. et al. (2008) On issue of brazing metals using powder braze alloys of different dispersity. *The Paton Welding J.*, **12**, 34–36.

EXPERIENCE OF INTRODUCTION
OF THE TECHNOLOGY OF RECONDITIONING
MICROPLASMA POWDER SURFACING
AT REPAIR OF HIGH-PRESSURE TURBINE BLADES
IN BATCH PRODUCTION

P.D. ZHEMANYUK, I.A. PETRIK and **S.L. CHIGILEJCHIK**

Company «MOTOR SICH»

15 Motorostroitelej Ave., 69068, Zaporozhie, Ukraine. E-mail: tb.ugmet@motorsich.com

Features of the technology of batch repair of blades for high pressure turbines of aviation engines applied at company «MOTOR SICH», equipment, technique and technology of microplasma surfacing, surfacing consumables and heat treatment are considered. The main types of reconditioned parts are presented, and an example of metal microstructure in repair zone is given. 7 Ref., 1 Table, 7 Figures.

K e y w o r d s : *high-temperature nickel alloys, service life, thermal fatigue cracks, microplasma powder surfacing, technology*

Since 1970s repair of blades of high-pressure turbines (HPT) in MOTOR SICH (reconditioning of worn edges and side walls of flanges of shroud platforms) has been performed by argon-arc surfacing process [1]. Note that our enterprise has been a pioneer in the USSR in repair of aviation blades from high-temperature nickel alloys, which at that time were regarded as absolutely unweldable. For a long time, this technology allowed performing batch-repair of such parts for a number of gas turbine engines [2].

In connection with increase of working temperature and service life on aviation engines, which were introduced comparatively recently (D18T, D436, AI222, AI450), HPT blades for operation at temperatures above 1000 °C began to be manufactured from higher alloyed high-temperature nickel alloys such as JS32-VI, JS26-VI [3–5]. At operating time of more than 6,000 h, thermal fatigue cracks of up to 6 mm depth were found on blades sent in for repair, in addition to operating wear of tips and side walls of shroud platforms. Argon-arc surfacing technology and consumable materials, available for this process, do not provide heat resistance properties of reconditioned surface, required for blade operation. Greater wear and, hence, deposited metal mass increased the hot cracking susceptibility at reconditioning by argon-arc process of these blades from modern complex-alloyed high-tem-

perature nickel alloys (with more than 60 % γ'-phase content).

The objective of this work is description of the features of development of surfacing technology, which allows increasing the repairability and extending the service life of HPT blades (with operating time of more than 6,000 h) from high-temperature nickel alloys JS32-VI and JS26-VI.

The main goals set by repair production for such a technology, were as follows:

• reconditioning of damaged blade sections after operation (shroud platforms, labyrinth seal edges, Z-shaped profiles and airfoil edges) on high-temperature alloys JS32-VI, JS26-VI, JS6K-VI and JS6U-VI, using filler material equivalent to base metal;

• improvement of surfacing technology through application of a constricted-arc source with precision adjustment of welding current and filler feed mechanization, that would enable surfacing performance with limited penetration depth, and mixing of deposited metal with base metal, respectively.

At that moment, PWI and SE «Ivchenko Progress» had experience of successfully solving this task. Special equipment was developed, and technology of microplasma powder surfacing (MPS) was introduced into production for reconditioning HPT blades from JS32-VI alloy for D18T engine [6]. Figure 1 shows the MPS block diagram. Deposition material in powder form is supplied by carrier gas into microplasma arc column, formed in argon atmosphere by plasma-forming nozzle channel. Heating in arc column, the powder is transferred into the weld pool, formed un-
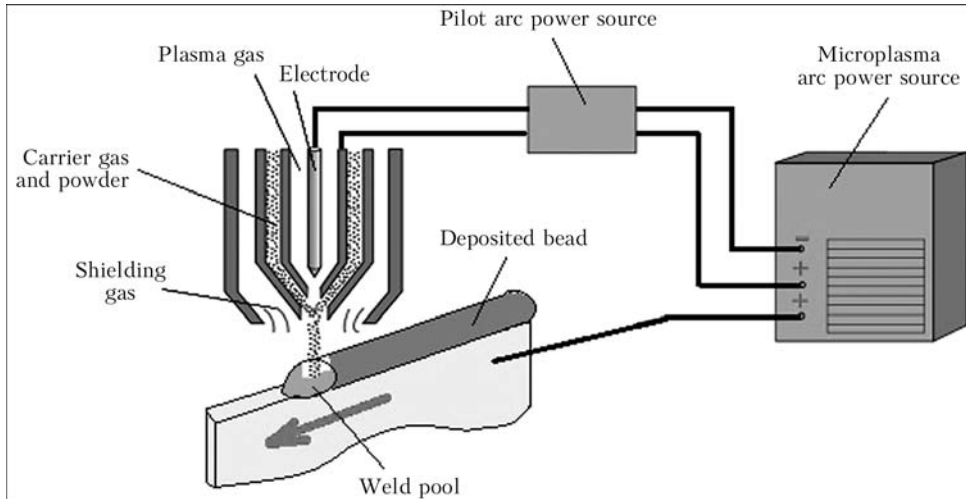
Figure 1. Schematic of MPS process

der the impact of heat flow of microplasma arc on the item (blade edge in our case). At that time, however, this process had a whole number of technological drawbacks, preventing MPS batch application at MOTOR SICH:

• broad deposited bead (more than 5 mm) that greatly increased the labour consumption for machining after surfacing and the hazard of grinding cracks;

• insufficient accuracy of adjustment of surfacing modes during blade reconditioning, particularly at up to 15 A currents;

• limited applicability — surfacing of just one layer; at deposition of two or more layers increased cracking susceptibility was manifested, both during surfacing, and during subsequent heat treatment;

• large overall dimensions of equipment, particularly, plasmatron, that impaired working conditions.

Allowing for available at PWI and SE «Ivchenko Progress» experience, both positive and negative, our enterprise experts developed statement of work and on its basis Deloro Stellite (currently Kennametal Stellite, Germany) de-
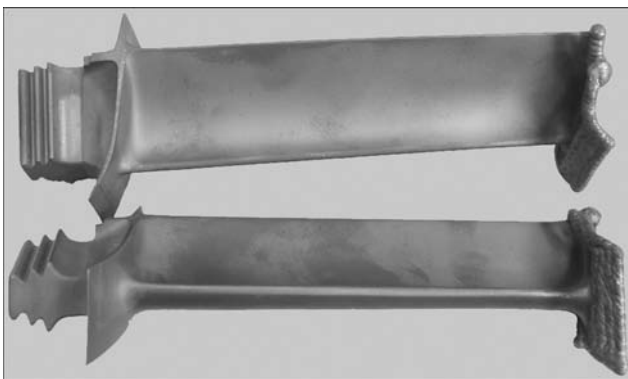
Figure 2. Blade after reconditioning of shroud platform (base metal is JS26-VI alloy, surfacing material is JS32 alloy)

signed and manufactured specialized system STARWELD 190H for MPS [7], which included:

• plasmatron HPH 80;
• pilot arc power source INV 50;
• main arc power source INV 190;
• gas feeding module GT-R5-20 (carrier and shielding gas);
• plasma gas feeding module GT-S 5;
• water-cooling module LT-01;
• powder feeder PR-S2;
• control module SIEMENS Somatic S 7-300.

A package of experimental and research work was performed, which resulted in development of a complex technology of repair of HPT blades from high-temperature nickel alloys JS32-VI and JS26-VI with the following sequence of process operations.

• Surface scraping to metallic luster (removal of scale, oxides and thermal barrier coatings) from edge being surfaced to the depth of 5–10 mm.

• Vacuum degassing annealing ($T = 1250 \pm \pm 10$ °C, soaking time of 20–30 min, medium is vacuum of $1 \cdot 10^{-3} - 1 \cdot 10^{-5}$ mbar).

• Penetrant inspection LYuM1-OV. Detected cracks are removed completely by machining.

• Building blade airfoil edge (see Figure 1) by MPS with powder from JS32-VI alloy (fraction of $+63 - -163$ μm) in 1–5 layers in STARWELD 190H system.

• Vacuum annealing ($T = 960 \pm 10$ °C, soaking time of 180–240 min, medium is vacuum of $1 \cdot 10^{-3} - 1 \cdot 10^{-5}$ mbar).

• Machining of deposited surfaces to required geometrical dimensions.

• Penetrant inspection LYuM1-OV.

• Coating restoration.

• Penetrant inspection LYuM1-OV.

Table 1 gives the main MPS parameters used in HPT blade reconditioning.

—

Main technological parameters of microplasma powder surfacing

Mode parameter	Value range
Welding current (for plasmatron HPH 80), A	3–30
Voltage, V	20–25
Plasma gas consumption, l/min	0.5–2.0
Shielding gas consumption, l/min	5–15
Plasma nozzle channel diameter, mm	1.6–3.2
Tungsten electrode diameter, mm	2.4
Powder feed efficiency, g/min	0.5–5.0

Effective heat input into base metal within 50–650 W is regulated by energy and thermal characteristics of microplasma arc. Used for this process are powders of nickel and cobalt alloys of +63 – −160 μm fraction, produced by the
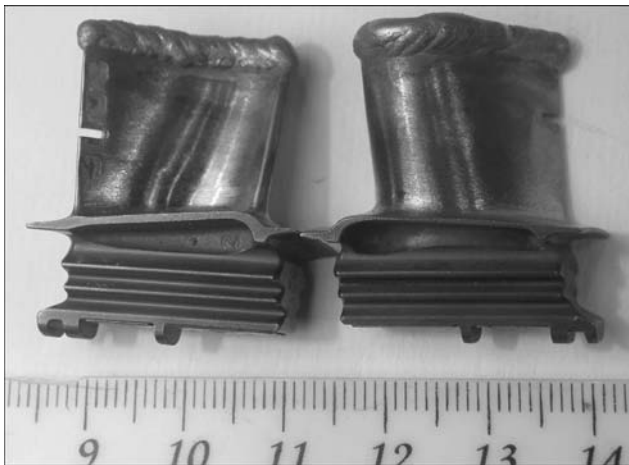
Figure 3. Blade after reconditioning of airfoil edge (base and deposited metal is JS32 alloy)
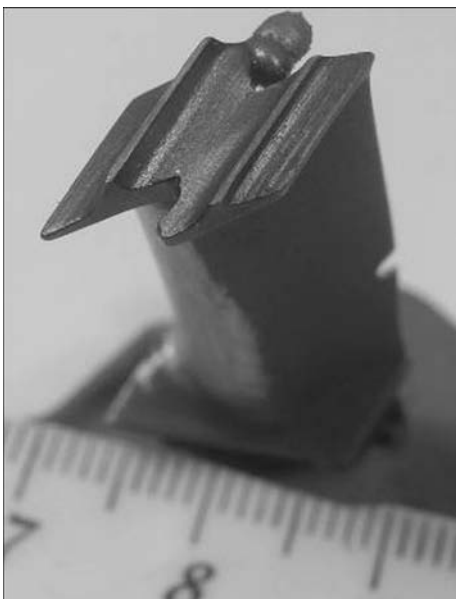
Figure 4. Blade after restoration of Z-shaped profile (base and deposited metal is JS6K alloy)
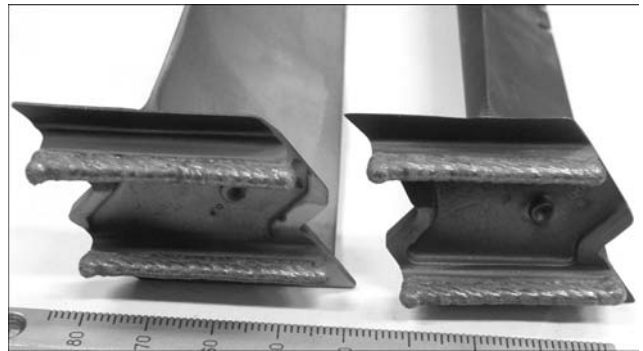
Figure 5. Blades after reconditioning labyrinth seal edges (base metal is JS6K alloy, surfacing material is Stellite 12)

method of dry atomizing of the ingot in argon atmosphere. The main used powders are from JS32-VI, JS6K-VI, V3K, Stellite 12 and Nistelle C alloys. Appearance of blades batch-reconditioned by MPS process is given in Figures 2–5.

Example of metallographic testing of reconditioned JS32-VI blade is given in Figures 6 and 7. Analysis of longitudinal and transverse sections showed that at 2-layer surfacing of airfoil edge by powder from JS32-VI alloy deposited layer height was equal to about 4 mm, and its thickness was 3.0–3.5 mm (see Figure 6). HAZ was small, structural changes were equal to about 0.1–0.2 mm (see Figure 7). No inadmissible defects of metallurgical nature were found in the deposited metal and HAZ.
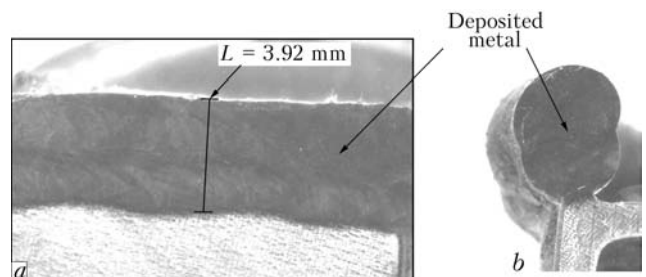
Figure 6. Appearance of longitudinal (*a*) and transverse (*b*) section of reconditioned seal element of the blade
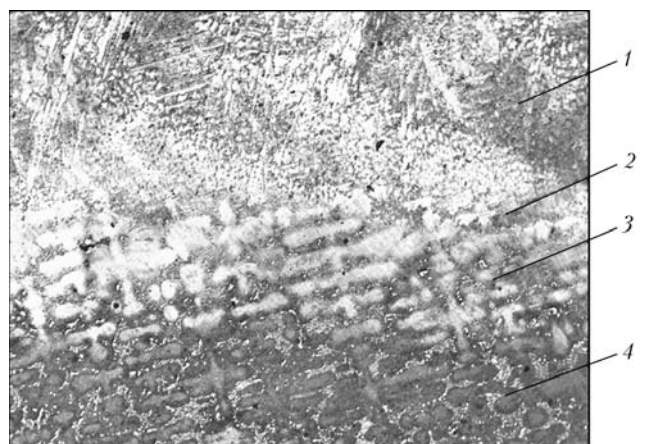
Figure 7. Microstructure (×100) of reconditioned seal element: deposited metal JS32 (*1*), fusion line (*2*), HAZ (*3*) and base metal JS32-VI (*4*)

Conclusions

MPS introduction at MOTOR SICH allowed improving the repairability of a considerable part of HPT blades with more than 6,000 h operating time. This was made possible due to mastering the technology of base metal reconditioning (surfacing in several layers) at considerable damage after operation of shroud platforms, labyrinth seal edges, Z-shaped profiles and airfoil edges from high-temperature alloys JS32-VI, JS26-VI, JS6K-VI and JS6U-VI with predominant application of equivalent filler material.

Technology of MPS of blade edges was improved through application of focused microplasma arc, precise adjustment of welding current, mechanization of disperse filler material feed and rational selection of the modes of pre- and postweld heat treatment.

1. Peremilovsky, I.A., Gejchenko, V.S., Frumin, I.I. (1976) Repair of turbine blades of aircraft engines by surfacing. *Avtomatich. Svarka*, **5**, 54–56.
2. Petrik, I.A., Peremilovsky, I.A. (2001) Further development of technology for strengthening of flange platforms of turbine blades from heat-resistant alloys. *Tekhnolog. Sistemy*, **3**, 90–92.
3. Bratukhin, A.G. (2003) *Modern aviation materials: Technological and functional peculiarities*. Moscow: Aviatekhinform.
4. Kablov, E.N. (2001) *Cast blades of gas turbine engines (alloys, technology, coatings)*. Moscow: MISiS.
5. Boguslaev, V.A., Muravchenko, V.M., Zhemanyuk, P.D. et al. (2003) *Technological assurance of service characteristics of parts of gas turbine engine. Blades of turbine*. Pt 2. Zaporozhie: Motor Sich.
6. Yushchenko, K.A., Savchenko, V.S., Yarovitsyn, A.V. et al. (2010) Development of the technology for repair microplasma powder cladding of flange platform faces of aircraft engine high-pressure turbine blades. *The Paton Welding J.*, **8**, 21–24.
7. (2010) Technological Seminar of Deloro Stellite in Zaporozhie. *Ibid.*, **1**, 46–49.

EROSION RESISTANCE OF Cr−Ni−Si METAL IN SURFACING IN DIFFERENT SHIELDING ENVIRONMENTS

Yu.I. LOPUKHOV

East Kazakhstan State Technical University

34, 30 Gvardejskoj Divizii Str., 070002, Ust-Kamenogorsk, Kazakhstan. E-mail: kanc_ekstu@mail.ru

Pipeline stop valves during operation should possess the erosion resistance of sealing surfaces. For this purpose they are subjected to mechanized arc surfacing with producing of high-alloyed Cr−Ni−Si deposited metal. Further improvement of erosion resistance can be achieved by additional alloying of deposited metal using nitrogen. The paper presents the results of comparative tests of the deposited metal on tear resistance in surfacing using flux-cored wire in argon, carbon dioxide, nitrogen and mixture of nitrogen with carbon dioxide. The best indicators of erosion resistance belong to the deposited metal produced during surfacing in mixture of nitrogen and carbon dioxide. 2 Ref., 3 Tables, 1 Figure.

For mechanized wear-resistant surfacing of sealing surfaces of the parts of pipeline stop valves under flux and in argon, flux-cored wires PP-AN133 (type 10Kh17N8S5G2T) and PP-AN157 (type 10Kh19N9S5M2RGT) are used. These materials are much cheaper as compared to the deficient cobalt stellites, which are finding wide spreading in industry instead of electrodes TsN-6L, TsN-12M. The deposited metal retains a sufficiently high resistance against corrosion and erosion wear and tears in the water-steam environment of high parameters and retains its characteristics during a long service life. The research and experience in application of these steels proves that the deposited coatings with a higher level of hardness show the higher tear resistance. However, their resistance against crack formation in this case falls, particularly abruptly at hardness of more than *HRC* 45 [1].

The hardness of surfacing Cr−Ni steels significantly depends on the presence of alloying elements, such as silicon and chromium in their composition, amount of ferrite phase and degree of its decay during heating. Therefore, a strict regulation of temperature and time modes of surfacing and heating of parts is necessary, including the mode of subsequent heat treatment. A slight deviation of chemical composition of the deposited metal as to chromium and, particularly, silicon, significantly reduces its service characteristics [1, 2]. As a result of dispersion hardening the sigma-phase is formed, which leads to embrittlement of deposited metal and formation of cracks in it. An important role belongs to the temperature-time conditions in surfacing of massive parts and to ageing of alloy at the long-term thermal loads at heat power plants with temperature of working environment of 450−600 °C, which generally reduces the service properties of the alloy [2].

In order to evaluate the possibility of improving the service characteristics the research was carried out on the effect of nitrogen alloying on changes in physical and mechanical properties of alloys 10X17N8S5G2T and 10Kh9N9S5M2RGT depending on temperature of annealing, tear and erosion resistance. The surfacing was carried out in argon and N_2-containing atmosphere.

Mechanical properties. The tests of specimens on impact bending were carried out on pendulum impact testing machine KM-0.3 using the optoelectronic system of fracture energy registration. The full reserve of potential energy of the pendulum was 300 J. The losses for friction in the axis of pendulum in all the cases did not exceed 0.4 %. The tests were conducted on specimens of type 1 according to GOST 9454−78 with V-notch. The hardness of deposited specimens at the normal temperature was determined in TK-2 durometer at loading of 0.29 kg and 30 s holding. The factographic investigations of surface of specimens after fracture at impact toughness tests were performed in scanning electron microscope JSM-6390LV.

The investigations of mechanical properties of the N_2-containing deposited metal (Table 1) show that nitrogen increases the strength and impact toughness of the investigated alloys.

The study of fractograms of the fractured surface of specimens after test on impact toughness (the Figure) shows that the surfacing in atmos-

Table 1. Mechanical properties of Cr−Ni−Si deposited metal

Deposited metal	Shielding atmosphere	Heat treatment mode	σ_t, MPa	KCV, J/cm^2
10Kh17N8S5G2T	Ar	Initial state	$\dfrac{88.2-92.5}{90.3}$	$\dfrac{5.2-5.6}{5.5}$
		Tempering at 650 °C, 3 h	$\dfrac{86.0-90.6}{88.3}$	$\dfrac{5.0-5.6}{5.3}$
		Tempering at 850 °C, 3 h	$\dfrac{66.8-77.2}{72.0}$	$\dfrac{2.8-4.6}{3.7}$
		Ageing at 650 °C, 1000 h	$\dfrac{62.4-68.3}{65.4}$	$\dfrac{0.25-1.10}{0.67}$
10Kh17N9S5G2T	N_2 + 30 % CO_2	Initial state	$\dfrac{94.2-115.0}{104.6}$	$\dfrac{10.6-12.4}{11.5}$
		Tempering at 650 °C, 3 h	$\dfrac{80.0-100.5}{90.2}$	$\dfrac{8.8-11.5}{9.9}$
		Tempering at 850 °C, 3 h	$\dfrac{68.2-78.4}{73.0}$	$\dfrac{5.6-6.4}{6.0}$
		Ageing at 650 °C, 1000 h	$\dfrac{63.8-67.9}{65.6}$	$\dfrac{2.3-3.8}{3.5}$
10Kh9N9S5M2GRT	Ar	Initial state	$\dfrac{86.0-99.2}{92.6}$	$\dfrac{3.5-5.2}{4.4}$
		Tempering at 650 °C, 3 h	$\dfrac{78.8-92.0}{85.4}$	$\dfrac{3.1-4.6}{3.9}$
		Tempering at 850 °C, 3 h	$\dfrac{79.8-94.0}{86.9}$	$\dfrac{2.6-4.2}{3.4}$
		Ageing at 650 °C, 1000 h	$\dfrac{71.2-84.6}{77.9}$	$\dfrac{3.1-4.6}{3.9}$
10Kh19N9S5M2GTRT	N_2 + 30 % CO_2	Initial state	$\dfrac{89.0-99.8}{94.4}$	$\dfrac{4.8-7.0}{5.9}$
		Tempering at 650 °C, 3 h	$\dfrac{79.4-94.0}{86.7}$	$\dfrac{4.1-6.3}{5.2}$
		Ageing at 650 °C, 1000 h	$\dfrac{71.2-85.4}{78.3}$	$\dfrac{3.1-4.6}{3.9}$

phere N_2 + 70 % CO_2 leads to a significant increase in the fraction of tough component in the fracture as compared to argon (Figure *b*). At the same time, fracture of steel may be characterized as a tough cup-shaped fracture with some inclusions of areas of brittle cleavage.

In the metal deposited in mixture of N_2 + 30 % CO_2, the fraction of tough component is increased and the dispersion of structure remains at a sufficiently high level (Figure *c*), that provides the higher values of impact toughness.

A further increase in percentage content of nitrogen in the mixture (over 70 %) results in growing tendency of the material to brittle fracture.

The metal deposited in atmosphere of 100 % N_2 with simultaneous strengthening the austenite leads to embrittlement. This is evidenced by appearance of cleavage sites with a distinct crystallographic orientation on the surface of fracture (Figure *d*).

Tests on tear resistance. In order to obtain the comparable data on service properties of sur-

facing consumables for sealing surfaces of stop valve gates, the complex experimental studies of alloys on the tendency to formation of tears and erosion under the parameters of environment and conditions close to the operating ones were carried.

The tests on tear resistance were conducted in the steam environment at 350 °C and specific pressure of 80−100 MPa at the specialized stand.

Alloys 10Kh17N8S5G2T and 10Kh19N-9S5M2RGT were investigated, produced by surfacing using wires PP-AN133 and PP-AN157, respectively, in Ar, CO_2, N_2, and CO_2 + N_2. The investigation of materials on tear resistance was carried out by modeling the process of contact force action on sealing surfaces of the parts of gate valves. The minimum specific load, at which the tests were started, was 10 MPa. Then, the load was increased stepwise by 10 MPa up to a tear or reaching the preset value of specific pressure. After the test the area of contact (friction) of specimens and tear depth were determined.
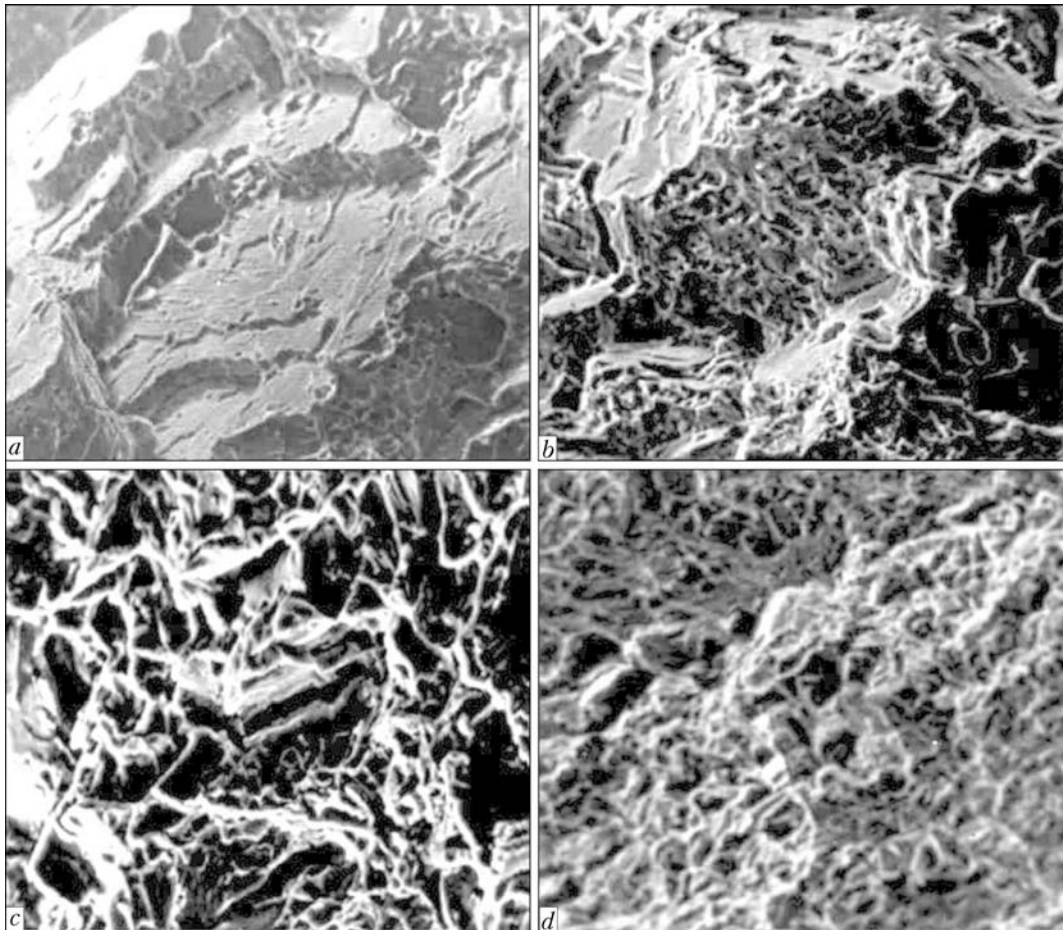
Evolution of type of fracture ($\times$580) in surfacing using flux-cored wire PP-AN133 and shielding atmosphere of Ar (*a*), N_2 + 70 % CO_2 (*b*), N_2 + 30 % CO_2 (*c*) and N_2 (*d*)

The measurements were carried out using microscope MIS-11. As a criterion of tear resistance the appearance of tear of 10 μm depth or more on the working (contact) surface of specimens was conditionally accepted. The specific loading, causing the tears of the preset value, was considered to be the maximum allowable one for the given material.

It follows from the presented data (Table 2) that all the pairs of specimens of alloy 10Kh17N8S5G2T, except of the specimens deposited in atmosphere of argon, have a sufficiently high tear resistance at specific pressures

of 91.2–96.6 MPa, however, the best properties belong to the metal deposited using wire PP-AN133 in N_2 + 50 % CO_2 (96 MPa) and N_2 + 30 % CO_2 (96.6 MPa) atmosphere.

During testing of dissimilar pairs of specimens 10Kh17N8S5G2T + 10Kh19N9S5M2RGT the high tear-resistant properties were registered in the metal, deposited using corresponding wires in mixture of N_2 + 30 % CO_2.

The tear-resistant properties of similar pair of alloy 10Kh17N8S5G2T, alloyed by nitrogen, are not inferior to these properties during testing of above-mentioned dissimilar pairs. The improve-

Table 2. Tear-resistant properties of investigated alloys

Type of alloy of investigated pairs of specimens	Content of shielding gas, %	Hardness *HRC*	Specific loads causing tear of more than 10 μm, MPa
10Kh17N8S5G2T	100 Ar	36	57.7
	100 CO_2	32	71.2
	100 N_2	36	93
	N_2 + 50 CO_2	35	96
	CO_2 + 30 N_2	33	93
	N_2 + 30 CO_2	35	96.6
10Kh17N8S5G2T (down)	100 N_2	32/36	70
10Kh19N9S5M2RGT (top)	N_2 + 30 CO_2	35/38	77

Table 3. Erosion properties of steel 10Kh17N8S5G2T

Steel	Shielding gas content, %	Tests parameters			Test results		
		P, MPa	T, °C	t, h	Wear depth, μm	Wear rate, μm/h	CRES
10Kh17N8S5G2T	100 Ar	17.0	200	254	15.95	0.064	1.03
		18.5	180	196	15.32	0.052	0.88
		18.5	180	196	9.32	0.047	0.97
	N_2 + 50 CO_2	17.0	200	254	12.15	0.051	1.29
		18.5	180	196	7.21	0.033	1.39
	N_2 + 30 CO_2	17.0	200	254	13.06	0.053	1.24
		18.5	180	196	7.52	0.035	1.31
	CO_2 + 70 N_2	17.0	200	254	12.33	0.032	2.06
		18.5	180	196	6.15	0.051	1.40
		18.0	180	196	10.86	0.049	1.53
12Kh18N10T	–	17.0	200	254	16.80	0.066	1
		18.5	180	196	8.70	0.046	1

ment of tear-resistant properties of the deposited metal is associated with producing a more uniform structure in surfacing in N_2-containing environments. In the structure of the alloys, alloyed with nitrogen, the quantitative ratio of α- and γ-phases is changed in the direction of increasing the austenite. Alloy 10Kh17N8S5G2T, alloyed with nitrogen from gas phase, is characterized by formation of fine-dispersed carbonitride particles uniformly distributed in the austenitic matrix, causing the strengthening effect.

Tests on erosion resistance. The working environment was water (18 MPa, 210 °C), feeding the boilers of industrial heat power plant. Simultaneously several pairs of specimens were subjected to tests, where at least in three of them the specimens of test material were present. The speed of environment in gap of 0.3×3 mm^2 between the investigated upper and lower specimen of 12Kh18N10T steel was about 100 m/s. The parameters of environment were maintained and recorded during the experiment using the monitoring system, composition of environment was controlled by hemical sampling at the heat power plant and at the test stand.

The degree of cavitation-erosion fracture of the investigated specimens was determined by weighing them in analytical scales before and after the tests with accuracy of ±0.0001 g. Besides, the working surface of specimens in the slotted water flow was evaluated according to the average depth of wear. The measurements were carried out at nine spots of the investigated surface.

During each experiment alongside with the specimens of the investigated material the upper specimen of steel of type 12Kh18N10T was also installed as a one being investigated, whose level of erosion resistance was taken as a unit. The coefficient of relative erosion resistance (CRES)

was calculated as the ratio of numerical values of erosion rate of the reference and investigated materials. The final indicators were determined as the simple average of relative erosion of tested pairs of specimens.

The average erosion rate was determined as the ratio of average depth of erosion fracture $\bar{h}$ per a unit of time $\tau - i = \bar{h}/\tau$ μm/h. For comparative evaluation of resistance to erosion of the investigated surfacing consumables the tests at changing operating conditions were carried out. It follows from the given results (Table 3) that all the investigated variants of alloys, produced by surfacing using wire PP-AN133 in N_2-containing atmospheres, have a high erosion resistance.

The comparative characteristics showed that the best indicators of erosion resistance belong to the metal deposited using wire PP-AN133 in N_2 + 30 % CO_2 and N_2 + 50 % CO_2 environment.

The phase composition of the deposited metal considerably influences the erosion properties. With increase in the content of austenite fraction, alloyed with nitrogen, the erosion resistance of steel increases. Improving of erosion properties of the N_2-containing deposited metal is obviously connected also with the formation of fine-dispersed nitrides with the lattice coherent to the lattice of austenite and provides their strong engagement in it.

1. Stepin, V.S., Starchenko, E.G., Andreev, A.A. (2006) Application of dispersion-hardened Cr–Ni–Si steels for valve components and cladding of seal faces of fittings of thermal and nuclear power plants. *Armaturostroenie*, **3**, 66–69.
2. Lopukhov, Yu.I. (2009) Formation of structure of chrome-nickel-silicon steel in conditions of gas-arc surfacing. *Fizich. Inzheneriya Poverkhnosti*, 7(**1/2**), 27–30.

PECULIARITIES OF RESTORATION OF WORKING PARTS OF DRILLING BIT MATRIX BODIES

B.V. STEFANIV, V.F. KHORUNOV, O.M. SABODASH, S.V. MAKSYMOVA and **V.V. VORONOV**

E.O. Paton Electric Welding Institute, NASU
11 Bozhenko Str., 03680, Kiev, Ukraine. E-mail: office@paton.kiev.ua

Peculiarities of defects of worn-out matrix drilling bits, occurred during service, were considered. The degree of wear of working parts of seats under diamond-hard-alloy cutters was investigated. Methods of preparation of worn-out areas of working parts for their restoration by arc surfacing were optimized. It is shown that to restore the defective areas of crosspieces of holes of diamond-hard-alloy cutters of body blades, alloy of Kh20N80 grade was recommended as the best one, while TeroCote 7888T alloy was the best one for hole substrates. It was found that protective coating TeroCote 7888T deposited on alloy VK10, provides the most effective protection from erosive and abrasive wears. Basing on the obtained data, the technology of restoration of working parts of blades of matrix bit bodies has been developed. These bits after their restoration were transferred to the customer and at present they are passing the industrial trials at the enterprise of the Poltava region in drilling gas and oil wells. 7 Ref., 4 Figures.

The competitiveness of modern gas-and-oil production enterprises depends mainly on efficiency and reliability of the industrial equipment being used. The efficiency of any drilling equipment or industrial complex is determined by a number of technological breaks or emergency stops for a scheduled on emergency repair.

This is connected to the largest degree with a wear of a drilling tool. The service life of drilling tool depends on the service life of all the working parts included into it. The drilling tool subjected to intensive wear (abrasive, erosion wear, cavitation, impact, pressure, etc.) has, as a rule, a short-time term of service, that reduces greatly the total service life of the tool and leads to the scheduled stops. The expenses, connected with the replacement of drill tool and standstill of equipment, are transformed into multimillion losses for enterprise.

The extension of life of the used rock destruction tool can be attained by applying the technology of restoration of working parts of bit bodies, surfacing of protective wear-resistant coating, that makes it possible to bring the worn-out bits to the condition of new ones.

The main task of present work was to evaluate the degree of wear of bit matrix bodies, equipped with polycrystalline diamond cutters (PDC) and restoration of the worn-out working parts.

The objects of investigations were the tools for rotational method of drilling, i.e. PDC matrix

bits for a continuous drilling. The body of matrix bit is made of composite material on tungsten carbide base, possessing higher wear resistance, as compared with steel one, and allowing drilling of abrasive rocks at a higher speed. The working parts of the matrix bit are equipped mainly with PDC of the leading manufacturers: Genesis, Smith Bits, Element Six Series (XT, HRC, HOT, SQC, GDC, etc.), and calibrating surfaces are made of hard alloys of B25 and B35 grades of SANDVIK Coromant production (Sweden) (analogs of domestic hard alloys VK6 and VK8, respectively).

To restore the worn-out matrix drilling bits, an experience of repair of working parts of steel bits was applied [1]. But the repair of matrix bodies is more complicated due to a poor weldability and problems in surfacing of hard alloys.

Technology of restoration of drilling bits, used for drilling of oil and gas wells by surfacing consumables [2–4], which are produced abroad and used in Ukraine, can be classified by a shape of manufacture and method of surfacing:

• manual surfacing with electrodes;
• arc surfacing with wear-resistant flux-cored wire;
• semi-automatic or automatic surfacing using solid wire, flux-cored wire, self-shielding flux-cored wire;
• gas-flame surfacing and spraying with alloys (surfacing powders);
• plasma surfacing and spraying;
• laser surfacing;
• induction surfacing;
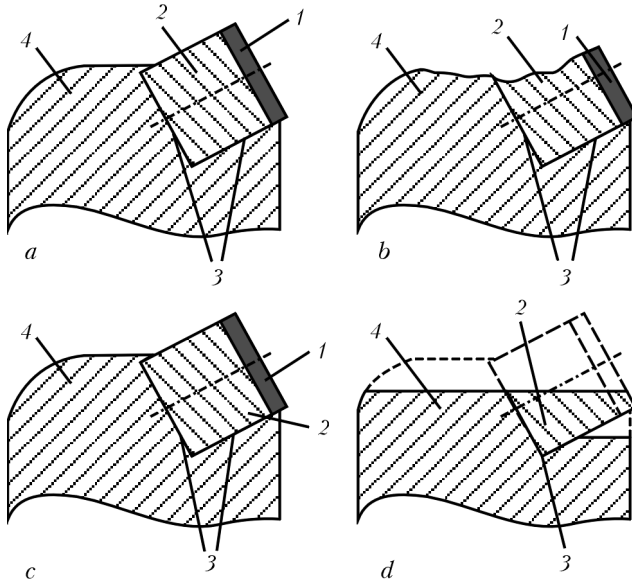
Figure 1. Schemes of wear of seat surfaces for matrix bit cutters: *a* — non-worn-out seat; *b*, *c* — repairable seat (wear of seat surface 10–30 %); *d* — seat not subjected to restoration (wear of seat surface for more than 30 %); *1* — diamond plate; *2* — tungsten-carbide substrate; *3* — seat surface for PDC; *4* — matrix bit body

- electroslag surfacing;
- electron beam surfacing.

In Ukraine only during the recent years the centers for repair and restoration of bits for continuous drilling and recovery of core began to be developed. In 2012 the specialists of enterprise «DP Service» (Poltava) mastered the new technology of repair of drilling bits of company «Polycrystalline Diamond Bits», which allows restoring the PDC bits with steel and matrix body.

In accordance with data [5] the market price of the new PDC-bit of 215.9 mm diameter is 15,000–40,000 USD. The cost of its restoration is different depending on character of damage and varied from 1,000 up to 10,000 USD, but

Figure 2. Appearance of seat wear and working parts of areas of matrix bit of 311.1 mm diameter

due to the possibility of multi repairs of one and the same bit, the customer can obtain the restored tool, which has a service life of that of the new one only for 10–30 % of its cost. On average one bit, as to their opinion, can be restored 3–5 times. But the repair of bits depends not only on the replacement of diamond-hard-alloy cutters (DHC) of working parts, but also, in the first turn, on degree of wear of working areas of layers of tungsten-carbide matrix of seats for DHC (Figure 1). If the working parts of the bit matrix body are worn out by more than 30 %, then the given bit cannot be restored because of a small thickness of tungsten-carbide matrix layer. From different estimations of the world manufacturers of matrix bits the thickness of tungsten-carbide matrix is from 5 up to 50 mm depending on the type and design.

Some features of restoration of bits with an abrasive wear are shown on the example of repair of worn-out working parts of two drilling matrix bits of 311.1 mm of «Smith Bits» production (USA).

The total life of one of these bits was 800 m. During examination of degree of wear of the working parts of six blades the areas with a plane abrasive wear of base metal and body core with damage of seats in a central region and negligible wear on the bit calibrating surface were observed. The most serious defect of damaged central region of the bit blade is wear of base metal of substrate of the working part (Figure 2), where DHCs are fixed into holes by brazing method. Due to the fact that the bit body was manufactured of the matrix material, which is characterized by the increased wear resistance, the works were carried out for determination of criteria of repairability for restoration of worn-out working parts of the given bit.

Let us take for example the fourth blade of the bit being examined, which has a wear both of substrate of seats around the perimeter of cutter and also crosspieces between them (Figure 3). The cause of this wear occurrence was the insufficient wear and impact resistances of the cutters, cooling of washing channels, as well as occurring rupture vibrations of bit in the well. In the given case the wear of seats and crosspieces between the seats was from 0.1 up to 5.0 mm on all the bit six blades.

Final evaluation of the given bit wear [6] according to Classification System, accepted by the International Association of Drilling Contractors (IADC) is 3 7 RO T 0 I (CT, BT, WT, FC) PR, i.e. «repairable». Basing on the results of our works for the creation of technological regulation

of repair of drilling bits of different assortment with DHC [1, 7], the investigations were carried out for the selection of method of deposition and material, which would correspond to all the physical-chemical properties of metal of the bit matrix body. To attain the aim, the properties of existing wear-resistant materials and technologies of restoration were investigated in this work, and methods of deposition of interlayers and protective coatings on the worn-out areas of damaged parts were developed.

To deposit the protective and wear-resistant layers of hard-alloy plates of VK10 grade, two methods of surfacing were investigated: manual argon-arc tungsten-electrode, and gas-flame (oxy-acetylene). And during deposition of protective coatings on defective areas of the working parts the arc surfacing was preferred. In the first turn, this is connected with difficulties of restoration of crosspieces between the blade holes and substrate of cutters, where DHCs are fixed. It is impossible in gas-flame surfacing to deposit bead of 3–5 mm thickness on the worn-out crosspiece because of possible fusion of its very thin layer by the torch flame, while in arc surfacing it is real to deposit a layer on the same worn-out area at keeping the optimum conditions.

During restoration of worn-out parts of the bit body the investigations for selection of material, which could correspond to physical-chemical properties of metal of the bit matrix body, were carried out. The optimizing of arc surfacing technology was performed on non-standard hard-alloy specimens: 1 — alloy VK10 + TeroCote 7888T; 2 — alloy VK10 + PANCh-11 + TeroCote 7888T; 3 — alloy VK10 + alloy of Kh20N80 grade; 4 — alloy VK10 + PANCh-11.

For surfacing of intermediate and protective coating on mock-up specimens the inverter welding machine «Korall-300» was used. The set optimum conditions of surfacing with the least heat inputs were: U = 10–12 V and I = 60–120 A. The obtained thickness of the deposited layer was in the range of 1–3 mm.

From the results of the carried out investigations two materials for restoration of defective areas of working parts were selected. The first one is TeroCote 7888T, which provides a good wetting γ the hard alloy and has no defects in surfacing the protective coating of substrates and perimeters of DHC holes. The second one is alloy of Kh20N80 grade, which is designed for restoration of thin crosspieces of holes, which, in its turn, contributes to a good machining of seats after surfacing and retains the geometry of holes for DHC fixation.
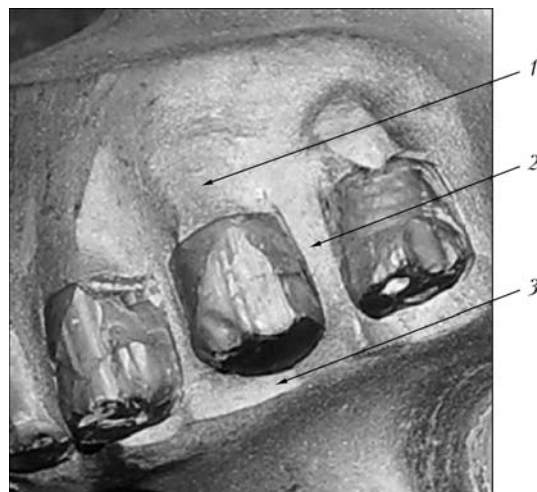
Figure 3. Scheme of wear of working part: *1* — seat substrate; *2* — seat crosspiece; *3* — perimeter of seat for DHC

Results of investigations were used in restoration of working parts of body blades of two worn-out matrix drilling diamond bits of 311.1 mm diameter. For example, at the area (Figure 4, *a*) after unbrazing of DHCs from the holes the works were carried out on machining of damaged areas of blade holes, i.e. wear of substrates and DHC crosspieces before repair was up to 30 % of the working part wear. For the restoration of worn-out crosspieces and substrates of DHC with the bit body the method of arc surfacing was used at a low heat input for reducing the level of residual stresses in the de-
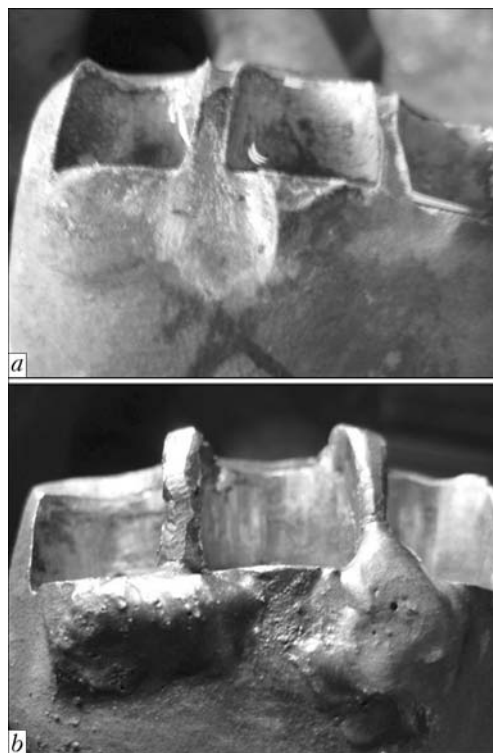
Figure 4. Appearance of worn-out part of blade after DHC unbrazing (*a*) and after surfacing of DHC crosspieces and substrates (*b*)

Figure 5. Appearance of matrix drilling bits of 311.1 mm diameter after restoration

posited layers (Figure 4, *b*). As a filler for restoration of crosspieces, the wire of 1.0 mm diameter of grade Kh20N80 was used. The optimum welding conditions of welding were U = 10−12 V and I = 60−100 A. For surfacing the DHC substrates, the protective wear-resistant material TeroCote 7888T (Castolin) of 5.0 mm diameter was used. Here, the surfacing conditions were U = 10−12 Vand I = 80−120 A.

The produced structure of the deposited metal provides a high hardness (*HRC* 43−49) of the surfacing zone and very effective protection from wear in drilling of medium and hard rocks. The applied method of increasing the wear resistance by using protective material TeroCote 7888T allows increasing significantly the service life of the restored areas of working parts of drilling bit bodies, operating in severe conditions of the erosion-abrasive wear.

Figure 5 shows drilling bits of 311.1 mm diameter after restoration of working parts. The described bits were tested in the Poltava region during drilling of gas wells.

Conclusions

1. Basing on the carried out investigations the challenging compositions of protective coatings were selected providing a good wetting of hard-alloy material (WC−Co) and good hardness at abrasive and erosion wear of the drilling bits.

2. Technology of deposition of interlayers and protective coating can be applied also for restoration of other defective areas of working parts of matrix bodies of the drilling bits for a continuous drilling.

3. Results of investigations can be used in mining and other branches of industry of Ukraine.

1. Stefaniv, B.V., Khorunov, V.F., Sabadash, O.M. et al. (2014) Features of reconditioning steel drill bit watercourse. *The Paton Welding J.*, **11**, 50−54.
2. Materials for brazing and surfacing TeroCote: *http*://www.castolin.com.ua/
3. Surfacing materials BAT-Servis: *http*://www.btrans.com.ua/qw/id/79/
4. Surfacing alloy relite of L3 type: *http*://www.re-source@aranei.com
5. DP Service repaired 13 drill bits of KUBGAZ: *http*://www.dp-service.com.ua/ru/nefterynok-magazine
6. Khorunov, V.F., Stefaniv, B.V., Sabadash, O.M. et al. (2012) Peculiarities of wear and criteria of repairability of drill bits with diamond-hard-alloy cutters. *The Paton Welding J.*, **10**, 39−43.
7. Khorunov, V.F., Stefaniv, B.V., Sabadash, O.M. et al. (2012) Specifics of repair technologies of drill bits with diamond-hard-alloy cutters. In: *Transact. on results obtained in 2010−2012*, 488−493. Kiew: PWI.

STATE-OF-THE-ART AND TENDENCIES OF DEVELOPMENT OF EUROPEAN MARKET OF JOINING TECHNOLOGIES
(Review of materials of economical-statistical data collection on welding production SVESTA-2014)

O.K. MAKOVETSKAYA

E.O. Paton Electric Welding Institute, NASU
11 Bozhenko Str., 03680, Kiev, Ukraine. E-mail: office@paton.kiev.ua

Paper gives the research data on volume of production and structure of joining technologies and services in EU countries, received by German Welding Society and European Welding Federation in 2007 and 2010 as well as volume of consumption of welding equipment in EU for 2012 and 2013 and volume of production of welding equipment in Germany in 2012 and 2013. 10 Ref., 13 Tables.

European Union (EU) market of joining technologies (JT) and services, including welding equipment market, makes around 30 % of world market, and the largest EU national market, namely German market, is around 30 % of EU market. Wide-range investigations on evaluation of input of JT in EU economy, carried out in 2007 and 2010 by German Welding Society (DVS) and European Welding Federation (EWF) allowed receiving the most complete evaluation of volume and structure of production

as well as EU market of JT and services. Added values and employment level, obtained as a result of JT application [1, 2], were also determined.

Investigation of cost volume of JT market in EU countries included evaluation:

• equipment and systems for welding, surfacing, brazing and cutting (including spare parts and accessories), adhesion and mechanical joints, thermal spraying, robots and robotized systems, laser technologies;

• accompanying goods and JT services: materials for welding, surfacing, brazing, coating deposition, adhesives, rivets, gases for welding and cutting, means for environment and individ-

Table 1. Volume of production of equipment and JT systems in the EU in 2007 and 2010

Joining technologies	Production volume, mln Euro		Portion, %	
	2007	2010	2007	2010
Welding and surfacing	3916[*]	3732	52	47
Brazing	629[*]		8	
Cutting	582[*]		8	
Spare parts and accessories	−	2202	−	28
Adhesion bonding	338	548	5	7
Mechanical joining	324	279	4	3
Thermal spraying	54	59	1	1
Robots / robotic systems	323	829	4	10
Laser technologies	1334	301[**]	18	4
Total	7500	7951	100	100

[*]Including spare parts and accessories.
[**]Data were provided only by Germany.

Table 2. Volume of production of accompanying goods and JT services in the EU in 2007 and 2010

Accompanying goods and JT services	Production volume, mln Euro		Portion, %	
	2007	2010	2007	2010
Welding and surfacing consumables	1717	2027	15	27
Materials for brazing	127		1	
Materials for thermal spraying	256		2	
Other materials (including adhesives)	6 040	1860	48	25
Welding gases	2232	1728	18	23
Rivets	500	552	4	7
Means for environment and individual protection	277	267	2	4
Vent equipment	50	–	1	–
Control means	723	688	5	9
Education	561	417	4	5
Total	12,483	7539	100	100

ual protection, control means, equipment for vent systems, education.

Data, obtained as a result of investigations in a period of 2007–2010 and statistical data on volume of welding equipment production in Germany in 2012 and 2013, published by DVS, allow evaluating conditions and tendencies of development of JT market and production in EU for 2012 and 2013 [3].

According to research data carried by DVS and EWF the volume of production in EU countries during post-crisis 2010 made 15.5 bln Euro, that is 22.6 % lower than the level of 2007. Tables 1 and 2 provide for data on volume of production of equipment and systems for separate JT in EU as well as accompanying goods and JT services.

After crisis of 2008, as can be seen from Tables 1 and 2, the growth of equipment production and JT systems was outlined in EU in 2009 as well as significant (40 %) reduction of volume of production of accompanying goods and JT services took place. Production of JT automation means is growing in EU. Volume of production of robots and robotics complexes rised 2.5 times for three years and exceeded 800 mln Euro in 2010. The International Robotics Federation predicts that volume of sales of industrial robots will increase in Europe by 4 % annually in 2014–2016. At that, it should be noted that portion of welding robots in annual sales had risen from 33 % in 2011 to 50 % in 2013. Volume of production of equipment for adhesion technologies also increases. Prediction of German experts relatively to rise of this technology application for materials joining was completely proved [4]. Reduction of production volume for accompanying goods took place mainly due to production re-

duction in «Other materials» category. Volume of production of materials for welding, surfacing, brazing and thermal spraying in 2010 virtually achieved sales level of 2007. DVS statistical data show 19.4 % increase of production of materials of this category in Germany in 2011, that allows predicting appearance of positive trend in whole for EU during this year [3]. It should also be noted that cost volume of welding consumables in Germany in 2012 and 2013 was reduced for 5 and 6.7 %, respectively, and made 550.7 mln Euro in 2013.

Tables 3 and 4 represent data on volume and structure of production of accompanying goods and JT services in 2007 and 2010.

Data given show significant change of structure except for substantial reduction of production volume of accompanying goods and JT services in a period of 2008–2010. Main portion (~50 %) in structure of production of accompanying goods and services in EU countries in 2007 falls to adhesives production; 18 % — for welding gas; 17 % — materials for welding, surfacing, cutting and thermal spraying. This structure was somewhat different in Germany, i.e. first place on volume of production was taken by welding gas — 28 %, the second is the materials for welding, cutting and thermal spraying (27 %), third is covered by adhesives production (13 %). Services on personnel education made significant portion in EU countries market and, especially, Germany, namely 4.5 and 11 %, respectively.

More than 3 times reduction of volume of adhesives production was noted in 2008–2010 in EU, at that its portion in general production volume of accompanying goods and services reduced to 25 %. This resulted in change of portion structure of production of accompanying goods

Table 3. Production of accompanying goods and services in JT field in Germany and the EU in 2007

Accompanying goods, services	Production volume, mln Euro		Portion, %	
	Germany	EU	Germany	EU
Materials in total, including for:	576	2100	27.3	16.9
welding and surfacing	415	1717	19.7	13.8
thermal spraying	78	256	3.7	2.1
brazing	83	127	3.9	1.0
Gas for welding and cutting	598	2232	28.4	17.9
Adhesives	271	6040	12.9	48.4
Rivets	134	500	6.4	4.0
Control equipment	229	723	10.9	5.7
Occupational safety	49	277	2.3	2.2
Vent equipment	9	50	0.4	0.4
Education	241	561	11.4	4.5
Total	2106	12,483	100	100

Table 4. Production of accompanying goods and services in JT field in Germany and the EU in 2010

Accompanying goods, services	Production volume, mln Euro		Portion, %	
	Germany	EU	Germany	EU
Materials for welding, surfacing, brazing, thermal spraying	549	2027	25.7	26.9
Gas for welding and cutting	544	1728	25.5	22.9
Adhesives	339	1860	15.9	24.7
Rivets	182	552	8.5	7.3
Control equipment	267	688	12.5	9.1
Occupational safety	56	230	2.6	3.1
Vent equipment	18	37	0.8	0.5
Education	179	417	8.5	5.5
Total	2135	7539	100	100

and services at absence of significant growth of production.

Quantitative volume of welding consumables consumption in EU by estimation of «The Japan Welding News for the World» made 530 thou t or 8.5 % of world consumption of welding consumables in 2013. Consumption of welding consumables reduced by 7 % in EU in 2012 and 2013 based on data of this publication. DVS notes 3 % decrease of production of welding consumables in Germany from 199.7 to 193.6 thou t [3, 5–7] in this period.

Structure of welding consumables consumption in EU included 56 % of solid and 20 % of flux-cored wires. Portion of these materials consumption continues growing, however, this process has become slower. Tables 5 and 6 provide data on volume and structure of consumption of main types of welding consumables in EU and in the world.

Main portion of production volume (more than 70 %) in the structure of production of equipment and JT systems in EU, based on DVS data, makes equipment and systems for welding, surfacing, cutting and brazing, including spare parts. Table 7 shows the data on production volume of equipment and JT system in EU and Ger-

Table 5. Volume of welding consumables consumption in the world and EU in 2013

Welding consumables	In the world		In the EU	
	thou t	%	thou t	%
Electrodes	2389.3	100	58.3	2.4
Flux-cored wire	863.7	100	106.0	12.3
Wire for SAW	706.2	100	68.9	9.8
Solid wire	2324.4	100	296.8	12.8
Total	6283.6	100	530.0	8.5

Table 6. Volume and structure of welding consumables consumption in the EU in 2011–2013

Welding consumables	2011		2012		2013	
	thou t	%	thou t	%	thou t	%
Electrodes	68	12	60	11	58	11
Flux-cored wire	108	19	105	19	106	20
Wire for SAW	75	13	77	14	69	13
Solid wire	319	56	308	56	297	56
Total	570	100	550	100	530	100

many in 2010 for main types of technologies accounting on the basis of costs.

In 2013 cost volume of production of equipment for welding and related technologies (brazing, surfacing, spraying, cutting) in Germany made 1663.8 mln Euro (considering production of spare parts 2430.4 mln Euro), and accounting on the basis of quantities it is 812,088 units. The largest portion, namely, 28 % in the cost structure of production of equipment for welding and related technologies is covered by expensive machines and apparatuses for resistance welding and 27 % in total go for equipment for plastics welding, cutting, laser and ultrasonic welding. At that, their portion is not great accounting on the basis of quantities and makes 1.8 and 5.8 %, respectively.

The largest portion in production of equipment for welding and related technologies in Germany accounting on the basis of quantities falls to arc welding — 56.8 % (461,536 units), from which equipment for automatic arc and plasma welding makes only 0.5 % (2369 units). At that portion of equipment for automatic arc and plasma welding accounting on the basis of costs makes 8 % and portion of other apparatuses for arc welding, including equipment for

MIG/MAG welding, is 12 %. Starting from 2010, the volume of production of automatic machines for arc welding increased from 336.5 to 464.7 mln Euro in 2013 or by 38 %.

Production volume of equipment for welding and related technologies in EU in 2013 can be evaluated on the level of 5 bln Euro and for JT is 10–11 bln Euro based on given above German statistical data and data of Table 7.

Equipment for arc and resistance welding dominate in all world markets, including EU market. Portion of EU in world consumption of welding equipment for arc and resistance welding accounting on the basis of quantities covers ~12 % of equipment for arc welding and ~22 % of equipment for resistance welding according to evaluation of «The Japan Welding News for the World». Portion of equipment for arc welding makes 93 % in the structure of consumption of these types of welding equipment in EU. Tables 8 and 9 provide data on consumption of equipment for arc and resistance welding in the world and EU for 2011 and 2012 accounting on the basis of quantities [8, 9].

The main manufacturers of equipment and accompanying goods and JT services in EU are Germany (as was mentioned above) and Italy,

Table 7. Volume of production of equipment and JT systems in Germany and EU in 2010

Joining technologies	Production volume, mln Euro		Portion, %	
	Germany[*]	EU[**]	Germany	EU
Welding, surfacing, brazing, cutting	1259	3732	47.3	47.0
Spare parts	535	2202	18.6	27.6
Adhesion bonding	309	548	10.7	7.0
Thermal spraying	17	59	0.6	0.7
Mechanical joining	89	279	3.1	3.5
Laser technologies	301[***]	301[*]	7.9	3.7
Robots/robotic systems	444	829	15.4	10.5
Total	2881	7951	100	100

[*]Data for 2011.
[**]Data for 2010.
[***]Data were provided only by Germany.

Table 8. Portion of consumption of equipment for arc and resistance welding in the world and EU in 2012

Welding equipment	In the world		In the EU	
	thou un.	%	thou un.	%
Arc machines	1301.70	100	152.5	11.7
Resistance machines	53.85	100	11.7	21.7
Total	1355.55	100	164.2	12.1

Table 9. Portion of consumption of equipment for arc and resistance welding in the EU in 2011 and 2012

Welding equipment	2011		2012	
	thou un.	%	thou un.	%
Arc machines	150	93.2	152.5	92.9
Resistance machines	11	6.8	11.7	7.1
Total	161	100	164.2	100

Table 10. Volume of production of equipment and systems as well as accompanying goods and JT services in the EU in 2007 and 2010 (mln Euro)

Country	2007			2010		
	Equipment and systems	Accompanying goods and services	Total	Equipment and systems	Accompanying goods and services	Total
Germany	2500	2110	4660	2881	2135	5016
Italy	1170	1800	2970	876	880	1758
France	320	1510	1830	518	940	1458
Great Britain	160	1190	1350	213	541	754
Poland	97	169	266	–	–	–
Check Republic	–	–	–	76	51	127
Netherlands	29	382	411	27	228	255
Other EU countries	3224	5319	8543	3360	2765	6125
Total for EU	7500	12,480	19,980	7951	7539	15,490

which covers half of production volume and consumption of equipment and accompanying goods and JT services in Europe.

Germany is an indisputable leader of the European market. Only Germany succeeded in recovery of production volume of goods and JT market and intensifying their production during post-crisis period. Data, given in Table 10, allow evaluating regional structure of JT market in EU following from contribution of national economies of EU countries.

Germany and Italy are also the main EU manufacturers of equipment for welding, cutting and brazing. In sum these two countries produce 70 % of all welding equipment in EU (only Germany produces around 43 %). Table 11 provides data on cost volume of production of equipment and systems for welding, cutting and brazing in series of EU countries in 2010.

Investigations, carried by DVS and EWF, showed the relevance of JT for EU economy. In 2010 a total added value, received as a result of JT application, made 65.1 bln Euro in EU for ~1.2 mln of work places. For comparison the total added value, received from JT in 2007 in Europe, was 86 bln Euro at more than 2 mln of work places [1].

Table 12 provides data on quantity of personnel working in the field of production of equipment and systems as well as accompanying goods

Table 11. Volume of production of equipment and systems for welding, brazing and cutting in the EU countries in 2010 (mln Euro)

Country	Equipment	Spare parts	Total
Germany	1259	535	1794
Italy	319	255	574
France	137	243	380
Great Britain	58	99	157
Check Republic	21	43	64
Other EU countries	1938	1028	2966
Total for EU	3732	2202	5934

Table 12. JT: Quantity of personnel involved in production for the EU and Germany in 2007 and 2010

Index	2007		2010	
	EU	Germany	EU	Germany
Quantity of personnel working in production of equipment and JT systems	55,000	15,000	45,000	18,332
Quantity of personnel working in production of accompanying goods and JT services	68,000	15,350	36,267	16,419
Total	12,3000	30,350	81,267	34,751

Table 13. JT application: Quantity of profession-engaged personnel in 2010

Country	Welders	Other professions[*]	Operators of welding robots	Involved in welding production, total	Other JT professions[**]	Involved in JT, total
Germany	156,146	19,611	82,570	258,327	74,157	332,484
France	51,068	11,357	26,052	88,477	14,751	103,228
Italy	112,829	19,667	23,806	156,302	54,785	211,087
Total for the EU	646,914	110,487	200,746	958,147	166,085	1,124,232

[*]Inspectors, NDT-inspectors, designers, researchers, instructors, planning engineers.
[**]Specialists on surfacing, brazing, cutting, thermal spraying etc.

and JT services in EU and Germany for 2007 and 2010.

Number of people working in the branches of industrial production, related with JT application, made 1.1. mln in EU. Table 13 includes data showing quantity of people engaged in welding production fields by their profession for Germany, Italy and France.

Economic crisis 2008 and 2009 had significant effect on European industry including for JT area, and revealed the necessity of its prompt updating. European Committee developed and adopted the plan of post-crisis recovery «Strategy 2020», which is based on new developed program of EU researches and innovations «Horizon 2020» for 2014−2020 with total financing volume 80 bln Euro. The aim of this framework research program is to increase the compatibility of Europe in global meaning, its economic rise and creation of new work places.

Development of progressive joining technologies was also referred to priority directions in scope of EU research and innovation program «Horizon 2020». Realizing the projects in given research direction provides for:

• 20 % reduction of consumption of expensive and critical materials;

• 30 % improvement of technical characteristics of products without increase of its final price;

• increase of automation level and reduction of production time in comparison with currently applied technologies [10].

1. (2009) The economic importance of welding and joining in Europe: Production values, values added and employees. *Welding and Cutting*, **5**, 292−296.
2. (2014) Study shows resilience of joining technology in Europe. *Ibid.*, **1**, 8−9.
3. (2014) 2013 — Kein gutes Jahr. *Schweissen und Schneiden*, 66(**9**), 500−513.
4. (2005) Neueste Machinery in der Fuegetechnik. *Stachlmarkt*, **8**, 58−59
5. (2014) General description for welding consumables. *The Japan Welding News for the World*, **67**, 4−5.
6. (2013) General description for welding consumables market, *Ibid.*, **63**, 4−5.
7. (2012) General description for welding consumables market. *Ibid.*, **59**, 5−6.
8. (2011) General description for welding machine's market. *Ibid.*, **55**, 5−6.
9. (2013) Worldwide demand for welding machines. *Ibid.*, **64**.
10. Horizont 2020. *http://www.joining-platform.com*